OPTIMAL SIZING OF A MICROGRID
INCLUDING RENEWABLE ENERGY SOURCES

A Dissertation

Presented to

Department of Electrical & Computer Engineering

by

Sofia Verigou

In Partial Fulfillment

of the Requirements for the Degree

ELECTRICAL & COMPUTER ENGINEER in the

TECHNICAL UNIVERSITY OF CRETE

Chania, 2018

OPTIMAL SIZING OF A MICROGRID
INCLUDING RENEWABLE ENERGY SOURCES

Approved by:

Prof. George Stavrakakis, Supervisor
School of Electrical & Computer Engineering
Technical University of Crete

Prof. Konstantinos Kalaitzakis
School of Electrical & Computer Engineering
Technical University of Crete

Dr. Eleftheria Sergaki, co-supervisor
School of Electrical & Computer Engineering
Technical University of Crete

Date Approved: July 16, 2018

ΜΕΛΕΤΗ ΒΕΛΤΙΣΤΟΥ ΣΧΕΔΙΑΣΜΟΥ ΤΟΥ ΜΕΓΕΘΟΥΣ ΜΙΚΡΟΥ ΗΛΕΚΤΡΙΚΟΥ ΔΙΚΤΥΟΥ ΠΟΥ ΠΕΡΙΛΑΜΒΑΝΕΙ ΑΝΑΝΕΩΣΙΜΕΣ ΠΗΓΕΣ ΕΝΕΡΓΕΙΑΣ

Μία διπλωματική που παρουσιάστηκε στο
Τμήμα Ηλεκτρολόγων Μηχανικών και Μηχανικών Υπολογιστών
από την
Σοφία Βερίγου

Ως μερική εκπλήρωση
των απαιτήσεων για την λήψη του διπλώματος
ΗΛΕΚΤΡΟΛΟΓΟΥ ΜΗΧΑΝΙΚΟΥ & ΜΗΧΑΝΙΚΟΥ ΥΠΟΛΟΓΙΣΤΩΝ στο
ΠΟΛΥΤΕΧΝΕΙΟ ΚΡΗΤΗΣ

Εξεταστική επιτροπή:

Καθηγητής Γεώργιος Σταυρακάκης, επιβλέπων
Σχολή Ηλεκτρολόγων Μηχανικών και Μηχανικών Υπολογιστών,
Πολυτεχνείο Κρήτης

Καθηγητής Κωνσταντίνος Καλαϊτζάκης
Σχολή Ηλεκτρολόγων Μηχανικών και Μηχανικών Υπολογιστών,
Πολυτεχνείο Κρήτης

Δρ. Ελευθερία Σεργάκη, συν-επιβλέπουσα
Σχολή Ηλεκτρολόγων Μηχανικών και Μηχανικών Υπολογιστών,
Πολυτεχνείο Κρήτης

Ημέρα Εξέτασης: 16 Ιουλίου, 2018

ACKNOWLEDGEMENTS

I would first like to express my sincere gratitude to my supervisor Prof. George Stavrakakis for the continuous support and his patience. He consistently allowed this thesis to be my own work, but steered me in the right direction whenever he thought I needed it. He taught me everything about renewable energy sources and he transferred that same passion to me.

I would also like to thank my thesis advisor Dr. Eleftheria Sergaki who was always there supporting me whenever i ran into a trouble spot or had a question about this project. I am gratefully indebted for as much as Without her participation and input, this thesis could not have been successfully conducted.

I would also like to acknowledge Prof. Konstantinos Kalaitzakis, for his very insigtful comments on this thesis.

Besides my thesis committee, I would like to thank Prof. Apostolos Dollas, for his guidance and motivation through all my years of study. With his valuable advices and his encouragement, he helped me find the division I would most enjoy working on.

Finally, I must express my very profound gratitude to my parents John and Maria, my sister Jenny and brother-in-law Elias and to my best friend Eleonora for providing me with unfailing support and continuous inspiration throughout all my years and especially through the process of researching and writing this thesis. Special thanks to Aggelos for his essential comments on this work. This accomplishment would not have been possible without them. Thank you.

TABLE OF CONTENTS

LIST OF TABLES

LIST OF FIGURES

LIST OF SYMBOLS AND ABBREVIATIONS

AC   Alternation Current

ADP   Advanced Dynamic Programming

AI   Artificial intelligence

BESS   Battery Energy Storage System

CHP   Combined heat and power system

COE   Cost of Energy

DC   Direct Current

DER   Distributed Energy Resources

DG   Distributed generation

DMS   Distribution Management System

DOD   Depth of Discharge

EMS   Energy Management System

EU   Europe

FCLs   Fault Current Limiters

GA   Genetic Algorithm

HPWS   Hybrid Photovoltaic/wind system

IEEE   Institute of Electrical and Electronics Engineers

LC   Load Controller

LCE   Life Cycle Emission

LCOE   Levelized Cost of Energy

LV   Low Voltage

MC   Microsource Controller

MG   Microgrid, μGrid

MGCC   Microgrid Central Controller

MOEA   Multi-Objective Evolutionary Algorithm

MPPT   Maximum Power Point Tracker

OMS   Outage management system

PCC   Point of common coupling

PES   Power and Energy Society

PEV   Plug-in electric vehicle

PHEV   Plug-in hybrid electric vehicle

PPC   Public Power Corporation

PSO   Particle Swarm Optimization

PV   Photovoltaic

R&D   Research & Development

RER   Renewable Energy Resources

RES   Renewable Energy Sources

ROR   Run of the River (hydroelectricity)

SCADA   Supervisory Control And Data Acquisition

SOC   State of Charge

SOH   State of Health

US   United States

WT   Wind Turbine

SUMMARY

In recent years, an increasing energy demand from a continuously growing population, combined with the advancement of greenhouse gasses (GHG) emissions and the depletion of fossil fuels have motivated the introduction of renewable energy systems (RESs) in a variety of disciplines and scales. As a consequence, the energy sector is facing a transition from a centralized network, composed of large and controllable power plants, to a decentralized grid, based on RESs. Within this framework, microgrids (MGs) provide a key solution to integrate each element of the grid, regardless of their operation status, either in a grid-connected or in an islanded mode. This study combines different RESs in order to create a functional power system which is able to cover the load of an autonomous small island, without the use of conventional energy sources. In more detail, the proposed model consists of photovoltaic (PV) panels and hydro turbines, a battery energy storage system (BESS) and a load. The main objective of this thesis is to present the optimal size of each component through an optimization software (HOMER).   Moreover, in order to facilitate the ability to adjust generation of load demand overtime, the simulation of four load prediction scenarios for the next five, ten and twenty five years is exercised with the HOMER software, while providing the optimal sizing of the PV subsystem and BESS in all cases (and generators in two scenarios), in regard to the simultaneous financial and energy load coverage optimization. The simulations conducted in the present study support our initial hypothesis, indicating that a small network can be electrically efficient and autonomous, without the need of the main grid to support it or the use of conventional energy sources, deemed as harmful as they could be to the environment, depending on the increase of the load demand.

ΠΕΡΙΛΗΨΗ

Τα τελευταία χρόνια, η αυξανόμενη ζήτηση ενέργειας από έναν συνεχώς αυξανόμενο πληθυσμό, σε συνδυασμό με την επιδείνωση του φαινομένου του θερμοκηπίου και την εξάντληση των ορυκτών καυσίμων, προκάλεσαν την εισαγωγή των ανανεώσιμων πηγών ενέργειας (ΑΠΕ) σε συστήματα ποικίλων κλάδων. Ως εκ τούτου, ο ενεργειακός τομέας αντιμετωπίζει τη μετάβαση από ένα κεντρικό δίκτυο, που αποτελείται από μεγάλες και ελεγχόμενες μονάδες παραγωγής ενέργειας, σε ένα αποκεντρωμένο δίκτυο, που βασίζεται σε ΑΠΕ. Στο πλαίσιο αυτό, τα μικροδίκτυα (microgrids) παρέχουν μια βασική λύση για την ενσωμάτωση κάθε στοιχείου του μικροδικτύου, ανεξαρτήτως της κατάστασης λειτουργίας του δικτύου, δηλαδή αν συνδέεται στο κυρίως δίκτυο (main grid ή macrogrid) ή λειτουργεί αυτόνομα). Η παρούσα μελέτη συνδυάζει διαφορετικές ΑΠΕ με σκοπό τη δημιουργία ενός λειτουργικού συστήματος ηλεκτρικής ενέργειας το οποίο είναι ικανό να καλύψει το φορτίο ενός αυτόνομου μικρού νησιού χωρίς τη χρήση συμβατικών πηγών ενέργειας. Ειδικότερα, το προτεινόμενο μοντέλο αποτελείται από φωτοβολταϊκά (PV) πάνελ και υδροστρόβιλους, σύστημα αποθήκευσης ενέργειας μπαταριών (BESS) και φορτίο. Ο κύριος στόχος αυτής της εργασίας είναι να παρουσιάσει το βέλτιστο μέγεθος κάθε μέρους μέσω ενός λογισμικού βελτιστοποίησης (HOMER). Επιπλέον, για να διευκολυνθεί η δυνατότητα προσαρμογής της ζήτησης φορτίου με την πάροδο του χρόνου, προσομοιώνονται τέσσερα σενάρια πρόβλεψης φορτίου για τα επόμενα πέντε, δέκα και είκοσι πέντε χρόνια με το λογισμικό HOMER. Παράλληλα, υπολογίζεται το βέλτιστο μέγεθος των υποσυστημάτων των φωτοβολταϊκών και των μπαταριών σε όλες τις περιπτώσεις (και γεννητριών σε δύο σενάρια), φροντίζοντας ταυτόχρονα την βελτιστοποίηση του κόστους και της ενεργειακής κάλυψης. Οι προσομοιώσεις που διεξήχθησαν υποστηρίζουν την αρχική μας υπόθεση, υποδεικνύοντας ότι ένα μικρό δίκτυο μπορεί να είναι ηλεκτρικά αποδοτικό και αυτόνομο, χωρίς την ανάγκη του κύριου δικτύου να το υποστηρίξει. Η χρήση συμβατικών πηγών ενέργειας επιβλαβών για το περιβάλλον κρίνεται αναγκαία μόνο ύστερα από μεγάλη αύξηση της ζήτησης φορτίου.

CHAPTER 1.   INTRODUCTION

1.1   Context

Globally, 1.4 billion people live without electricity and many people around the world face recurrent power outages. Growth of electricity demand, together with concerns related to climate change and suitability of other technologies has stirred interest in renewable energy technologies. Efficient use of diverse renewable energy sources can pave a path for sustainable development. Therefore, careful design and planning for utilizing renewable energy sources is required for sustainable development of a society. Renewable energy sources are capable of addressing global problems of energy security, climate change and sustainable development, so there is a pressing need to accelerate the development of renewable energy technologies. A brief description of various renewable energy sources along with their current status are presented next.

1.1.1   Renewable Energy

In the past, the power system used to rely heavily on coal, oil, and natural gas for its energy. Fossil fuels are non-renewable, that is, they draw on finite resources that will eventually dwindle, becoming too expensive or too environmentally damaging to retrieve. Energy crisis emerging from the early 1970s with increased environmental concern was the key factor for setting the foundation for development of renewable sources for electric power generation. Countries like Denmark, Germany and the United States led the green energy mission by creating critical markets and policy targets for development of renewable energy. Awareness on climatic change and its adverse effects further fueled this tremendous drive to reduce emissions and generate environment-friendly energy. In contrast with fossil fuels, the many types of renewable energy sources (RES) -such as wind and solar energy- are constantly replenished and will never run out. As a result, today and in the future, the power system is characterized by sharing of RES. The sharing of variable renewable sources in Greece – currently, as well as the predictions until the goal of 40% participation in 2020- is shown in Figure 1.1.
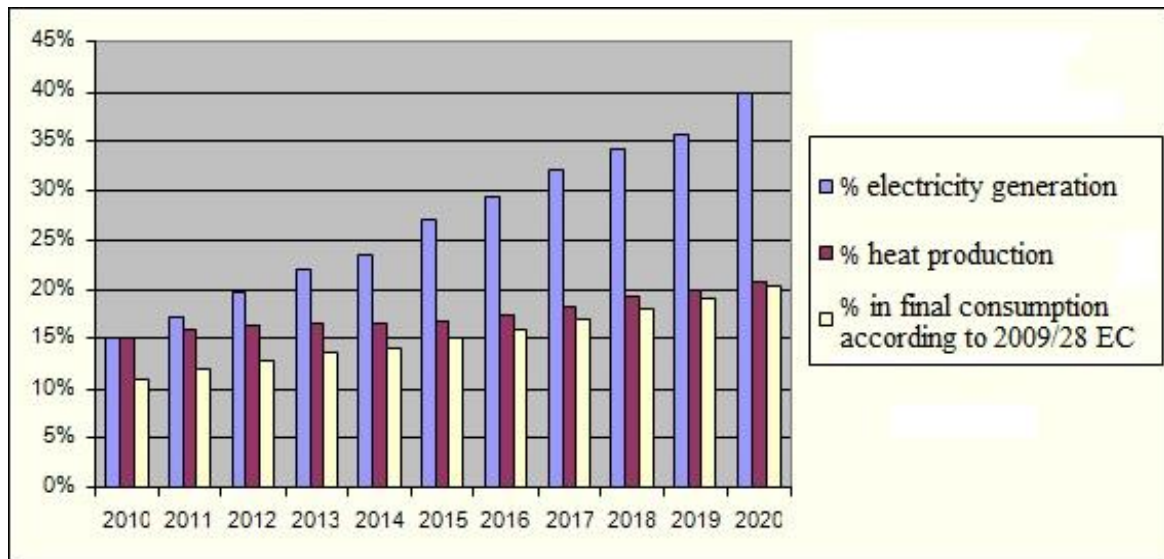
Figure 1.1: The sharing of variable renewable sources in Greece

(Source: http://www.ypeka.gr/Default.aspx?tabid=285&language=el-GR)

The Greek power system involves power generation by lignite, fuel oil, hydroelectric and natural gas power plants, as well as by renewable energy sources. It also involves power transmission via the National Interconnected System to the mainland, as well as power supply to consumers via the distribution network. The load dispatching is effected by the National Center for Energy Oversight, located in Agios Stefanos, Attica. Most of the islands are supplied with electric power generated by autonomous fuel oil power plants, while the use of renewable energy sources (wind, solar) is increasingly gaining ground.

Figures 1.2 shows a continuous huge increase of the installed power of renewable sources over the years.
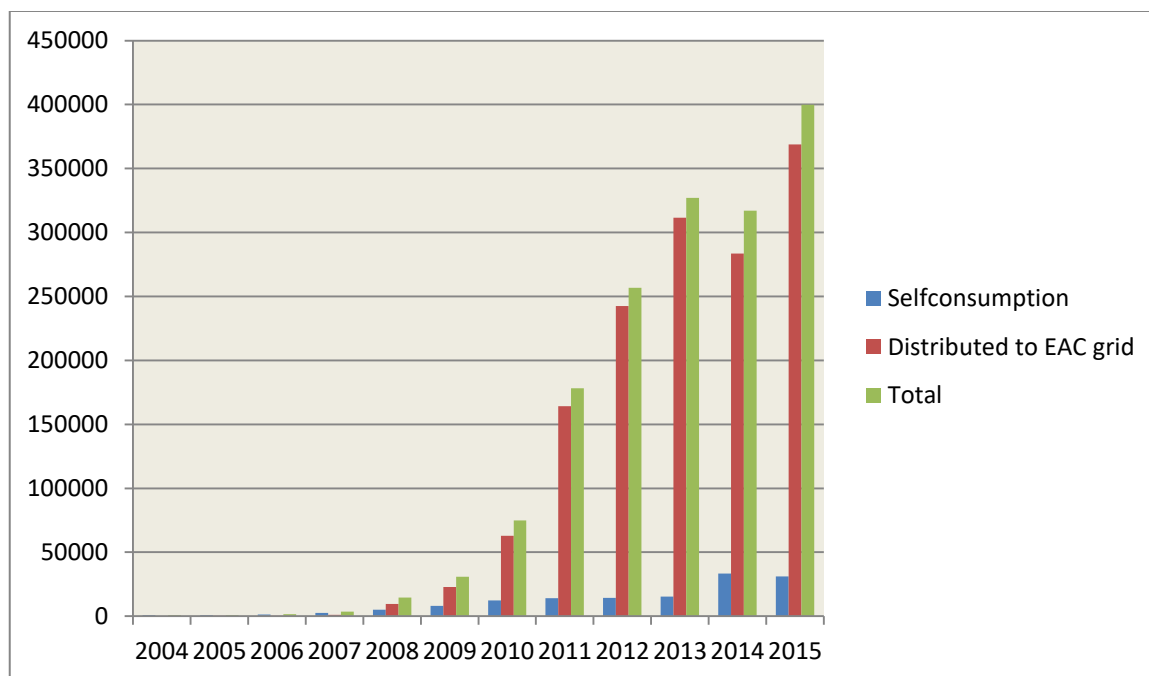
Figure 1.2: Gross production of electricity from RES in Greece (KWh), 2004-2015

(Source:http://www.mof.gov.cy/mof/cystat/statistics.nsf/energy_environment_81main_gr/en ergy_environment_81main_gr?OpenForm&sub=1&sel=4, Energy Statics)

The production of electricity by RES category in Greece is demonstrated in Figure 1.3. As can be seen from this Figure, the photovoltaic and wind energy productions are given as the fastest growth. Specifically, the solar installed is given up to 126.7MWh in 2015 in counter to 6.4MWh in 2010 and just 0.6MWh in 2005.
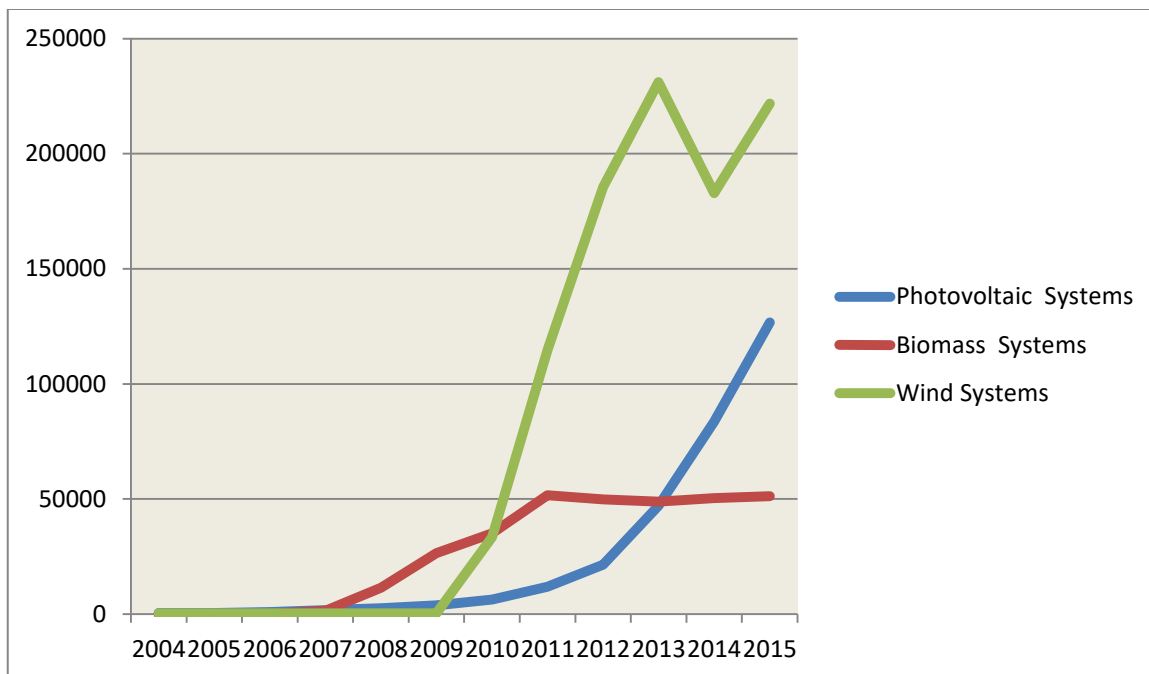
Figure 1.3: Production of electricity by RES category in Greece (KWh), 2004-2015

(Source:http://www.mof.gov.cy/mof/cystat/statistics.nsf/energy_environment_81main_gr/energy_environment_81main_gr?OpenForm&sub=1&sel=4, Energy Statics)

Public Power Corporation (PPC) ensures the energy efficiency of the country through its vast projects. Until recently PPC was the country's only electricity provider. As of 2007, the 34 major thermal and hydroelectric power plants and the 3 Aeolic parks of the interconnected power grid of the mainland, as well as the 61 autonomous power plants located on Crete, Rhodes and other Greek islands (39 thermal, 2 hydroelectric, 15 Aeolic and 5 photovoltaic parks) form PPC's industrial colossus constitute the energy basis of all financial activities of the country.

During the past few years the company, apart from the construction of new thermal (lignite, fuel oil and natural gas) and hydroelectric power plants, has also been investing on alternative energy resources (wind, sun and geothermal).

The total installed capacity of the 98 PPC power plants was 12.76MW with a net generation of 53.90TWh in 2007.
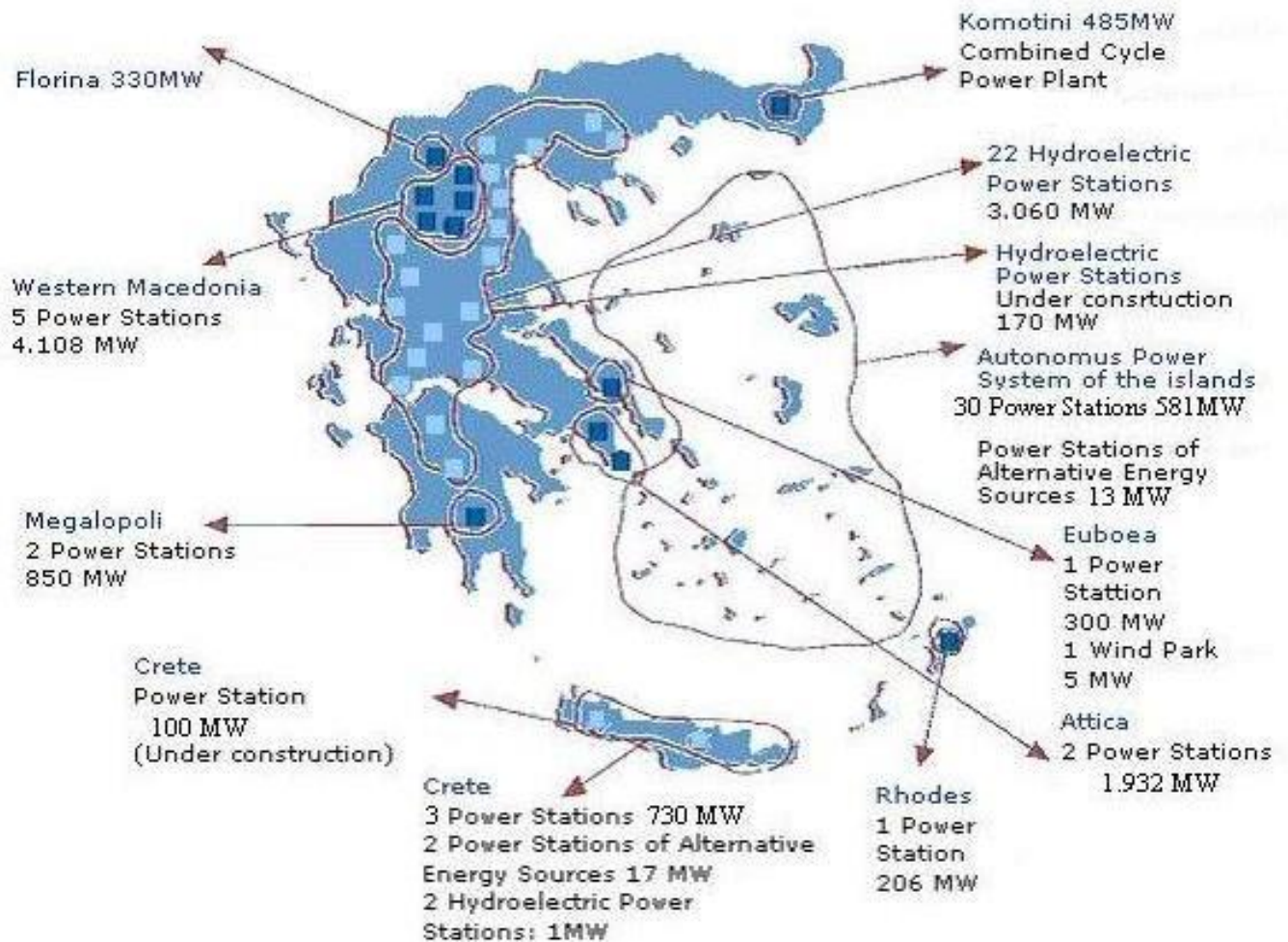
Figure 1.4: Detailed map of power plants in Greece (KWh), 2007

(Source: https://www.dei.gr/en/i-dei/i-etairia/tomeis-drastiriotitas/paragwgi/analutikos-xartis-stathmwn)

1.1.2 Development of photovoltaic

The PV effect was observed as early as 1839 by Alexandre Edmund Becquerel, and was the subject of scientific inquiry through the early twentieth century. In 1954, Bell Labs in the US

20

introduced the first solar PV device that produced a useable amount of electricity, and by 1958, solar cells were being used in a variety of small-scale scientific and commercial applications. The energy crisis of the 1970s saw the beginning of major interest in using solar cells to produce electricity in homes and businesses, but prohibitive prices (nearly 30 times higher than the current price) made large-scale applications impractical. Industry developments and research in the following years made PV devices more feasible and a cycle of increasing production and decreasing costs began which continues even today. The next Figure shows the PV installations and average system price in the US from 2000 until 2013. As can be seen from this Figure the average price of a completed PV system has dropped by 33% since the beginning of 2011.

Installations (MW)	2000	2001	2002	2003	2004	2005	2006	2007	2008	2009	2010	2011	2012	2013
Residential	1	5	11	15	24	27	38	58	82	164	246	304	494	792
Non-Residential	2	3	9	27	32	51	67	93	200	213	339	831	1,072	1,112
Utility	0	3	2	3	2	1	0	9	16	58	267	784	1,803	2,847
Total Installations	4	11	23	45	58	79	105	160	298	435	852	1,919	3,369	4,751

Figure 1.5: US PV installations and average system price, 2000-2013

(Source: http://www.seia.org/policy/solar-technology/photovoltaic-solar-electric)

21

Figure 1.6 illustrates the installed power from photovoltaic applications in Greece from 2007 until 2015.

Greek photovoltaic market

	2007	2008	2009	2010	2011	2012	2013	2014	2015
■ Annual installed power	2	10	35	152	425	912	1.043	17	10
■ Total installed power	2	12	47	199	624	1.536	2.579	2.596	2.606
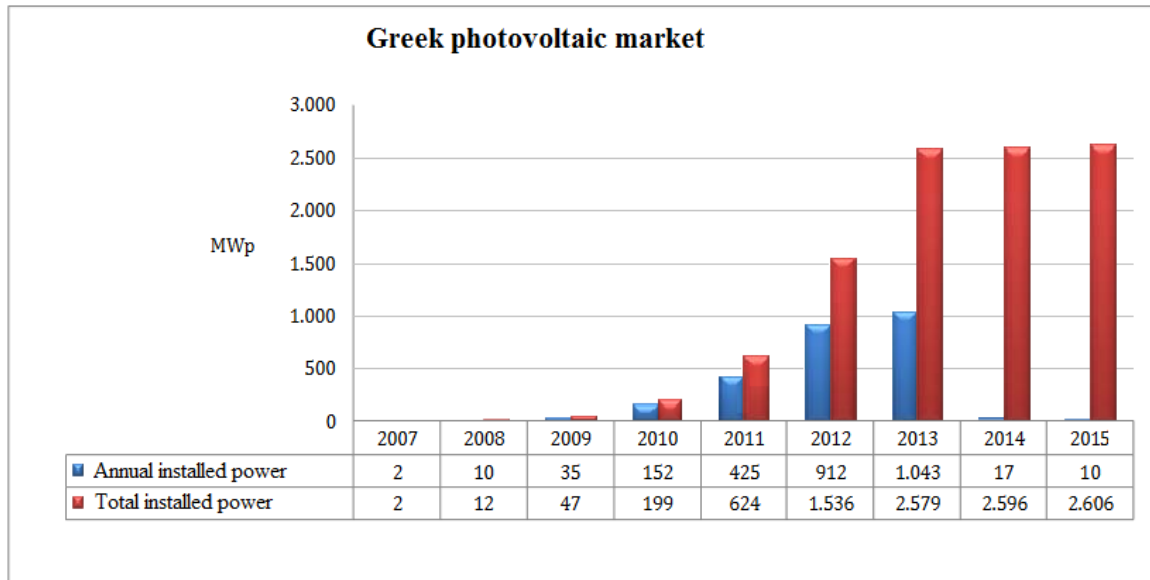
Figure 1.6: Installed Power from Photovoltaics in Greece (MWp), 2007-2015

(Source: http://helapco.gr/wp-content/uploads/pv-stats_greece_2015_10Feb2016.pdf)

In the last two years there has been a downward trend in photovoltaic applications in Greece as a consequence of the political choices that froze the market. However, because of the earlier impressive growth, in 2015 Photovoltaic applications covered 7.1% of the total of the country's electricity needs, bringing Greece (for the third consecutive year) to the second place internationally in terms of the contribution of photovoltaic applications to total energy consumption.

1.1.3   Development of hydropower systems

Hydropower or hydroelectricity refers to the conversion of energy from flowing water into electricity. It is considered a renewable energy source because the water cycle is constantly renewed by the sun.

Humans have been harnessing water to perform work for thousands of years. The evolution of the modern hydropower turbine began in the mid-1700s when a French hydraulic and military engineer, Bernard Forest de Bélidor wrote Architecture Hydraulique.

In 1880, a dynamo driven by a water turbine was used to provide arc lighting– a technique where an electric spark in the air between two conductors produces a light – to a theatre and storefront in Grand Rapids, Michigan, and in 1881, a dynamo connected to a turbine in a flour mill provided street lighting at Niagara Falls, New York; both of which used direct current technology. The breakthrough of alternating current, the method used today, allowed power to be transmitted at longer distances and ushered in the first US commercial installation of an alternating current hydropower plant at the Redlands Power Plant in California in 1893. The Redlands Power Plant utilized Pelton waterwheels driven by water taken from the nearby Mill Creek and a 3-phase generator which ensured consistent power delivery.

The past century of hydropower has seen a number of hydroelectric advancements that have helped it become an integral part of the renewable energy mix in the United States and all around the world. Now they are mostly used for electric power generation. Water turbines are mostly found in dams to generate electric power from water kinetic energy. In July 26 of 2016 Hydropower Vision Report was released. This report establishes an ambitious roadmap to usher in a new era of growth in sustainable domestic hydropower over the next half century.

In table 1.1 are presented some hydroelectric plants in Greece and their configuration.

Table 1.1 – Hydroelectric plants in Greece

NAME	LOCATION	CONFIGURATION
Alfios	Arcadia (PP)	2x3.7 MW Pelton
Aoos	Ioannina (EP)	2x115MW Pelton
Ghiona	Fokis (GC)	1x8.5MW Francis
Gitani	Thesprotia (EP)	2x2.1MW S-tyrbine
Louros	Preveza (EP)	2x2.5MW, 1x5.3MW Francis
Manesaikos	Arcadia (PP)	2x1.08MW Pelton
Mousda	Drama (MT)	1x970kW, 1x508kW Francis
Platanovrisi	Drama (MT)	2x61MW Francis
Polyphyton	Kozani (MW)	3x125MW Francis
Pougakia	Fithiotis (GC)	2x523 kW Pelton
Pournari	Arta (EP)	3x103MW Francis, 2x15MW bulb
Theodoriana	Arta (EP)	1x1.3MW, 1x2.6MW Francis
Thermorema	Fithiotis (GC)	3x680kW Pelton

It's quite difficult to make generalizations about the cost to build hydro systems because of the different combinations of head (the change in water levels between the intake and discharge) and maximum flow rate, and how that affects the maximum power output and choice of turbine type. Also the extent of any civil engineering works is very site dependent, with some new-build sites requiring everything to be built from scratch, while other retrofit projects can make use of and adapt the existing civil engineering structures.

However, it is possible to install systems for a lower cost, particularly if the existing infrastructure at the site lends itself to easy adaption for a modern hydropower system so only modest or no civil engineering works would be needed. The Next figure shows an example of how the cost for every kW installed may evolve in a project depend on the project's size.
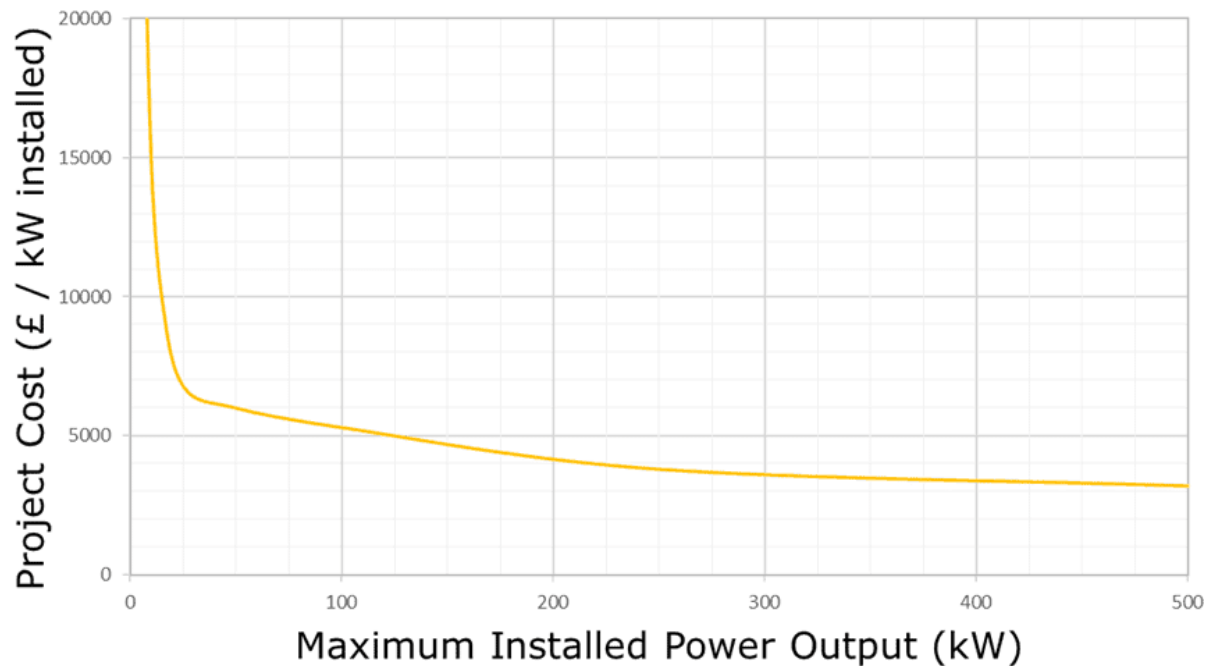
Figure 1.7: Cost of Hydropower Systems per kW of installed power

(Source: https://www.renewablesfirst.co.uk/hydropower/hydropower-learning-centre/how-much-do-hydropower-systems-cost-to-build/)

Very small hydropower systems are disproportionately expensive, and this is because hydro projects of any size have to include a substantial fixed-cost element at the design and consenting stages, and to a slightly lesser degree during the installation stage. This is why the maximum power output of an economically-viable hydropower system will have to be at least 25kW, and preferably at least 50kW. Smaller systems can make sense, particularly at sites with higher heads or if other intangible benefits, such as sustainability, environmental protection or publicity, are valued as much as return on investment.

1.1.4   Development of electrochemical energy storages

At any moment in time, the consumption of electricity has to be perfectly matched with the generation of electricity. This balance is necessary in all electricity grids to maintain a stable and safe electricity supply. Energy storage can help deal with fluctuations in demand and generation by allowing excess electricity to be 'saved' for periods of higher electricity demand.

Table 1.2 - Energy storage R&D investment in Europe

Public funding available through national mechanisms (EU, NO &CH)	EUR	59 million
Public funding available at EU level*	EUR	1 million
Corporate R&D Investment	EUR	1,516 million
Number of companies identified in the corporate investment sample		284
Number of countries represented in the corporate investment sample		20

*indicative; not all funding could be allocated by technologies

The storage technologies that exist currently in the market with their capacity and discharge time are described in Figure 1.8.
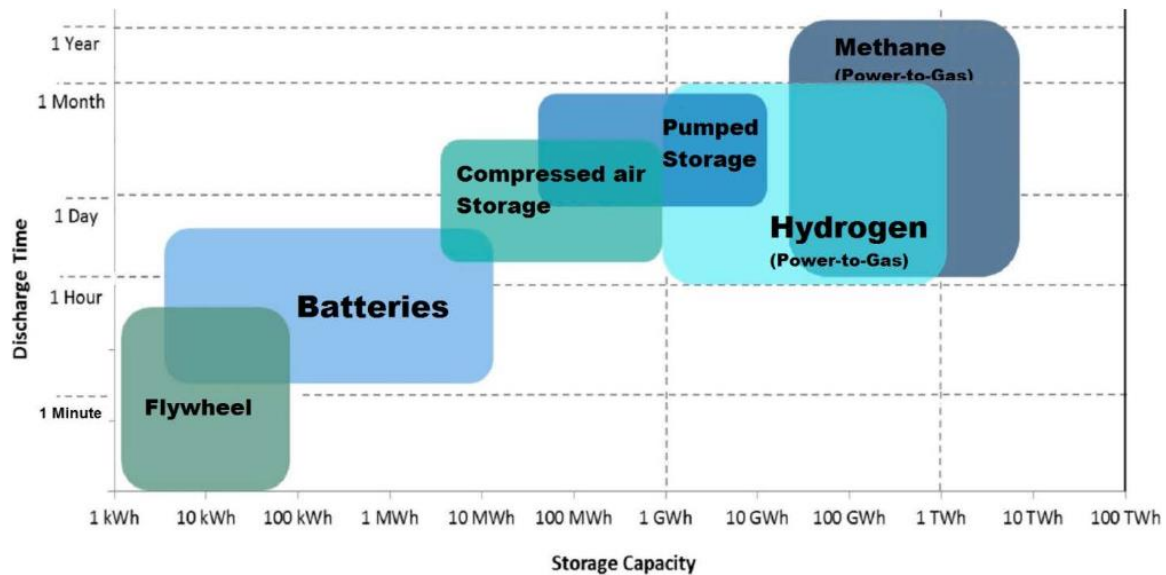
Figure 1.8: Available storage technologies, their capacity and discharge time

(Source: School of Engineering, RMIT University, 2015)

The variation in sun radiation may lead to over-production of electricity from solar PV generators at one time, and lack of production to satisfy the energy demand at another time. As a result, solar PV systems demonstrate a low-level of reliability in power systems. However, the grid must be balanced at each instant; therefore, the generated electricity must meet the varying demand. An energy storage technology would play a significant role in increasing the reliability of solar power generation systems. The battery prices were prohibitive for large-scale power grids utilizing photovoltaic panels. Next Figure shows the storage technology cost (and storage services revenue) in the US during 2013 as well as near-term and long-term predictions until 2023.As figure 1.9 clearly demonstrates, the price is steadily dropping while the technology advances, a combination that makes the use of energy storage rather promising..
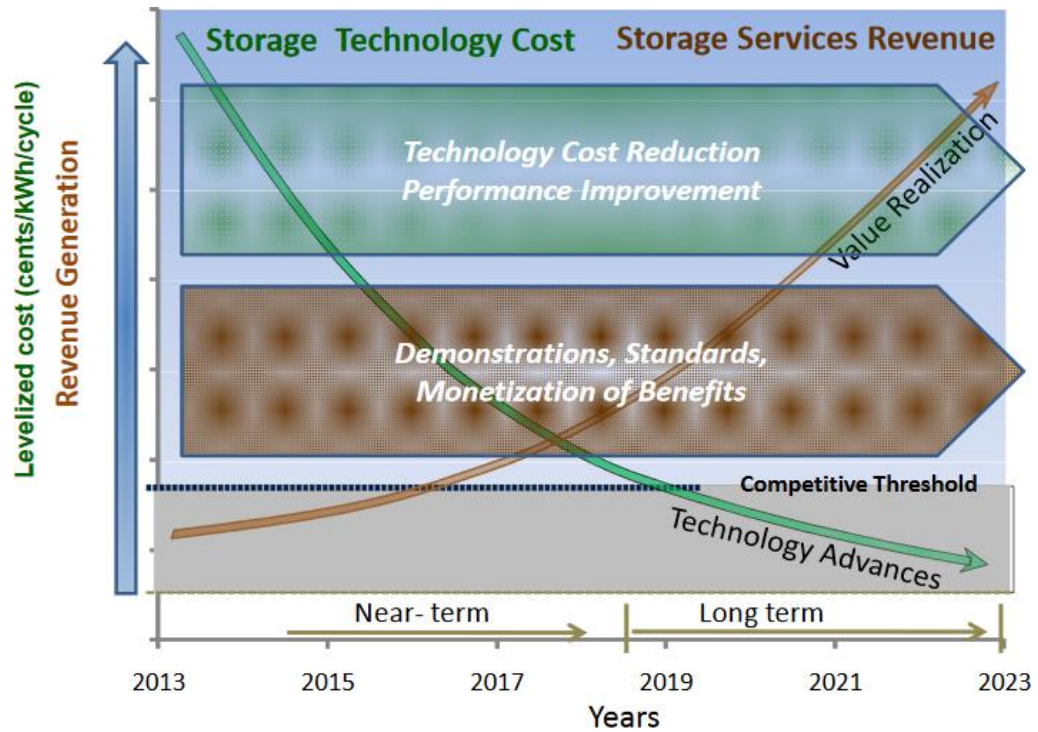
Figure 1.9: Storage technology cost in US - 2013

(Source:https://energy.gov/sites/prod/files/2014/09/f18/Grid%20Energy%20Storage%20Dec
ember%202013.pdf)

Figure 1.10 shows the installed energy storage capacity used in microgrids by battery
category from 2014 until the predictions in 2024.
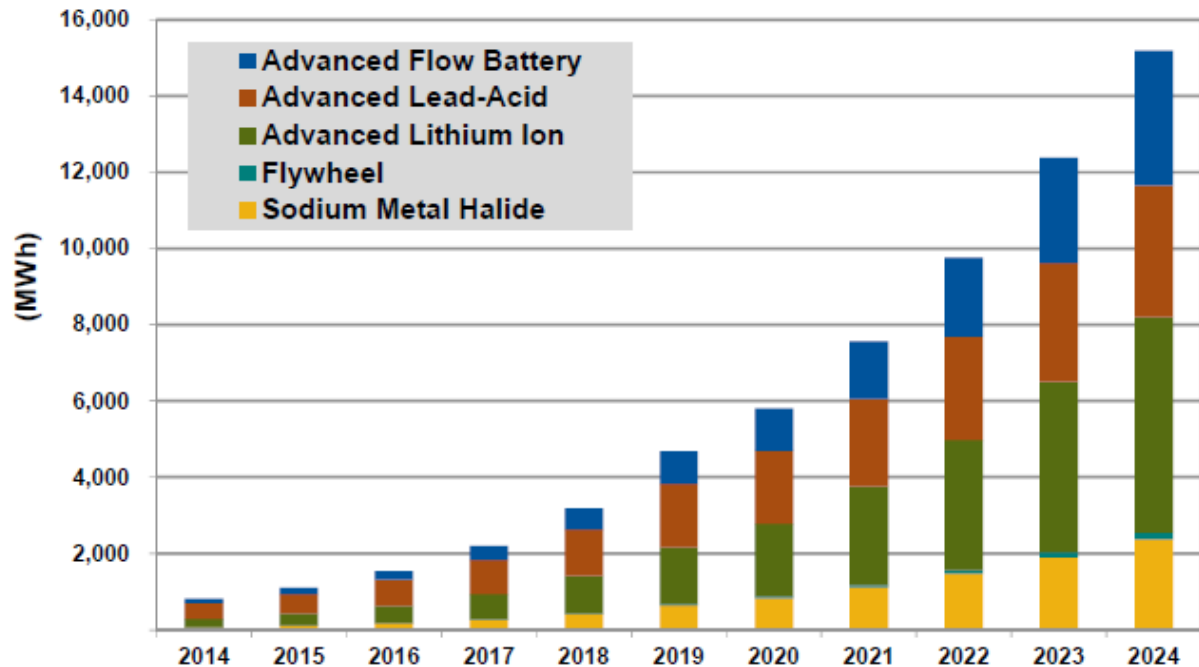
Figure 1.10: Installed energy capacity in microgrids, World Markets: 2014-2024

(Source: Navigant Research)

In conclusion, energy storage is absolutely necessary to any grid with renewable energy sources and some of the roles of this are mentioned below:

- Area regulation,
- Electric supply reserve capacity,
- Voltage and transmission support,
- Transmission and distribution upgrade deferral,
- Demand charge management,
- Electric service reliability and power quality,
- Dynamic operating benefits,
- Reduced generation fossil fuel use,
- Reduced air emissions from generation,
- Flexibility of the grid.

1.1.5 Microgrid

A microgrid is a localized grouping of electricity sources and loads that normally operate connected to and synchronous with the traditional centralized grid (macrogrid or main grid), but can disconnect and function autonomously as physical and/or economic conditions dictate. Note that there is no reference to the actual generation or other DER technologies involved, and in fact, many microgrids will involve a combination of resources, sometimes a quite complex one. There is no reference on the size of microgrids either, since the focus of the definition is on two features:

- It is a locally controlled system.
- It can function both connected to the traditional grid (grid connected mode) or as an electrical island (island mode) and handling the transitions between these two modes.

More specifically, in the island mode, the production is required to meet the loads demand. On the other hand, when the microgrid is connected to the grid, it can either receive or inject power into the main grid. Furthermore, the grid connected microgrid can provide power supporting to its local loads demand. When a disturbance occurs, the microgrid is disconnected from the distribution network as soon as possible in order to avoid any further damage. In that case, the microgrid will operate in an island mode.
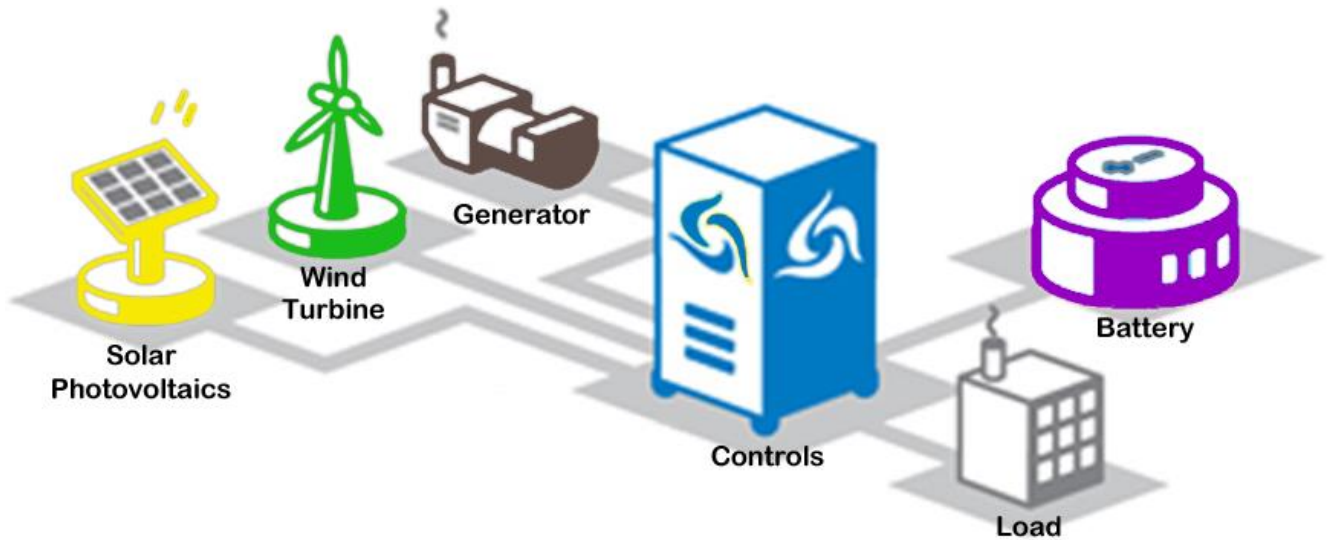
Figure 1.11: Graphic representation of a microgrid

(Source:https://www.civicsolar.com/support/installer/articles/microgrid-regulatory-policy-us)

Microgrid allows and facilitates integration of renewable energy generation such as photovoltaic, wind and fuel cell generations without requiring re-design of the distribution system. Modern optimization methods can also be incorporated into the microgrid energy management system to improve the efficiency, economics, and resiliency.

The base scenario of annual total microgrid capacity by region until 2020 is presented in Figure 1.12. As it can be seen from the Figure the microgrid capacity is expected to continue to develop tremendously during the next 3 years.
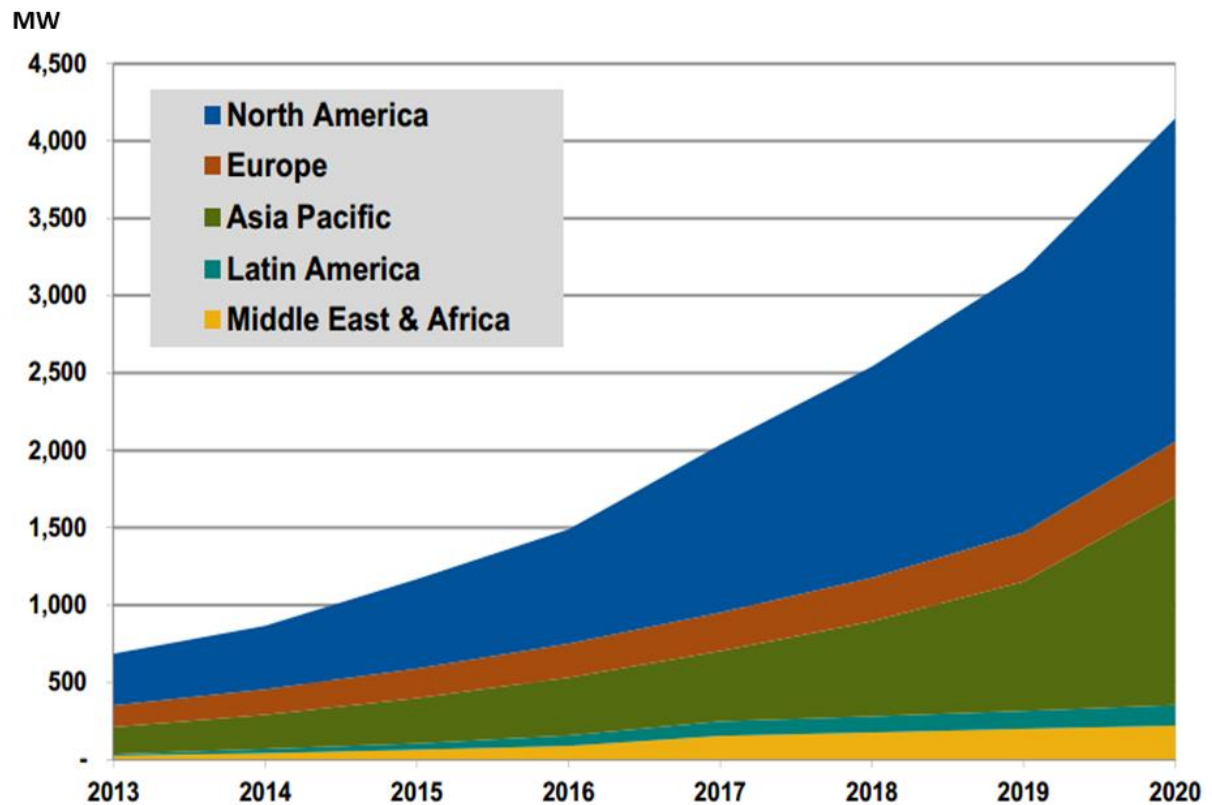
Figure 1.12: Annual total Microgrid Capacity by Region, Base Scenario, World Markets: 2013-2020

(Source: Navigant Research)

1.2 Literatures review

The purpose of the literature review is to gain insight into the concepts of microgrids and optimization, which includes optimal sizing, control and energy management. This thesis is focused on optimal sizing of microgrids. Therefore, the main topic of the present literature review is the classification and comparison of the different optimization strategies towards sizing.

1.2.1 Optimization technics

First, several methods for optimal sizing have been proposed in the literature. According to the optimal operation strategy of the microgrid, the optimal configuration of the system will accrue through the artificial intelligence (AI), genetic algorithms (GA), iterative method or any other methodology which is described in detail in the next sub-chapter.

Second, when a microgrid has more than two DERs, the energy management system (EMS) is needed to impose the power allocating among DER, the cost of energy production and emission. Figure 1.13 describes an example of EMS in a microgrid. As can be seen from this Figure, the forecast values of load demand, the distributed energy resources and the market electricity price in each hour on the next day are denoted as inputs. Furthermore, the operation objectives are considered to optimize the energy management. There are three basic options: economic, technical and environmental, but it is possible to choose a combined objective.
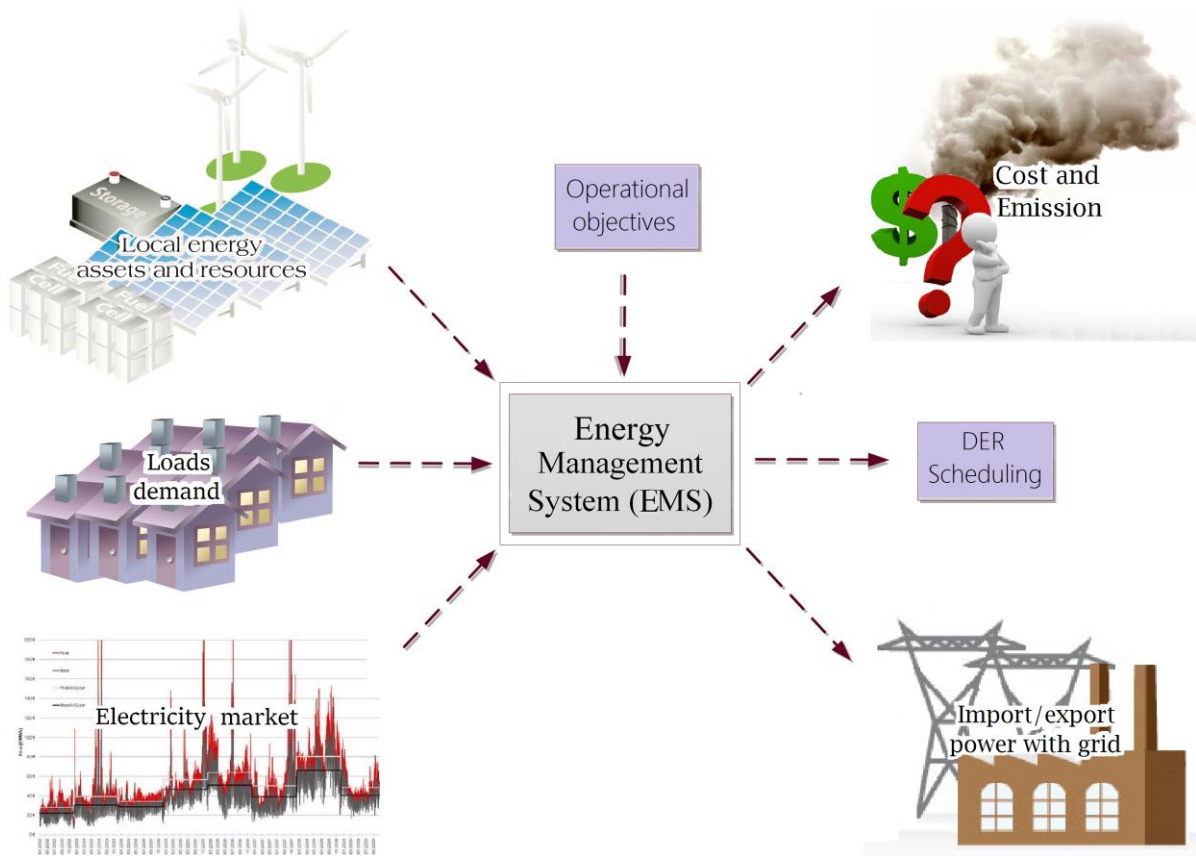
Figure 1.13: The energy management system (EMS)

Some algorithms for the optimization of microgrid energy management are presented in [1] using a rule-based management, [2] with fuzzy logic, [3] with Game Theory and multi-objective optimization and [4] by advance dynamic programming (ADP).

Last, microgrid control is essential for the smooth operation of the system. The local controllers for DER can enhance the efficiency of microgrid operation by using the conventional methods, such as single master (centralize control), master/slave and droop control. Figure 1.14 shows the architecture of a microgrid control.
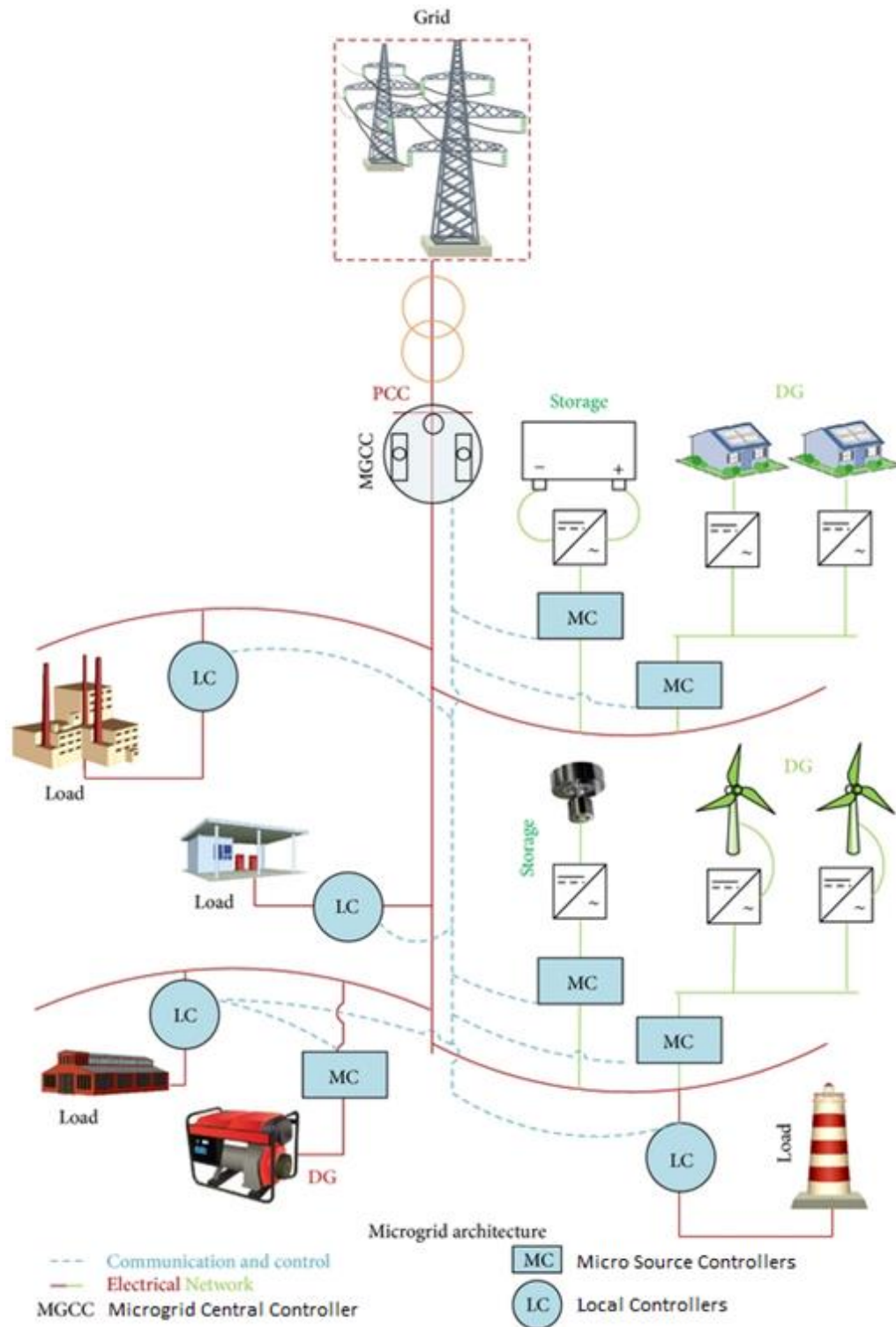
Figure 1.14: The microgrid control architecture

(Source: https://www.hindawi.com/journals/je/2013/937614/fig1/)

Microgrid control is also addressed in some literature. The European R&D project is presented in [5]. The hierarchical microgrid control is proposed in [6], while the centralized control can be found in [7]. Very important is droop control which is presented in [8], alongside with master/slave control.

1.2.2   Optimal sizing of a microgrid

The optimization sizing has been presented in the literature. In [9] is developed a methodology of performing the optimal unit sizing for distributed energy resources in MG which is aimed at finding the configuration, among a set of systems components, which meets the desired system reliability requirements, with the minimum cost of energy (COE).

An island mode microgrid has two main aspects, which are the architecture sizing and the energy fluxes. Dealing with these problems, various simulation and optimization software tools on PV hybrid systems have been reviewed in [10], [11] and [12] On the other hand, two main methods of optimization that are iterative and artificial intelligence (AI) based methods have been proposed in [13]. In [14] a methodology based on genetic algorithm was proposed in order to find the optimal sizing of stand-alone PV/WT systems. The Genetic Algorithm (GA) is used to optimize a hybrid PV/diesel generator system which is divided into two parts, in [15]. The first part aims to find the optimal configuration of the system. Then, the latter part optimizes the operation strategy by using each calculated configuration in the first part. The optimal configuration is the one that leads to the minimum cost of the system. A multi-objective optimization for a stand-alone PV-Wind-diesel system with battery storage by using Multi-Objective Evolutionary Algorithms (MOEAs) is described in [16]. The levelized cost of energy (LCOE) and the equivalent CO_2 life cycle emission (LCE) are known as the objectives. An iterative optimization technique for a stand-alone hybrid photovoltaic/wind system (HPWS) with battery storage was proposed in [17]. The aim is to find the optimum system size in order to respond to the demanded load and to analyze the impact of different parameters on the system size.

In [18] a multi-objective evolutionary optimization algorithm (MOEA) was developed in order to solve the problem of determining optimal size and placement of distributed energy storage in microgrid.

For a grid-connected microgrid, in [19], a method is proposed to determine the size of battery storage for a grid connected PV system. The objective is to minimize the cost considering the net power purchase from the grid and the battery capacity loss (state of health). A methodology for the optimization sizing and the economic analysis dedicated to PV grid-connected systems is presented in [20]. In which, the number, type of the PV units and converters are given as the decision variable. In [21], the author uses GA to determine the optimal allocation and sizing of PV grid connected systems. On the other hand, the Particle Swarm optimization (PSO) is used for optimal sizing of a grid connected hybrid system in [22]. A comparison between the two methods which are PSO and genetic algorithm (GA) is carried out in advance to evaluate the efficiency of the proposed method.

1.3 Objective of the thesis

The aim of this thesis is to present optimal configuration to ensure secure, reliable and efficient operation of a microgrid including photovoltaic productions (PV), battery energy storage system (BESS) and a small hydropower plant. In this thesis, the optimal sizing is designed to find the minimum cost considering the optimization of the operating conditions with highest reliability and without emissions.

1.4 Thesis contributions

The contribution of this thesis lies in the comparison of the multiple scenarios, in both pure RESs depending and fossils depending microgrids, with HOMER's optimization and sensitivity. These simulations were performed for different load demand, different types of operating strategies, and applied to microgrids' optimum size problem.

1.5 Thesis organization

This thesis comprises seven chapters. Contents of each chapter are briefly described as follows:

- Chapter 1: introduces the context, the literature review, the thesis objective, the thesis contribution and the thesis outline.
- Chapter 2: presents the microgrid concept with the definition of microgrid, microgrid operation, microgrid control and microgrid protection.
- Chapter 3: brings out the mathematical modeling of the microgrid components: photovoltaic productions (PV), battery energy storage systems, hydro.
- Chapter 4: analysis and process of data: loads and weather conditions.
- Chapter 5: proposes the optimal sizing for microgrid in island mode through HOMER software and simulates every component.
- Chapter 6: Simulation modelling of four additional scenarios for load prediction.
- Chapter 7: contains the conclusion and future works.

CHAPTER 2.   MICROGRID CONCEPT

Microgrids will play a critical role in the transformation of the existing electricity grid towards the smart grid of the future. They can be defined as low voltage distribution networks consisting of renewable energy sources (RESs), back up controllable energy sources such as diesel generators, storage systems and controllable loads. They can help to integrate the previous components into the grid, enhancing its reliability and reducing the reliance on carbon-emitting fossil fuels for power generation. Moreover, they are fundamental in supporting deep penetration of plug-in electric vehicles (PEVs) and plug-in hybrid electric (PHEV) vehicle.

Figure 2.1: Four good reasons for community microgrids

(Source: http://www.obg.com/insights/four-good-reasons-for-community-microgrids)

2.1   Definition of microgrid

Many research groups around the world are pioneering various µGrid concepts, also written as microgrids, as an alternative approach for integrating small scale distributed energy

resources (DER of < approx. 1MW) into low-voltage electricity systems. Many other terms are in common use to describe similar concepts, e.g. virtual power plants, minigrids, smart grids, smart distribution networks, embedded generation, distributed or dispersed generation.

Currently, there are a lot of microgrid definitions presented in various reports by researching organizations in all over world. Some descriptions of microgrids are shown as follows:

− The definition from the EU research projects [23] and [24] is provided as follows: "Microgrids comprise LV distribution systems with distributed energy resources (DER) (micro-turbines, fuel cells, PV, etc.) together with storage devices (flywheels, energy capacitors and batteries) and flexible loads. Such systems can be operated in a non-autonomous way, if interconnected to the grid, or in an autonomous way, if disconnected from the main grid. The operation of micro-sources in the network can provide distinct benefits to the overall system performance, if managed and coordinated efficiently."

− From the Office of Electricity Delivery & Energy Reliability (US Department of Energy) the definition of microgrid [25] is provided as follows:
 "A microgrid is a local energy grid with control capability, which means it can disconnect from the traditional grid and operate autonomously."

− Mohommed Shahidehpour, bodine Distinguished Chair Professor and Director at Illinois Institute of Technology, presented a simple definition of microgrid [26]:
"A microgrid is essentially nothing more than an electrical grid that can operate from its own power without a long-distance transmission system or connection to a broader grid."

− The US San Diego (University of California) presents a Microgrid definition in [27]:
A small-scale version of a traditional power grid, a microgrid draws energy from clean sources such as wind and solar power, as well as from conventional technology. A microgrid can be connected to a larger electric grid, but can also work independently. Power generation may be produced from several key sources: solar, a fuel cell and a cogeneration plant. These assets are integrated with energy storage and the sophisticated software that controls it all.

– The Berkeley Lab Has provided the following definition of Microgrids in [28]. It has a slight difference with the above descriptions:

"A microgrid is a semiautonomous grouping of generating sources and end-use sinks that are placed and operated for the benefit of its members, which may be one utility "customer," a grouping of several sites, or dispersed sites that nonetheless operate in a coordinated fashion. The supply sources may include reciprocating engine generator sets, micro-turbines, fuel cells, photovoltaic and other small-scale renewable generators, storage devices, and controllable end-use loads. All controlled sources and sinks are interconnected in a manner that enables devices to perform the μGrid control functions unnecessary for traditional DER. For example, the energy balance of the system must be maintained by dispatch, and non-critical loads might be curtailed or shed during times of energy shortfall or high costs. While capable of operating independently of the macrogrid, the μGrid usually functions interconnected, purchasing energy and ancillary services from the macrogrid as economic, and potentially selling back at times."

From these definitions, the features of a microgrid include:

o Microgrid is an integration of micro-sources, storage units and controllable loads located in a local distribution grid.
o A microgrid can operate in grid-connected or disconnected modes.
o The energy management and coordination control between available micro-sources are demonstrated in a microgrid.

2.2 Microgrid structures and components

In the very beginning of rural electrification, several microgrid structures had been installed. Later, the economic benefits of an interconnected utility grid with large power plants led to today's power system structures.
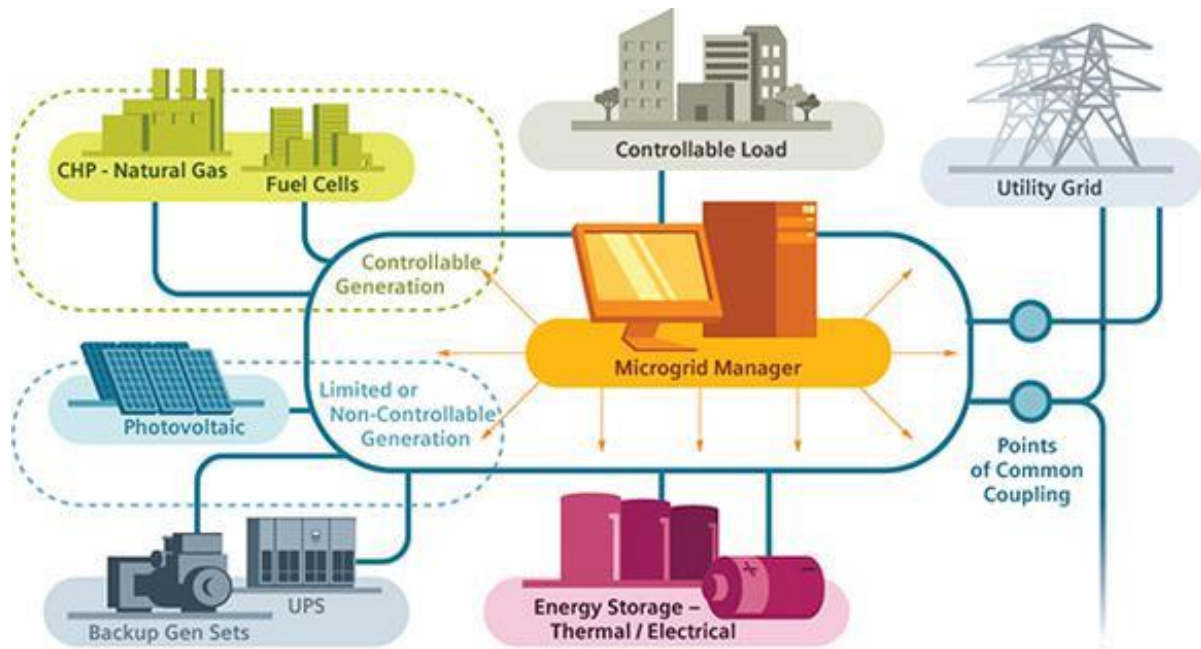
Figure 2.2: A studied microgrid structure

Expectations on today's microgrid structures significantly exceed the capabilities of the initial systems, especially in terms of physical characteristics, and the number and size of distributed generators within the microgrid. A modern microgrid will include renewable and fossil-fueled generation, energy storage facilities, and load control. And this new system will be scalable, which means that growing load may require the installation of additional generators without any negative effect on the stable and reliable operation of the existing microgrid. Typical distributed energy resources for microgrids are wind and solar powered generators, combined heat and power systems (CHP), and biogas and biomass systems. DERs can be divided into two main groups:

(i)   DER directed-coupled conventional rotating machines (e.g., an induction generator driven by a fixed-speed wind turbine), and

(ii)   DER grid-coupled with the inverter (e.g. Photovoltaic, fuel cells, etc.). Distributed energy storage devices can be charged with the power excess and discharge to cover the power deficit. Thus, helping to enhance the reliability of the microgrid as well as making it efficient and economical.

The diagram of a microgrid which includes many systems: PV, hydropower turbines and a battery energy storage system is shown in Figure 2.3. Each distributed energy resource is interfaced with its corresponding bus through a power-electronic converter. The microgrid is connected to the upstream network at the Point of common coupling (PCC). The power is furnished from a Low-voltage (LV) transmission grid, through a substation transformer. The microgrid operates with two modes: the grid-connected mode and the islanded mode. In the grid-connected mode, the PCC is closed and the microgrid is connected with the main grid. It leads that the microgrid can exchange energy with the main grid. When the upstream network occurs the disturbance or the microgrid gets the optimal operation state, the switch at PCC can be opened to disconnect the microgrid. Thus, the microgrid can continue to operate in the so-called islanded mode.
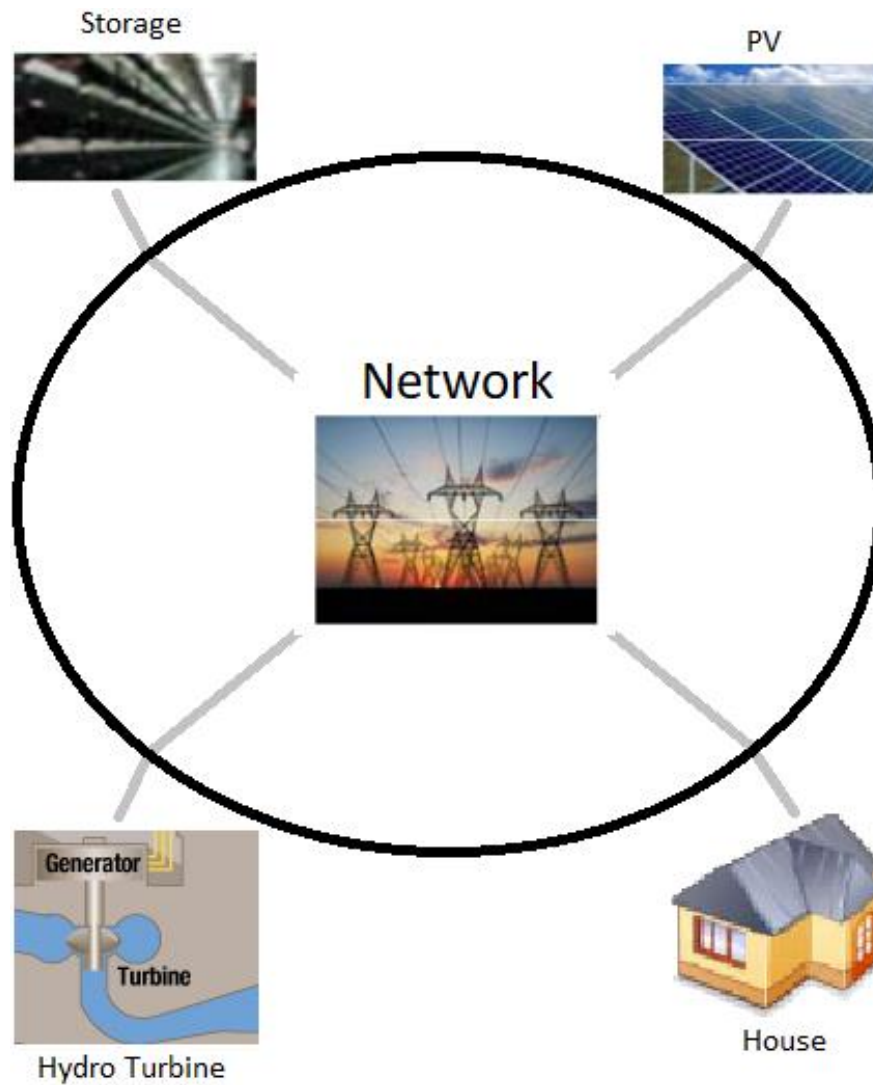
Figure 2.3: Diagram of a microgrid

2.3 Microgrid operation

2.3.1 Operational Modes in Microgrid

There are two main working modes of a microgrid power system. The first is called "grid-connected" mode. When it is connected to the utility grid, the static switch closes all the

feeders that are being equipped by the utility grid, and the Microgrid can then give surplus power to the main grid. Figure 2.4 shows the point of common coupling (PCC) which is the point in the electric circuit where a microgrid is connected to the main grid.
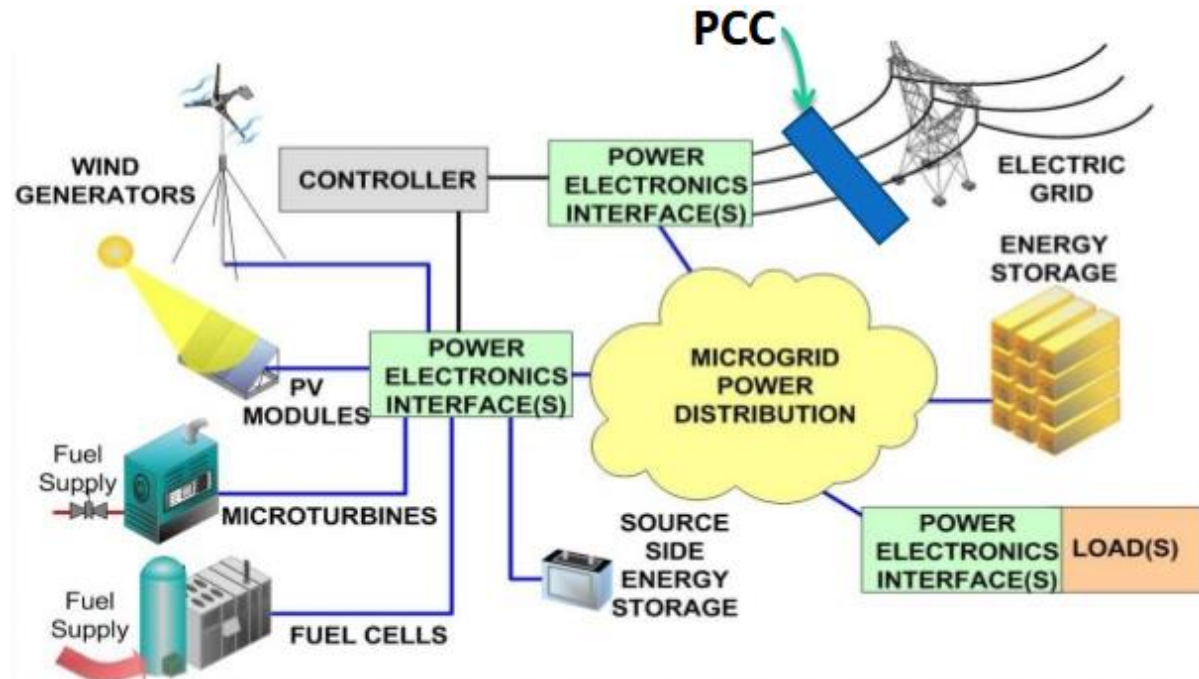
Figure 2.4: Point of common coupling in a microgrid

(Source: https://www.slideshare.net/VipinPandey9/concet-of-microgrid)

The second mode is called "island" mode. The utility grid does not provide power once the static switch is open. The Microgrid can be operating alone preventing power outages once the utility grid isn't obtainable. When a microgrid is operating in island mode the installed power must meet the needs of load. Figure 2.5 presents a microgrid in island mode due to a malfunction of the main grid. The microgrid now operates autonomously, in a similar way to the electric power systems of the physical islands.
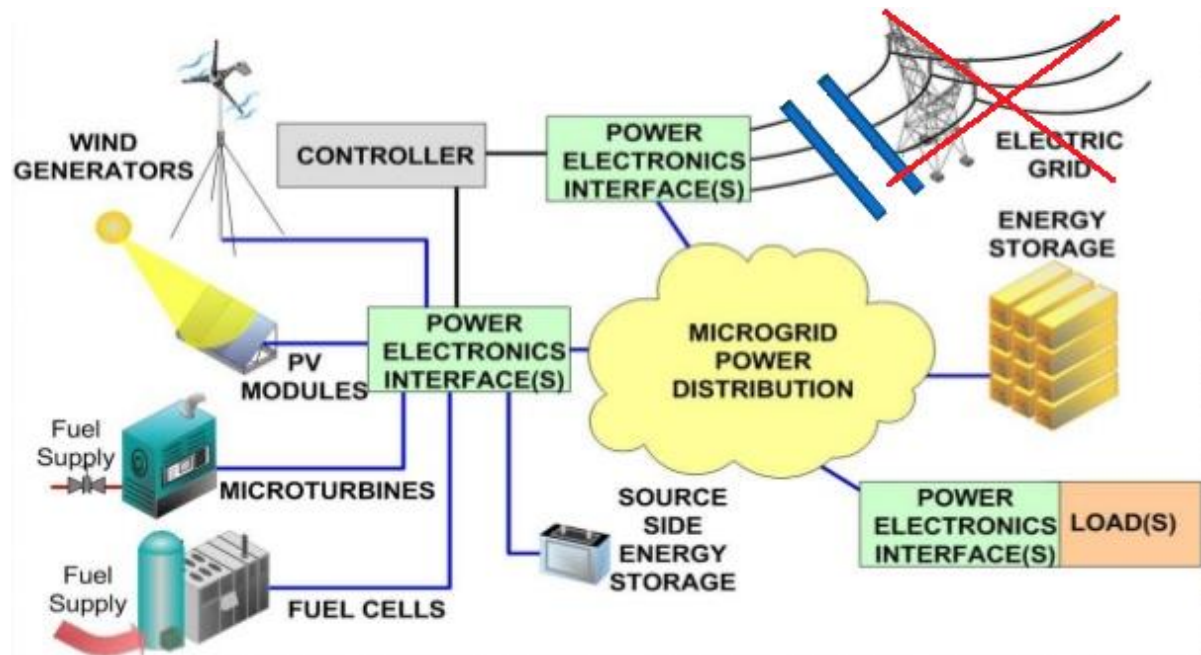
Figure 2.5: Microgrid in island mode.

2.3.2   Microgrid Operational Strategies

In every microgrid there are goals to be achieved, such as technical optimization, economic growth and reduction of any potential harmful environmental impact. Evidently, conflicting interests among different stakeholders involved in electricity supply, such as system/network operators, DG owners, DER operators, energy suppliers, and so on, as well as customers or regulatory bodies may influence the operational strategy of the microgrid towards a specific objective.

The microgrid operational strategies are presented in Figure 2.6.
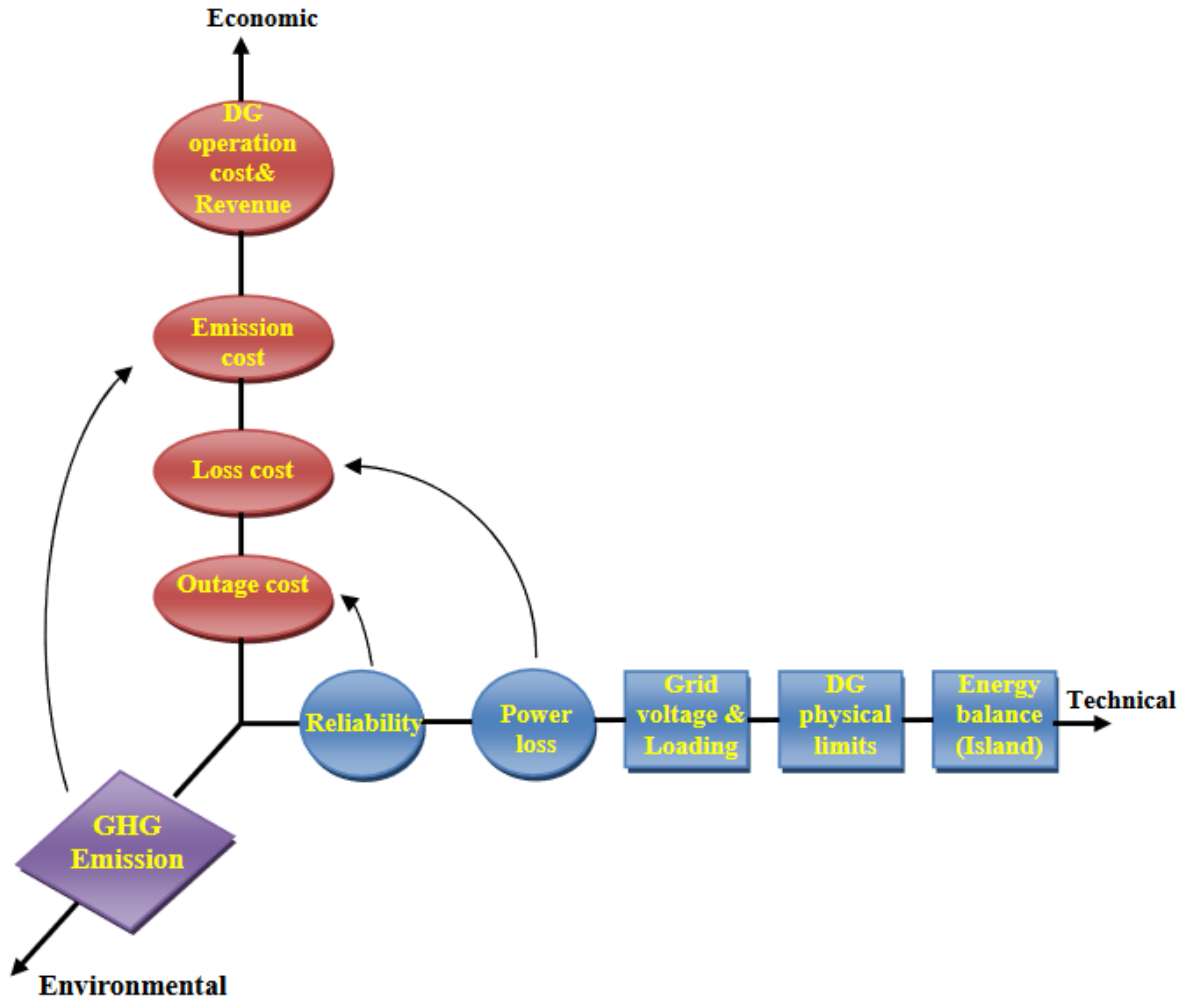
Figure 2.6: Microgrid Operational Strategies

(Source: Ngoc An Luu, Control and management strategies for a microgrid, Electric power.
     Université de Grenoble, 2014)

There are three main operational options and of course the combined objective option.

Firstly, in the economic mode, the objective function is to minimize total costs of DER operation and revenue. This option underestimates lost cost and emission obligations. The constraints are expressed as the physical constraints of DERs and energy balance.

Subsequently, in the technical mode of microgrid operation, the power loss is demonstrated as the objective function. The voltage variation and device loading, DER physical limits and energy balance are the constraints.

Furthermore, the environmental mode of microgrid operation indicates the DER units with lower specific emission levels to be target of choice without taking into consideration the financial or technical aspects. The emission cost is given as the objective of this option.

To conclude, the combined mode solves a multi-objective problem to satisfy all of the economic, technical and environmental aspects. The objective function includes the economic and the economic equivalents of the technical and environmental constraints from the voltage variation and loading, DER physical limits and the balance energy.

2.4   Microgrid Control

A brief description of microgrid control is presented in this part. The objective of this thesis is to analyze the optimal sizing of a microgrid. As a result only basic knowledge of control methods will be described.

A typical microgrid control structure is shown in Figure 2.7. As it is observed, a microgrid control includes Micro Source Controllers (MC), Local Controllers (LC), a Microgrid Central Controller (MGCC) and a Distribution Management System (DMS).
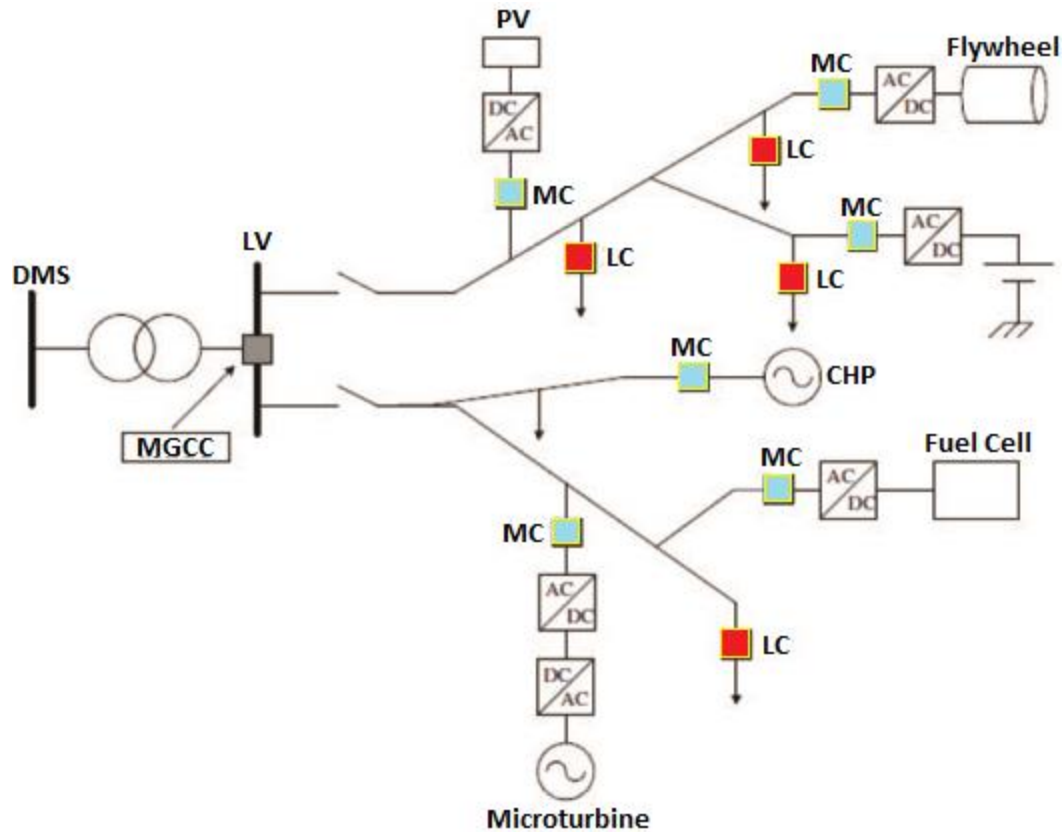
Figure 2.7: A typical microgrid control structure

(Source: http://www.ee.co.za/article/development-renewable-energy-based-mini-micro-
    nano-grids.html)

2.4.1   Microsource Controller

MC is responsible to control and monitor distributed energy resources, storage devices and loads, including electrical vehicles. The power electronic interface of the microsource is used for the microgrid source controller. The local information is measured for controlling the voltage and frequency of the microgrid. The basic configuration of the microsource is shown in Figure 2.8 and includes the microsource, a DC-link (capacitor), DC-AC (grid-side) inverter, a low pass LC filter (which cancels out high order harmonics) and a coupling inductance.
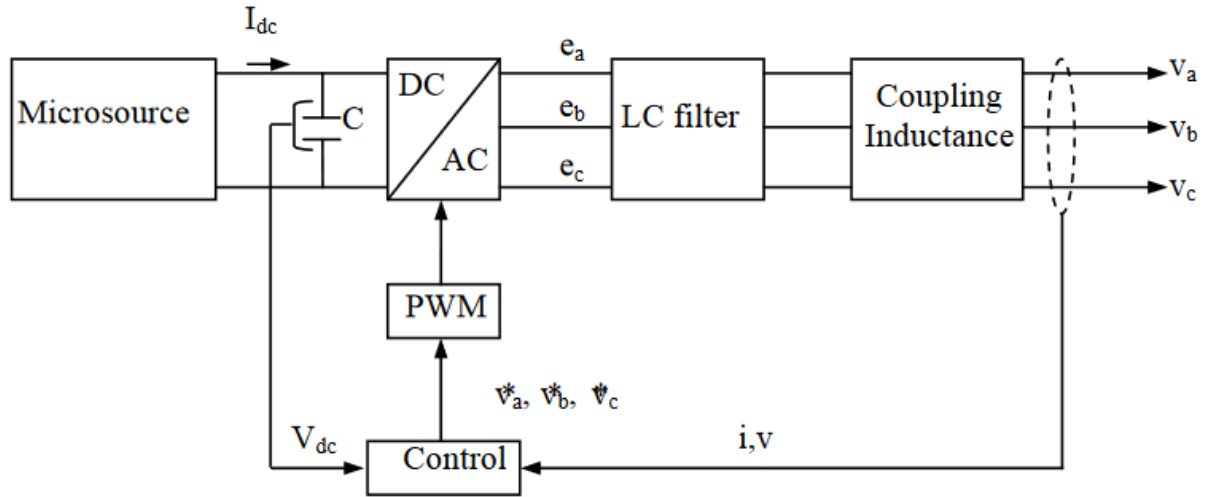
Figure 2.8: The basic configuration of the microsource

(Source: Ngoc An Luu, Control and management strategies for a microgrid, Electric power.
    Université de Grenoble, 2014)

In more detail, inverters connected to the Microgrid could be controlled in two methods. In the first method, the microsources could operate at a particular set of active and reactive power references. This method arguably works reasonably well in the grid connected mode since any short fall or excess could be taken from the utility network. However, local voltage control is not achieved. More importantly, the Microgrid would not operate to control frequency and voltage when the system is isolated from the utility due to generation-demand mismatch. Thus a set reference active and reactive power method is not suitable for use as the only control method of microsources in a Microgrid.

Droop line control is the presently favoured control technique, which can be used to control each inverter independently. In this method, frequency and voltage are given as references. The frequency is varied with output active power and the voltage is varied with reactive power. This method works well with both utility connected and islanded operating modes. Figure 2.9 presents a typical droop line characteristic used for the inverters' control.

(a) Active power – frequency control   (b) Reactive power – voltage control
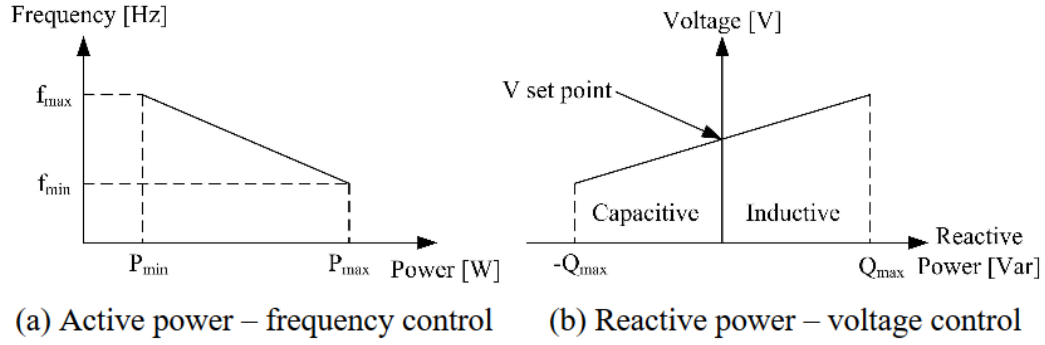
Figure 2.9: Active and reactive power control of a microsource

(Source: https://www.research.manchester.ac.uk/portal/files/54592900/FULL_TEXT.PDF)

2.4.2 Microgrid Central Controller

A Micro-Grid Central Controller (MGCC) is the link between Electrical utility and load through Local controllers. Renewable Energy Resource (RER) and other small power production resources are connected to local Controllers and supply the power to own connected load, so MGCC in addition to controlling the connection to the main grid, manages the controllable loads –for demand reduction and load shedding– and the microsource controllers –for power dispatch, as it can be seen in figure 2.10. It is assumed that the MGCC periodically receives information regarding the consumption/generation levels from the load controllers and microsource controllers, and it also stores information on technical characteristics of the microsources, e.g. active and reactive power limits.

51
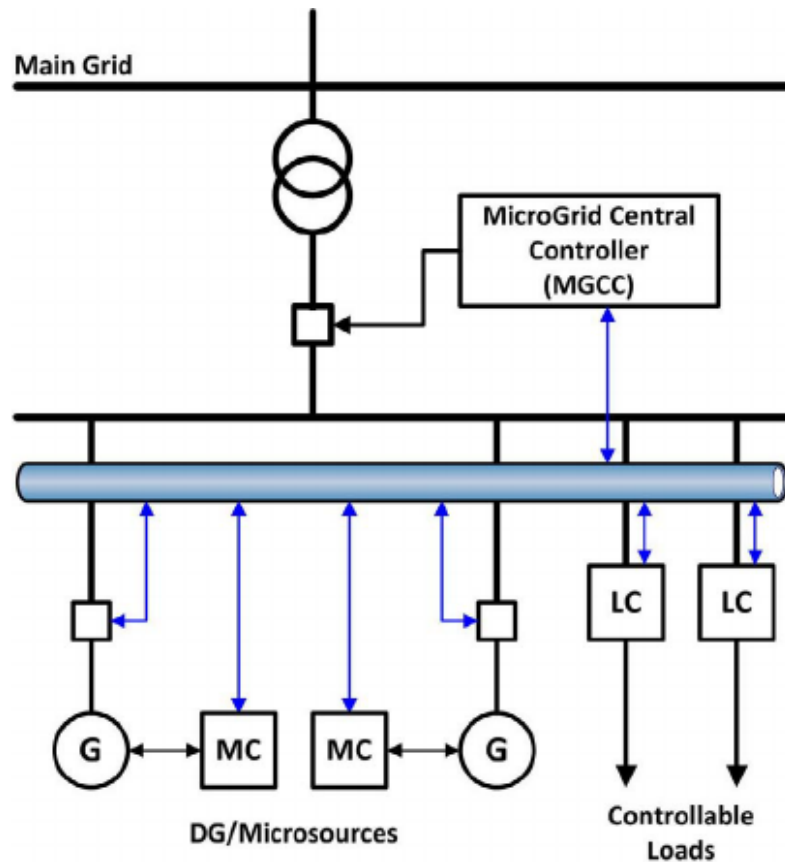
Figure 2.10: Microgrid Central Controller (MGCC)

(Source: https://www.researchgate.net/figure/224233967_fig1_Fig-1-Schematic-diagram-of-
a-typical-microgrid-The-controllable-loads-and-the)

The MGCC is able to provide set-points for the MCs or simply monitor or supervise their operation. Generally, a microgrid can be controlled in a centralized or decentralized fashion.

1. Through the centralized approach, the MGCC can optimize the microgrid's performance depending on the market price (price of electricity, gas and fuel costs) and security constraints. This can be very similar to an economic dispatch process

adopted at the utility level, since the MGCC responsibilities are the maximization of using microgrid value and the optimization of its operation.

2. The decentralized approach, on the other hand, requires decision making based on local information available. This way, the microgrid would act as a combination of autonomous energy agents that operate in such a way that it optimizes their individual objective functions –mostly influenced by the market price. That being said, the overall performance of the microgrid can be improved due to the coherent responsibility of all the MCs (which is to optimize the microsourse, to meet the demand and provide the maximum possible export power to the grid following the current market prices), even if each MC alone isn't able to achieve the maximum revenue of its corresponding unit.

However, the boundary between the centralized and decentralized approach is not definite. It can be imagined that at a centralized approach, some of the decisions are made locally, for instance, demand responsive actions by the controllable loads are subject to the local policies defined. Likewise, a decentralized approach could also provide links between the agents and the MGCC, or links between the neighboring agents for exchange of data and/or commands. With multiple microgrids in the network, the issue of interactions between them and the utility arises. Although microgrids are assumed to be inherently autonomous, it is possible for the utility to establish a hierarchical energy management system to coordinate their actions as seen from the grid's standpoint.

2.4.3   Distribution Management System

The definition of DMS from the IEEE Power and Energy Society (PES) Task Force is provided as follows [29]: "A DMS is a decision support system that is intended to assist the distribution system operators, engineers, technicians, managers, and other personnel in monitoring, controlling, and optimizing the performance of the electric distribution system without jeopardizing the safety of the field workforce and the general public and without jeopardizing the protection of electric distribution assets."

The DMS includes a distribution supervisory control and data acquisition (SCADA) system and various advanced applications such as an advanced metering infrastructure, an outage management system (OMS), and a geographic information system. A typical DMS is illustrated in Figure 2.11.
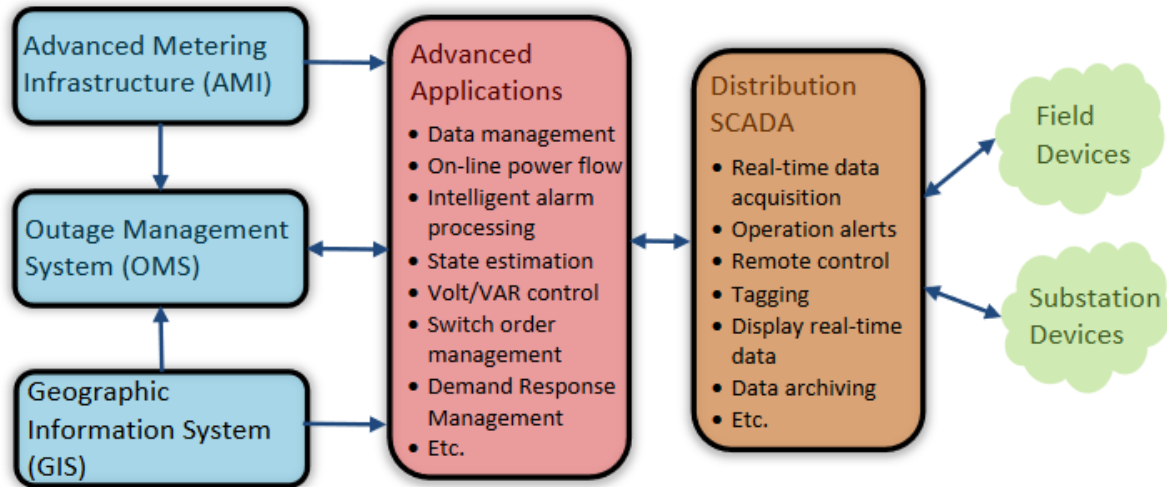
Figure 2.11: A typical Distribution Management System (DMS)

(Source: http://info.ornl.gov/sites/publications/files/Pub68309.pdf)

The main control functionalities of DMS are the participation of the market, the decision for island/interconnected (grid-connected) mode and the upstream coordination.

2.5 Microgrid Protection

With the microgrid connected to a network, the structure of the traditional radial distribution network has been broken to become a multiple-source system that challenges traditional protection schemes. Moreover, it is impossible for traditional protection schemes to protect a microgrid in islanded mode. Therefore, innovative protection for network with grid-connected microgrid and the microgrid in islanded mode should be explored. The protection

system should ensure the stable operation of both Microgrid and utility network. Any fault within the Microgrid should be dealt with internally and the utility should not view the fault. In case of a fault in the utility network, the Microgrid may be disconnected from the utility to ensure stable operation within the Microgrid.

A suitable scheme to protect the micro-grid should be able to respond to both utility grid and micro-grid fault incidents. Over the last few years, numerous schemes for the protection of micro-grids have been devised and reported as shown in Figure 2.12.
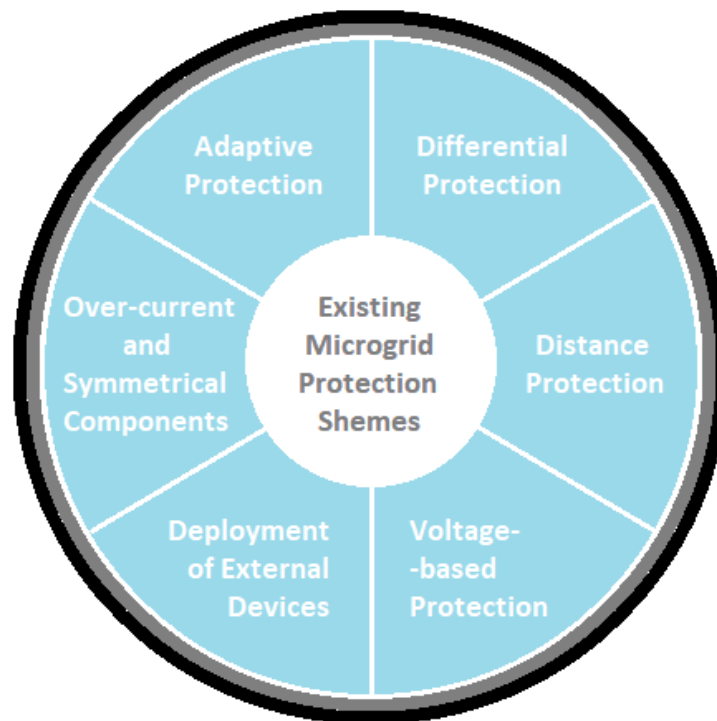
Figure 2.12: Existing Microgrid Protection Shemes

1. Adaptive protection schemes: An Adaptive protection scheme could solve problems arising from both modes of grid connected and islanded operation. In this protection scheme, automatic readjustment of relay settings would trigger when the microgrid changes from the grid connected mode to the islanded mode or vice versa. It is an online system that could modify the preferred protective response to change under

system conditions or requirements in a timely manner through external generated signals or control actions.

2. Differential protection schemes: Differential protection compares the currents that enter and leave a protected zone and will only operate when the differential between these currents exceeds a pre-determined magnitude.

3. Distance protection schemes: The impedance of a line is proportional to its length, thus it is appropriate to use a relay that can measure the impedance of a line up to a predetermined point (the reach point) for distance measurement. Such a relay is called a distance relay and it is designed to operate only for faults that occur between the location of the relay and the selected reach point.

4. Voltage-based protection schemes: Substantially, voltage-based protection techniques employ voltage measurements in protecting the microgrids against different kinds of faults.

5. Protection schemes with the deployment of external devices: As stated earlier, the challenge faced in micro-grid protection is associated with the huge difference between the fault current level in the grid-connected mode and the autonomous mode. Hence, it is imperative to implement an adequate protection scheme which is able to operate suitably in both grid-connected and autonomous modes. Substantially, these protection schemes are based on modification of the short-circuit level when the microgrid operation mode changes from grid-connected to autonomous, or vice versa. These devices can be classified into the following two groups: (a.) Fault Current Limiters (FCLs) can be employed to reduce the aggregated contribution of many distributed generation units, and it is capable of adequately changing the short circuit current level to exceed the design limit of different equipment components. (b.) Energy storage devices can be used to provide supplementary short-circuit level to the network such as flywheels and batteries, due to the fact that the short circuit current level in the microgrid is limited to approximately 2–3 times of the rated current because of the existence of inverter-based DGs.

6. Protection schemes based on over-current and symmetrical components: These protection strategies evolved mainly from the current symmetrical components

analysis and they attempt to improve the conventional over-current protection performance and provide a robust microgrid protection system.

The purpose of a microgrid is to meet the reliability and power quality needed by the customers. Nevertheless, some significant challenges are faced in the emergence of micro-grids and protection of a microgrid and its entity is among them. One major relevant challenge to microgrid protection is to find an effective protection strategy for both grid-connected and islanded mode of operation. In the past few decades, various strategies have been introduced to provide adequate protection for microgrids. A robust protection scheme should have the capability to protect the micro-grid against all kinds of faults and provide assured safe and secure operation in both grid-connected and autonomous mode.

CHAPTER 3.   MATHEMATICAL MODELING OF MICROGRID COMPONENTS

3.1   Introduction

In this chapter, the model of each component within the microgrid is illustrated. An archetypical micro-grid is considered in this thesis, that of a Hydro-PV-BESS hybrid system which includes photovoltaic power generation, hydro turbine generation, and energy storage. Without loss of generality, the sum of the photovoltaic power generators, hydro turbine power generators or energy storage systems is equivalently regarded as one PV system, one hydro system or one storage system respectively. The presented microgrid includes the above systems, and the load to be covered. In each system, one will concentrate on presenting the mathematical model, which is designed to apply for optimal sizing of a microgrid and is described in chapter 5.

3.2   Photovoltaic System Modeling

3.2.1   Photovoltaic Module

A single PV cell is a thin semiconductor wafer made of two layers of highly purified silicon (PV cells can be made of many different semiconductors but crystalline silicon is the most widely used). This PV cell converts sunlight into direct (DC) electricity. The amount of current is determined by the number of electrons that the solar photons knock off. Bigger cells, more efficient cells, or cells exposed to more intense sunlight will deliver more electrons. A PV module consists of many PV cells connected together. The module is encapsulated with tempered glass (or some other transparent material) on the front surface, and with a protective and waterproof material on the back surface. PV panels include one or more PV modules assembled as a pre-wired, field-installable unit. A PV array is the complete power-generating unit, consisting of any number of PV modules and panels. In Figure 3.1 the development of PV from cell to array is presented.
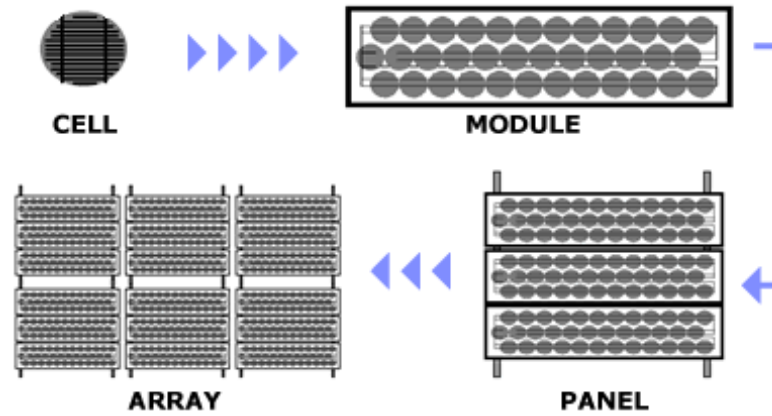
Figure 3.1: Photovoltaics: From Cell to Array

(Source: http://www.solardirect.com/pv/pvlist/pvlist.htm)

Currently, there are four possible structure topologies of the inverters: (a) module, (b) string, (c) multi-string, and (d) central inverter. Structure topologies with the type of supply system are shown in Figure 3.2.
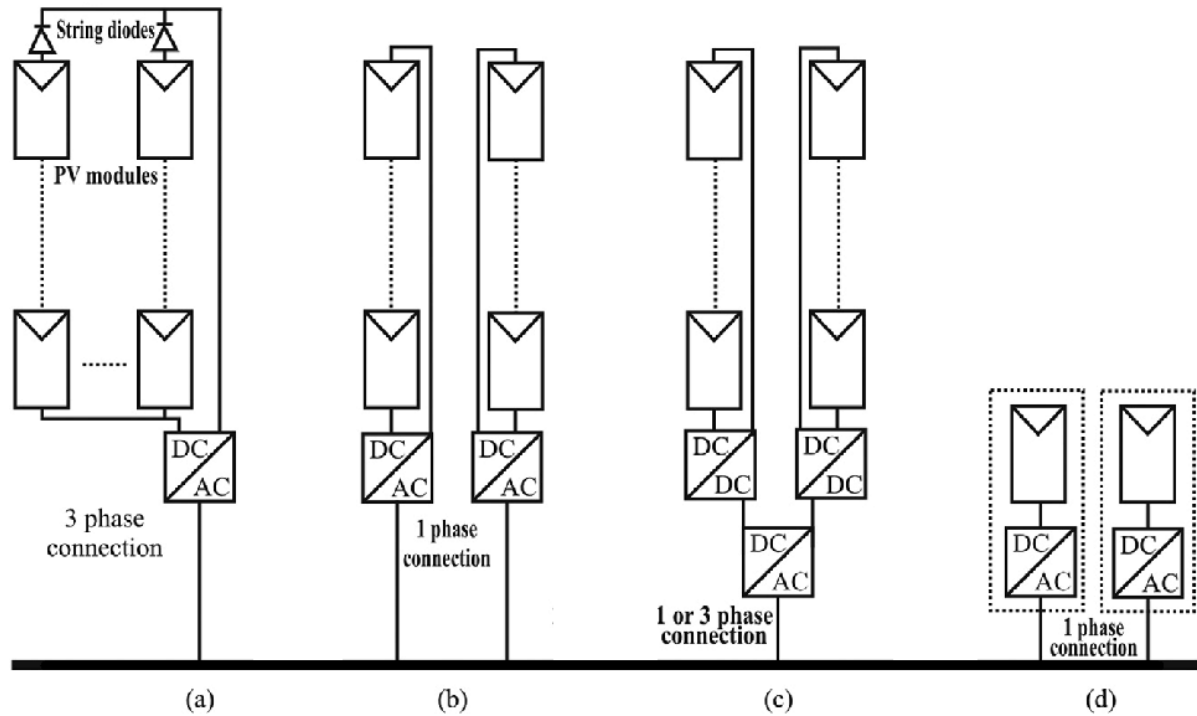
Figure 3.2: Types of grid-tied PV inverters (a) central, (b) string, (c) multi-string and (d) module inverter

(Source:https://www.researchgate.net/publication/308415753_Comprehensive_Overview_of
_Grid_Interfaced_Solar_Photovoltaic_Systems)

A centralized inverter topology (a) is based on a central inverter that interfaces a large PV array to the utility grid. The array consists of PV modules divided into series connections known as strings to generate high voltage. These strings are connected in parallel, through string diodes, to generate high powers of 10–250kW.

In the string inverter system (b) a single PV string is coupled to an inverter. The input voltage may be high enough to avoid voltage amplification. This topology has the minimum losses due to which it has the advantage of increased energy yield and enhances the supply reliability.

The multi-string inverter (c) is the further development of the string inverter. In this type of topology, several strings are interfaced with their own DC-DC converter to a common DC-AC inverter. Every string can be controlled individually. The application area of the multi-string inverter covers PV plants of 3–10kW.

In the module integrated inverter system (d), where an AC module consisting of a single solar PV panel and its own inverter is connected to the utility grid. It removes the mismatch losses between PV modules, as well as supports optimal adjustment between the PV module and the inverter.

3.2.2   Photovoltaic System Modeling

In order to model a simpler photovoltaic system, one will need a current source and its power (P/Q) control. This control causes the output active and reactive power to follow the set-point value of P_{sp} and Q_{sp}, respectively. The maximum power point tracker (MPPT) regulates the value of P_{sp} and Q_{sp} is zero. [9] In figure 3.3 the operation of this model is presented as follows.
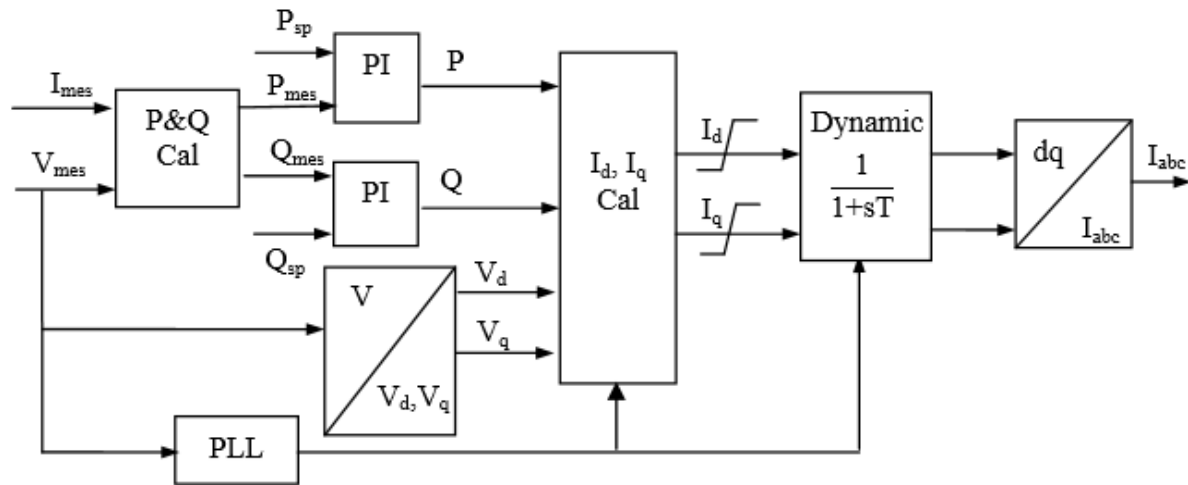
Figure 3.3: Photovoltaic system with power electronic interface – P/Q control

(Source: https://hal.archives-ouvertes.fr/tel-01144941v2/document)

- Block: P&Q Cal

The information of instantaneous values of line-to-line voltages and line currents is required to calculate the values of active and reactive power. The equations are presented below [30]:

$$P_{mes} = V_{bc}i_c - V_{ab}i_a$$

$$Q_{mes} = \frac{V_{bc}(2i_a + i_b) + V_{ca}(2i_b + i_a)}{\sqrt{3}}$$

- Block: V / V_d, V_q

The voltage magnitude component converts the voltage from Polar to Cartesian [30]:

$$V_d = \frac{V_c - V_b}{\sqrt{3}}$$

$$V_q = \frac{2}{3}\left(V_a - \frac{1}{2}V_b - \frac{1}{2}V_c\right)$$

- Block: I_d, I_q

The direct and quadratic currents are determined as follows:

$$I_d = \frac{2}{3}\frac{\left(P.V_d + Q.V_q\right)}{\left(V_d^2 + V_q^2\right)}$$

$$I_q = \frac{2}{3}\frac{\left(P.V_q - Q.V_d\right)}{\left(V_d^2 + V_q^2\right)}$$

–   Block: PI

The two proportional integral (PI) blocks help to adjust the active and reactive power at their reference value. The coefficient k_i and k_p are calculated with the help of a loop control of active power, as shown in figure 3.4.
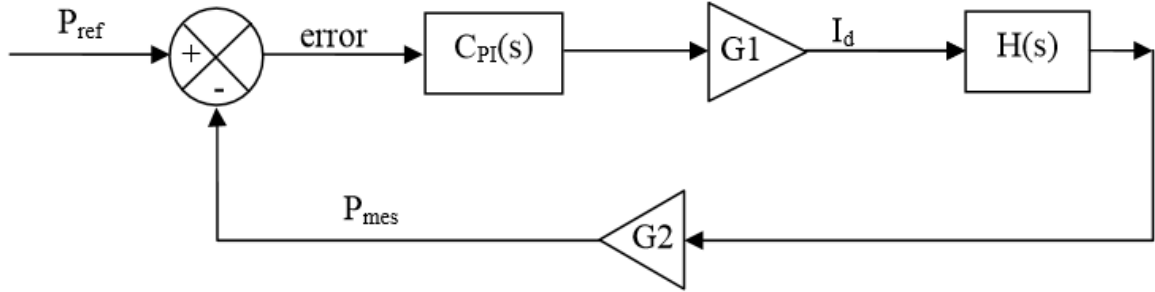
Figure 3.4: Control loop for active control

(Source: https://hal.archives-ouvertes.fr/tel-01144941v2/document)

The transfer functions G1 and G2 are calculated from the equations of the direct and quadratic currents above, with V_d constant and V_q equal to zero. G1 and G2 are presented below [31]:

$$G_1 = \frac{2}{3V_d}$$

$$G_2 = \frac{3}{2}V_d I_d$$

The transfer function H(s) of the dynamic block (figure 3.4) is expressed as follows:

$$H(s) = \frac{1}{1 + \tau s}$$

Lastly, the two-order transfer function of the loop control is presented below:

$$K(s) = \frac{N(s)}{1 + \frac{2\xi}{\omega_n}s + \frac{1}{\omega_n^2}s^2} = \frac{C_{PI}(s)G_1H(s)}{1 + C_{PI}(s)G_1G_2H(s)} = \frac{G_1(k_ps + k_i)}{1 + \frac{G_1G_2k_p + 1}{G_1G_2k_i}s + \frac{\tau}{G_1G_2k_i}s^2}$$

Thus,

$$\frac{2\xi}{\omega_n} = \frac{G_1G_2k_p + 1}{G_1G_2k_i}$$

And

$$\frac{1}{\omega_n^2} = \frac{\tau}{G_1G_2k_i}$$

While $\omega_n = \frac{1}{\tau}$ and $\xi < 1$, the coefficient k_i, k_p are calculated as follows [31]:

$$k_i = \omega_n$$

$$k_p = 2\xi - 1$$

Similar to the loop for reactive power, the same results are obtained with both the correction coefficients.

3.3 Electrochemical storage Modeling

Electrochemical capacitors are sometimes also referred to as "supercapacitors" or "ultracapacitors". There are three types of electrochemical storage: rechargeable battery, flow battery and Ultrabattery. In this thesis, rechargeable batteries are used. Common rechargeable battery chemistries include:

- Lead-acid battery
- Nickel-cadmium battery (NiCd)
- Nickel-metal hydride battery (NiMH)
- Lithium-ion battery
- Lithium-ion polymer battery.

The typical charge and discharge voltammetry characteristics of an electrochemical capacitor are presented below, in figure 3.5.
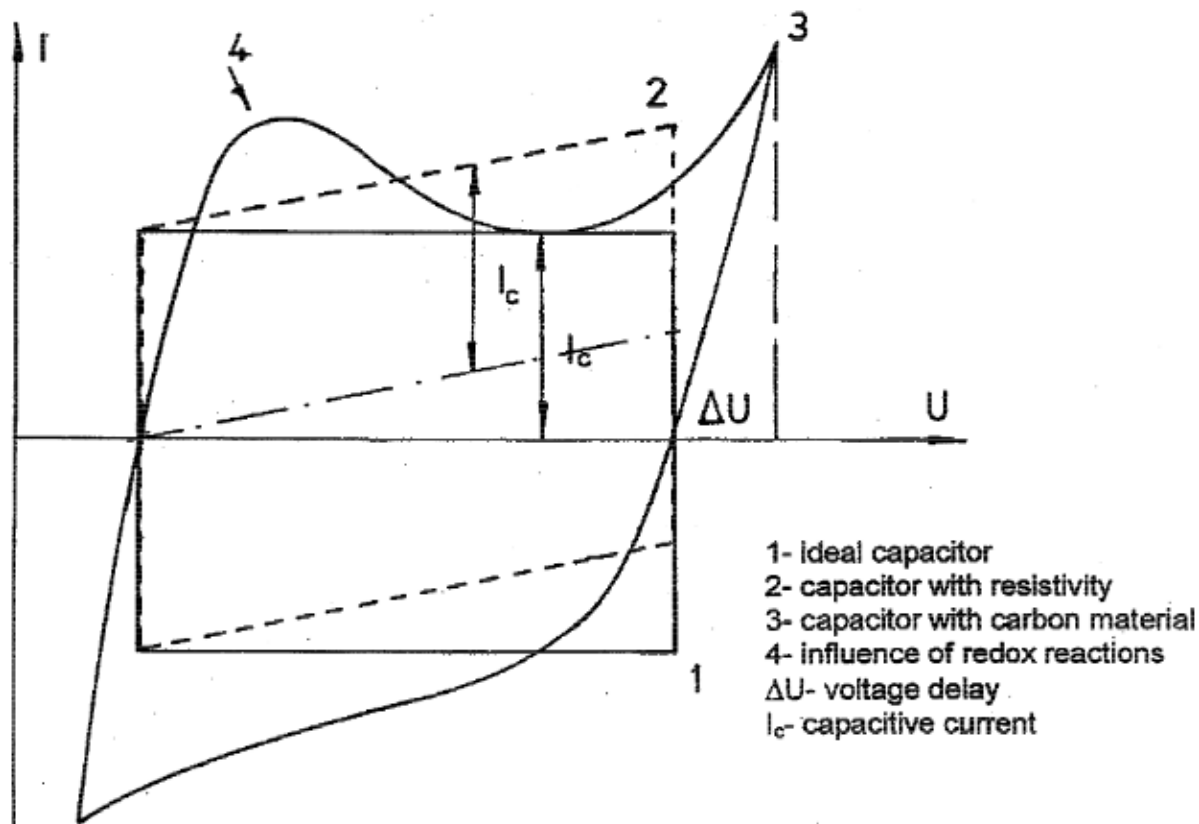
Figure 3.5: Typical charge/discharge voltammetry characteristics of an electrochemical capacitor

(Source: Carbon materials for the electrochemical storage of energy in capacitors, Elzbieta Frachowiak, Francois Beguin)

3.3.1 Battery parameters

– Voltage Estimation

Battery voltage is related to the sum of reduction and oxidation potentials. Electrical energy is produced when the chemicals in the battery react with one another. The rate of the chemical reaction varies with the following conditions [32]:

1. State of charge
2. Battery storage capacity
3. Rate of charge/discharge
4. Environmental temperature
5. Age/Shelf life.

There have been many proposals for lead-acid battery models. In figure 3.6 one of them is presented, the Thevenin equivalent circuit, which is a simple way of demonstrating the behaviour of battery voltage (V_b). This circuit contains the electrical values of no-load voltage (V_{oc}), internal resistance (R_1) and overvoltage (parallel combination of C and R_2), as constants, so one must consider that this is not a realistic model.
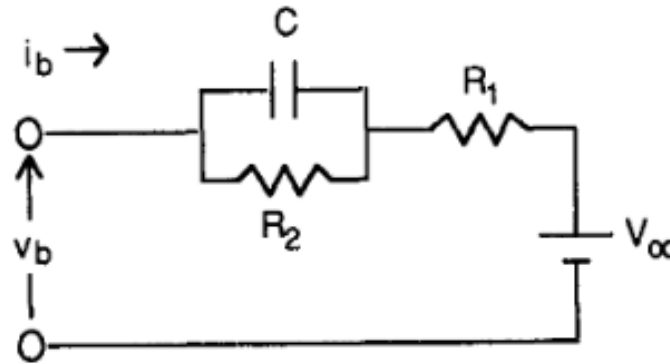
Figure 3.6: Thevenin Battery Model

(Source: A Mathematical Model for Lead-Acid Batteries, Ziyad M. Salameh, Margaret A.
Casacca, William A. Lynch, University of Lowell)

Another approach calculates voltage through charge/reset and during the discharge period from experimental results carried out at the INES institute [33]:

- If $I_{Bat} \geq 0$ (Charge/reset)

$$V_{Bat}(t) = (12{,}94 + 1{,}46 SOC(t))N_{Bat}$$

- If $I_{Bat} \leq 0$ (Discharge)

$$V_{Bat}(t) = \left(12{,}13 - 1{,}54(1 - SOC(t))\right) N_{Bat}$$

Where,

$V_{Bat}(t)$: Battery Voltage at time t,

SOC(t): State Of Charge at time t,

N_{Bat}: 12V batteries number connected in series.

    –   Charge Level Estimation

State Of Charge (SOC) is the percentage of capacity or energy with which a battery is charged at a given time and is calculated as follows:

$$SOC = \frac{C(t)}{C_{ref}}$$

Where,

C(t): the capacity of the batteries at each instant,

C_{ref}: the reference capacity.

C(t) is estimated as presented below:

$$C(t) = Q(t_o) + Q_c(t) + Q_d(t)$$

Where,

$Q(t_0)$: the initial quantity of charge,

$Q_c(t)$: the quantity of charge exchange during the charge,

$Q_d(t)$: the quantity of charge exchange during the discharge.

Conversely, the Depth Of Discharge (DOD) is the percentage of capacity or energy at which the battery is discharged.

   – State Of Health

The State Of Health (SOH) of batteries is defined as follows [34]:

$$SOH = \frac{C_{ref}(t)}{C_{ref,nom}}$$

Where,

C_{ref}(t): the new capacity reference at each time t,

$C_{ref,nom}$: the nominal capacity of reference available from the manufacturer data.

C_{ref}(t) is calculated as presented below:

$$C_{ref}(t) = C_{ref}(t - \Delta t) - \Delta C_{ref}(t)$$

Where,

ΔC_{ref}(t): the capacity loses at each time t.

The capacity loses ΔC_{ref}(t) is estimated as follows:

$$\Delta C_{ref}(t) = C_{ref,nom} Z(SOC(t - \Delta t) - SOC(t))$$

Where,

Z: linear ageing coefficient.

From all the above equations the SOH can be expressed as presented below:

$$SOH(t) = \frac{C_{ref}(t - \Delta t)}{C_{ref,nom}} - Z(SOC(t - \Delta t) - SOC(t))$$
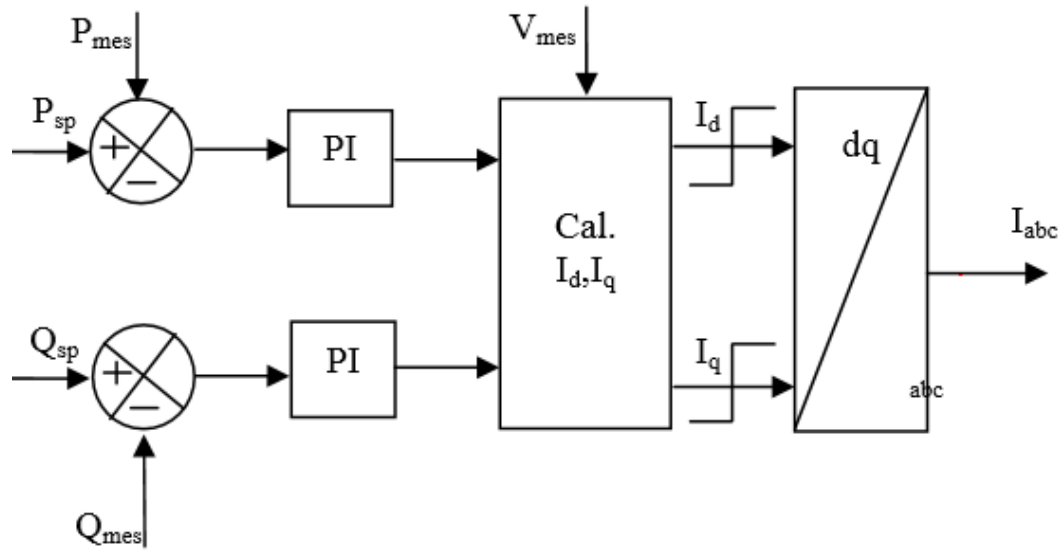
Figure 3.7: Battery model with power electronic interface – P/Q control

(Source: https://hal.archives-ouvertes.fr/tel-01144941v2/document)

The BESS (Battery Energy Storage System) is connected to the grid via a power electronic interface which the power can be fed into or taken from the grid directly. In figure 3.7 the P/Q control is presented. The P_{sp} and Q_{sp} are given as input of this control.

3.4   Hydroelectric System Modeling

Modern hydro plants produce electricity using turbines and generators, where mechanical energy is created when moving water spin rotors on a turbine. This turbine is connected to an electromagnetic generator, which produce electricity when the turbine spins.

3.4.1 Types of Hydropower plants

There are three main types of hydro plants:

1. Impoundment facilities are the most common technology which uses a dam to create a large reservoir of water. Electricity is made when water passes through turbines in the dam.
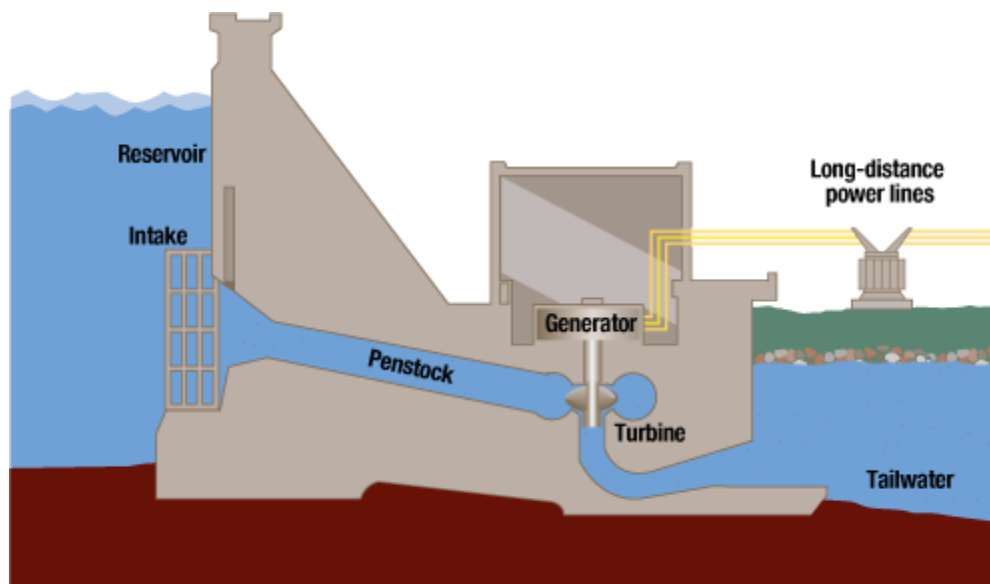
Figure 3.8: Hydroelectric Dam Diagram

(Source: https://www.e-education.psu.edu/earth104/node/1067)

2. Pumped storage facilities are similar but have a second reservoir below the dam. Water can be pumped from the lower reservoir to the upper reservoir, storing energy for use at a later time.
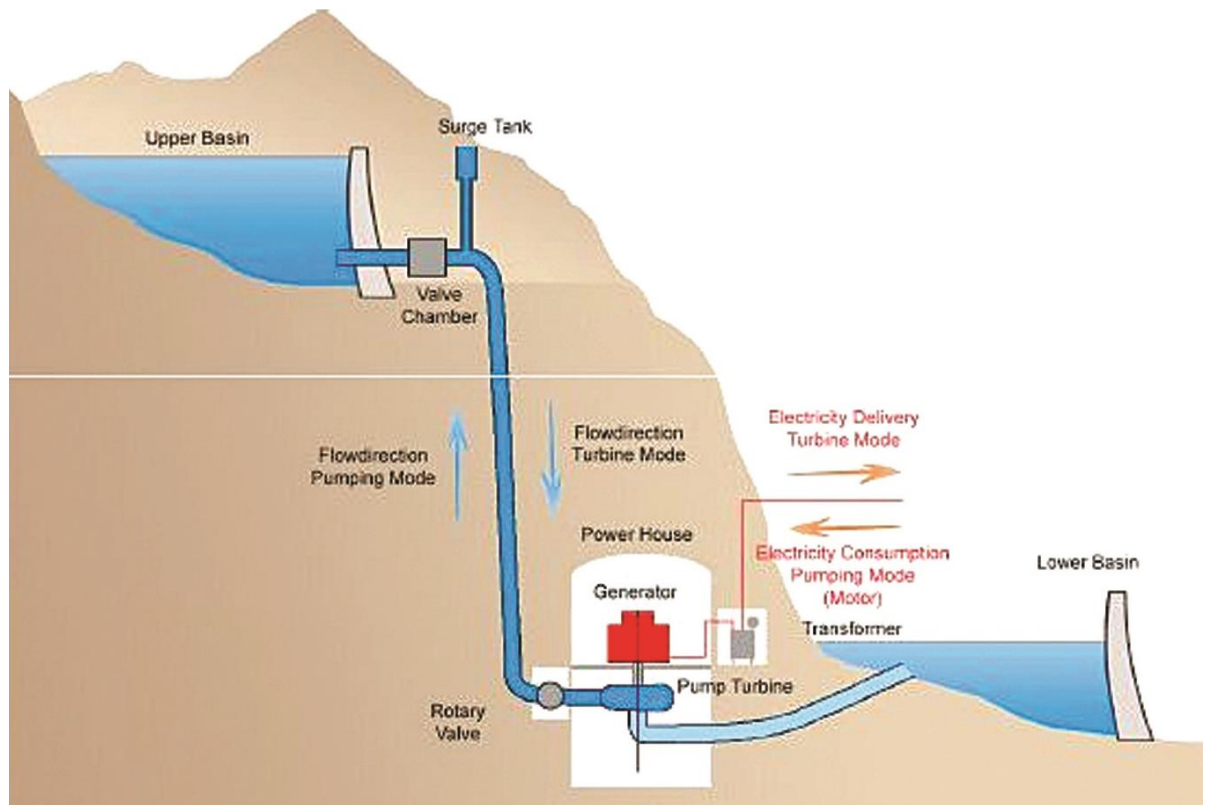
Figure 3.9: Pumped hydroelectric storage system

(Source: http://www.nwhydro.org/events-committees/pumped-storage-workshop/)

3. Run-of-river facilities rely more on natural water flow rates, diverting just a portion of river water through turbines, sometimes without the use of a dam or reservoirs. Since run-of-river hydro is subject to natural water variability, it is more intermittent than dammed hydro.

In more detail, run-of-the-river hydroelectricity (ROR) or run-of-river hydroelectricity is a type of hydroelectric generation plant whereby little or no water storage is provided. Run-of-the-river power plants may have no water storage at all or a limited amount of storage, in

which case the storage reservoir is referred to as pondage. A plant without pondage has no water storage and is, therefore, subject to seasonal river flows. Thus, the plant will operate as an intermittent energy source while a plant with pondage can regulate the water flow at all times and can serve as a peaking power plant (power plants that generally run only when there is a high demand) or base load power plant (energy station devoted to the production of base load supply).

ROR hydroelectricity is considered ideal for streams or rivers that can sustain a minimum flow or those regulated by a lake or reservoir upstream. A small dam is usually built to create a headpond ensuring that there is enough water entering the penstock pipes that lead to the turbines which are at a lower elevation. Projects with pondage, as opposed to those without pondage, can store water for daily load demands. In general, projects divert some or most of a river's flow (up to 95% of mean annual discharge) through a pipe and/or tunnel leading to electricity-generating turbines, then return the water back to the river downstream.

ROR projects do not have most of the disadvantages associated with dams and reservoirs, which is why they are often considered environmentally friendly. Substantial flooding of the upper part of the river is not required for run-of-river projects as a large reservoir is not required. As a result, people living at or near the river don't need to be relocated and natural habitats and productive farmlands are not wiped out. In addition, a ROR power plant can be operated where larger forms of hydroelectric structures with reservoirs etc. may not be feasible. For example, a small floating power plant uses no or only minimal land beside rivers, which makes it perfect for small islands with a river.
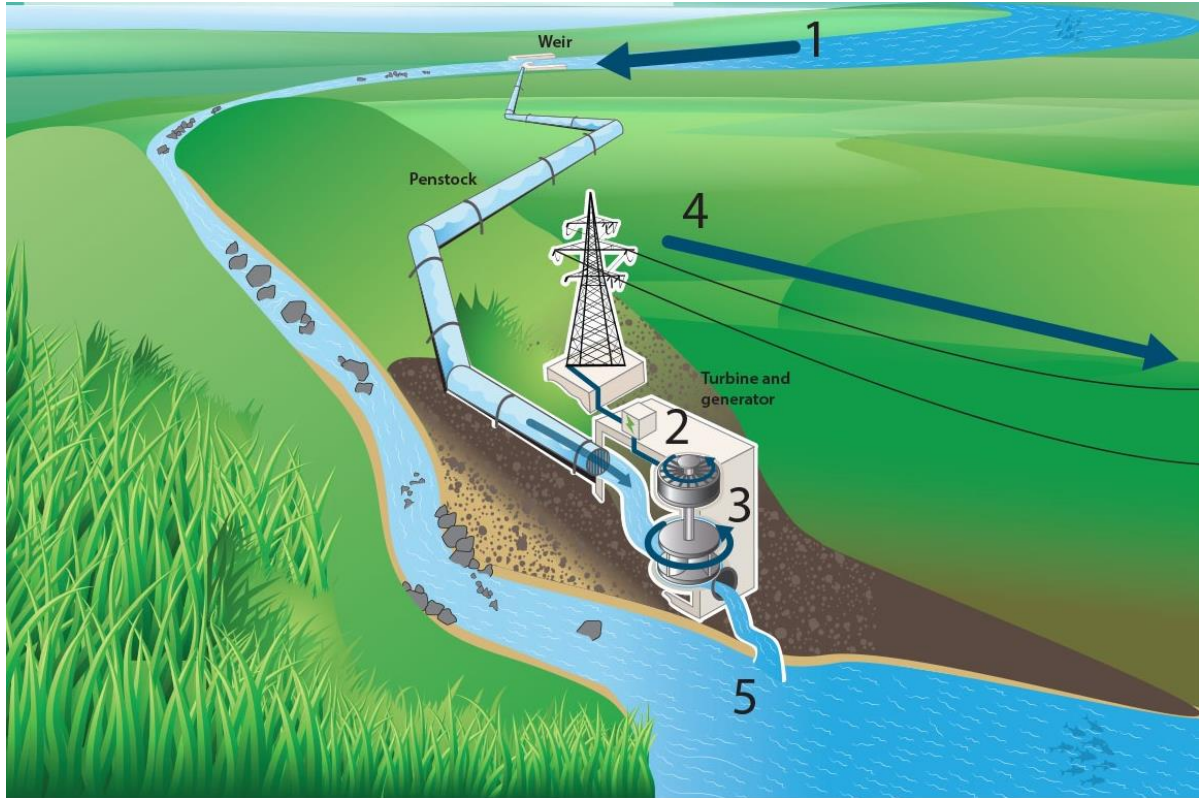
Figure 3.10: Run-of-the-river Hydropower plant

(Source: http://ruahaenergy.com/hydro/)

As it can be seen from the Figure 3.10 a portion of the flow is been channeled in the penstock (1) and through the penstock to the turbine (3). The turbine is connected to a generator (2) to produce electricity, which afterwards gives it back to the network (4). Finally, the flow of the river is been restored (5).

3.4.2   Model formulation of RoR Hydropower plant

The run-of-river system is considered as a shallow river to be able to be transformed in equations in order to produce its mathematical model. To create a model of the shallow river

system, the Saint-Venant equations will be used. These equations describe the behaviour of the river and consist of both mass and momentum balances, and are solved using the Finite Volume method with staggered grid [35].

The fact that the RoR system is considered as a shallow river means that the water level and width of the river is much smaller than the length of the river, and the slope of the river is not too steep. This also means that the depth of the river has little variation. In this case the Hydrostatic pressure approximation can replace the vertical variation of the water motion, and the flow velocity is approximated by the depth-average flow velocity [36]. Another assumption is that the fluid (water of the river) is incompressible and the streamline curvature is small. It is important to mention that only gravity force is taken into consideration. The effect of friction in the penstock can be estimated with formulas related to steady flow (as the Manning Formula or the Chezy Formula).

The discretization of the Saint-Venant equations for the mass Balance with Finite Volume method results in [37]:

$$\frac{dh_i}{dt} = \frac{\dot{V}_{i-1} - \dot{V}_{i+1}}{w \cdot \Delta x} + \frac{\dot{V}'_i}{w} \quad , \qquad i = 3, 5, \dots, 2N_{\dot{V}} - 1$$

Where

h_i: the water level along the river, where i = 1, 3, …, 2N$_{\dot{v}}$+1,

$\dot{V}_i$: the volumetric flow rate along the river, where i = 2, 4, …, 2N$_{\dot{v}}$,

w: width of the river,

Δx: length of each segment of volumetric flow,

$\dot{V}'_i$: lateral inflow per length unit, where i=1,3,…, 2N$_{\dot{v}}$+1,

N$_{\dot{V}}$: momentum balance/volumetric flows.

For i=1 the previews equation will be as follows:

$$\frac{dh_1}{dt} = \frac{\dot{V}_{in} - \dot{V}_2}{w \cdot \frac{\Delta x}{2}} + \frac{\dot{V}'_1}{w}$$

Where

$\dot{V}_{in}$: inlet volumetric flow rate.

For i=2 N_V+1 the previews equation will be as follows:

$$\frac{dh_{2N_V+1}}{dt} = \frac{\dot{V}_{2N_V} - \dot{V}_{out}}{w \cdot \frac{\Delta x}{2}} + \frac{\dot{V}'_{2N_V+1}}{w}$$

Where

$\dot{V}_{out}$: outlet volumetric flow rate.

The discretization of the Saint-Venant equations for the momentum balance with Finite Volume method results in [35]:

$$\frac{d\dot{V}_i}{dt} = \frac{\frac{\dot{M}_{i,i}}{\rho} - \frac{\dot{M}_{o,i}}{\rho}}{\Delta x} + g \cdot \cos\theta \cdot w \cdot \frac{h_{i-1}^2 - h_{i+1}^2}{2\Delta x} + \bar{A}_i \cdot g \cdot \sin\theta - \frac{g}{C_i^2} \frac{\bar{\varphi}_i}{A_i^2} |\dot{V}_i| \dot{V}_i$$

for i = 2, 4, …, 2N$_{\dot{V}}$, where:

76

ρ: density of water,

θ: angle of river slope,

g: the gravitational acceleration,

cross sectional area A and wetted perimeter φ and their averages between neighboring segments, $\bar{A}$ and $\bar{\varphi}$ respectively, are defined as follows:

$$A_i = w \cdot h_i$$

$$\varphi_i = w \cdot 2h_i$$

$$\bar{h_\iota} = \frac{h_{i-1} + h_{i+1}}{2}$$

$$\bar{A_\iota} = \bar{h_\iota} \cdot w$$

$$\bar{\varphi_\iota} = \frac{\varphi_{i-1} + \varphi_{i+1}}{2}$$

Also, the Chezy friction coefficient C is defined in relation to Strickler's friction factor k_s as presented below:

$$C_i = k_s \cdot R_i^{\frac{1}{6}}$$

Where R_i is the hydraulic radius and is defined as:

$$R_i = \frac{A_i}{\varphi_i}$$

Lastly, the momentum input and output flow per density ($M_{i,i}$ and $M_{o,i}$ respectively) are presented below:

$$\frac{\dot{M}_{i,i}}{\rho} = \begin{cases} \dfrac{\dot{V}_{in}}{A_1}, & i = 2 \\[2ex] \dfrac{\left|\dot{V}_{i-2}\right|}{\bar{A}_{i-2}} \cdot \max(\dot{V}_{i-2}, 0) + \dfrac{\left|\dot{V}_{i+2}\right|}{\bar{A}_{i+2}} \cdot \max(-\dot{V}_{i+2}, 0), & i = 4,6,\dots,2N_{\dot{V}} - 2 \\[2ex] \dfrac{\left|\dot{V}_{2N_{\dot{V}}-2}\right|}{\bar{A}_{i-2}} \cdot \max\left(\dot{V}_{2N_{\dot{V}}-2}, 0\right), & i = 2N_{\dot{V}} \end{cases}$$

and,

$$\frac{\dot{M}_{o,i}}{\rho} = \begin{cases} \dfrac{\dot{V}_i^2}{\bar{A}_i}, & i = 2,4,6,\dots,2N_{\dot{V}} - 2 \\[2ex] \dfrac{\dot{V}_{out}}{A_{2N_{\dot{V}}+1}}, & i = 2N_{\dot{V}} \end{cases}$$

CHAPTER 4. THESIS RESOURCES AND MATERIAL FROM CORVO ISLAND

4.1 Introduction

The data needed in this research is gathered from island Corvo in Portugal, northernmost island of the Azores archipelago (located in the north Atlantic ocean, about 2 hours from Europe and 5 from North America) assuming there is a similar island in Greece, in order to solve a realistic model with the existing constraints of Greece. Corvo island is located at a latitude of 39,7° N, with an area of only 17.1 km^2, about 6 km long and 4 km wide, with a population of approximately 512 inhabitants (in 2011).

Tables 4.1 and 4.2 show the kind of data that were used to develop this thesis.

Table 4.1 - Load Demand Dataset

NAME	CorvoLoadAverage
DATA	Load
TIME FRAME	Per hour, Average per year
PERIOD	1999-2010
PLACE	Corvo island, Portugal

Table 4.2 - Water Dataset

NAME	WaterData
DATA	Rainfall, evaporation, inflow rain, outflow evap, outflow pub
TIME FRAME	Per hour
PERIOD	One year
PLACE	Corvo island, Portugal

4.2 Load

From the load demand dataset the Figure 4.1 is created, which presents the load demand in 1999 and in 2010.
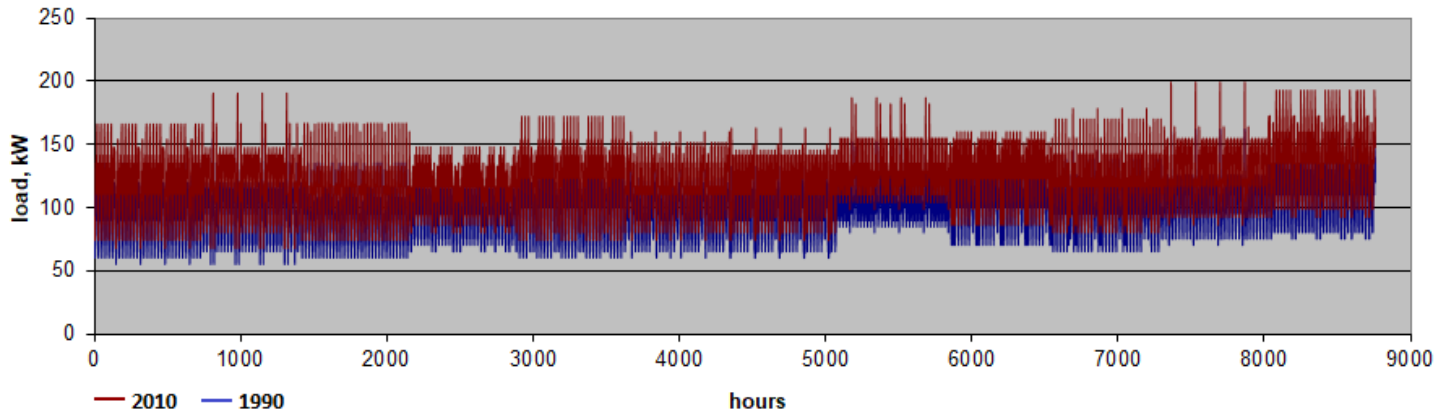
Figure 4.1: Load Curve, 1999 and 2010

(Source: Excel file "CorvoLoadAverage.xls")

In Figure 4.2 the same curve is divided into four different color regions, one for each season.
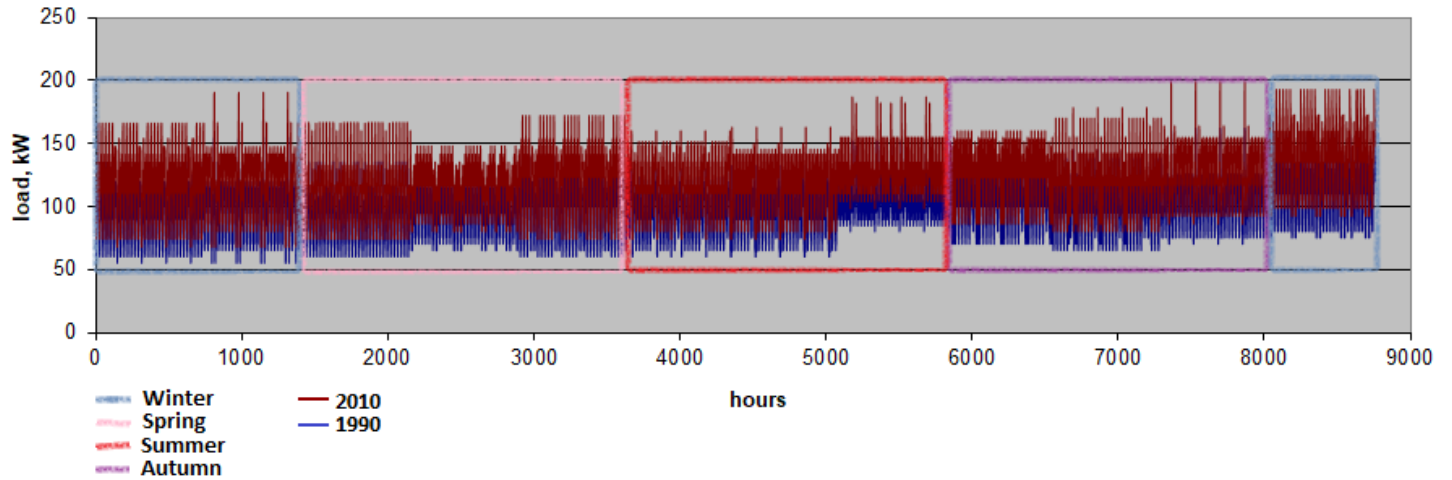
Figure 4.2: Load Curve per season, 1999 and 2010

(Source: Excel file "CorvoLoadAverage.xls")

For this project, in order to calculate the average load demand all the data will be used as discrete values to avoid any loss of information. Consequently, the average load demand of 2010 has been calculated in 135kW, and:

$$\bar{E}_{tot} = \bar{P}T_{tot}$$

In a period of one year Ttot is 8760h, and the previews equation is:

$$\bar{E}_{tot} = 135kW\ 8760h = 1182MWh$$

4.2.1   Sampling of Load Demand

In figure 4.3 the load of four days is presented, one (example) of every season.
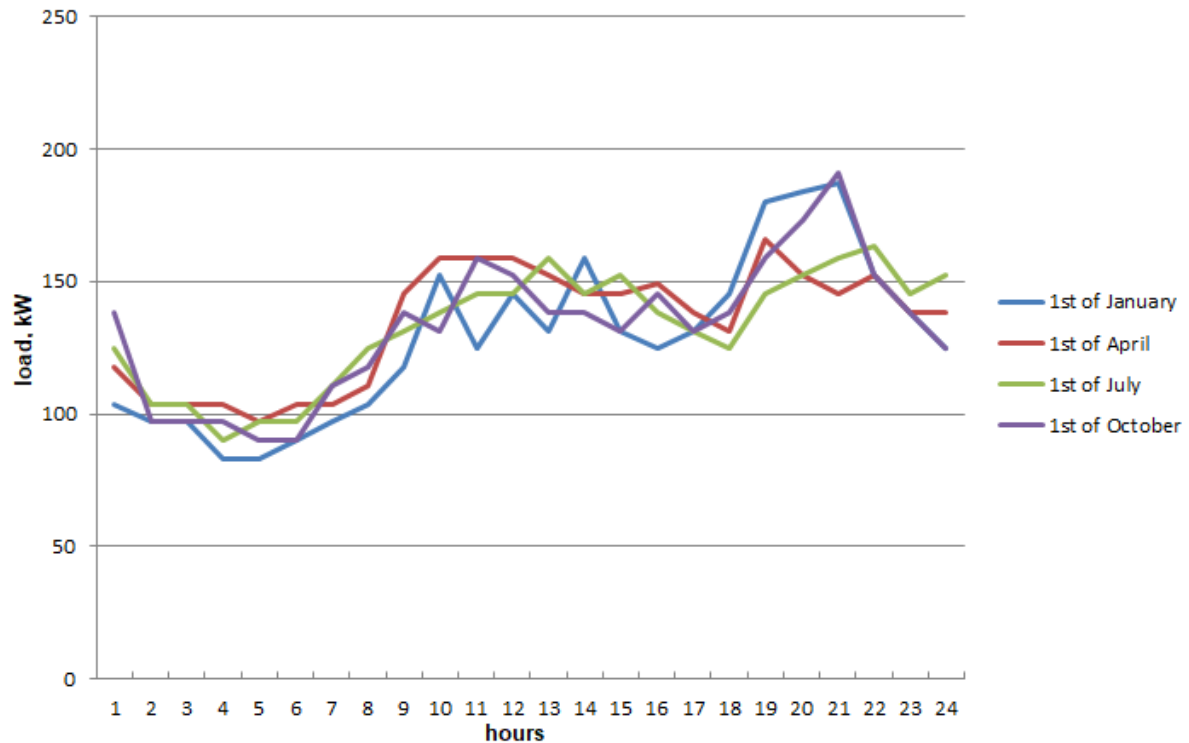
Figure 4.3: Load Curves of four days, 2010

(Source: Excel file "FourDaysLoadCorvo2010.xlsx")

In order to model the load, a Matlab file was created. The goal was to fit a curve to the set of data of one day of each season. Thus, there would be a better overview of the load demand as it changes depending on weather conditions. This was made possible using the "fit" function. This function creates a curve for the model, but the type of the curve is specified by the user. In this case -that the edges were too valuable to smooth out during the fitting process- the type that was used is called "cubicintepr" and is piecewise cubic interpolation.

- 1st of January:

In figure 4.4 is presented the load demand for the first of January of 2010. The cyan circles represent the data gathered from Corvo, while the black line shows the fitted curve created in the Matlab file.
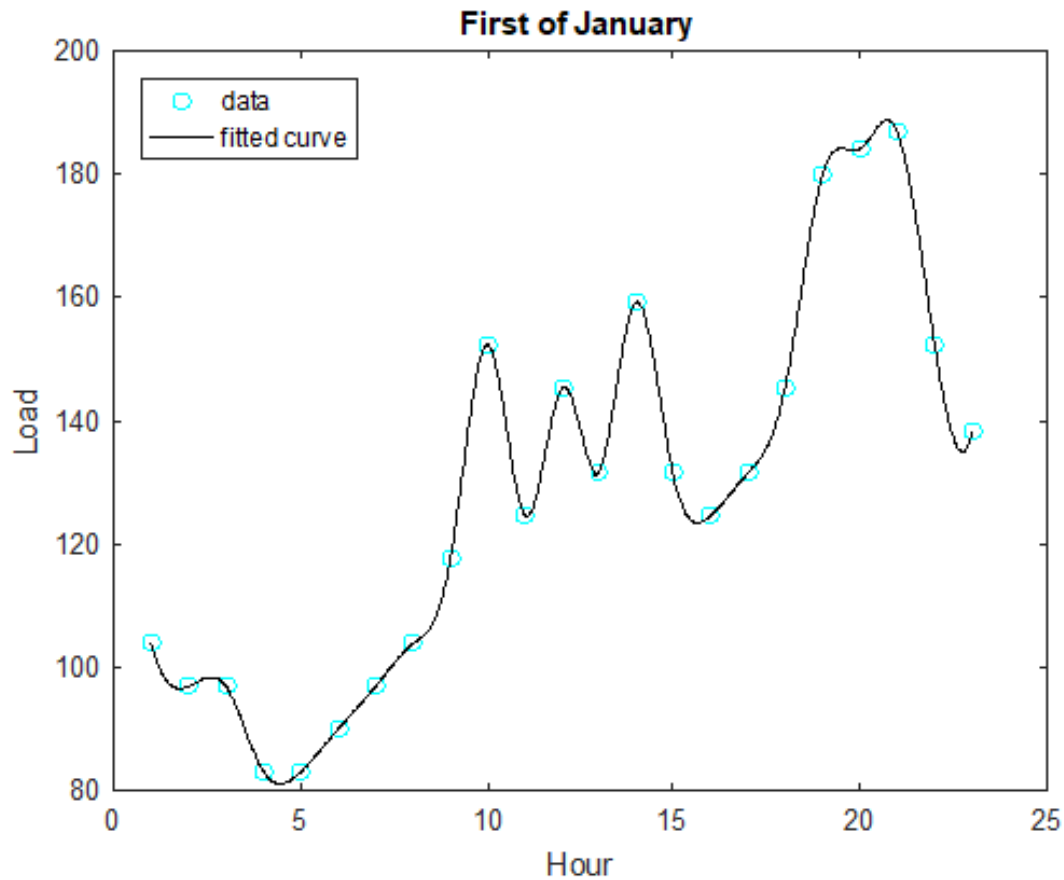
Figure 4.4: Load Curve of the 1st of January 2010

(Source: Matlab file "SamplingOneDayOfEachSeason.m")

- 1st of April:

In figure 4.5 is presented the load demand for the first of April of 2010. The cyan circles represent the data gathered from Corvo, while the black line shows the fitted curve created in the Matlab file.
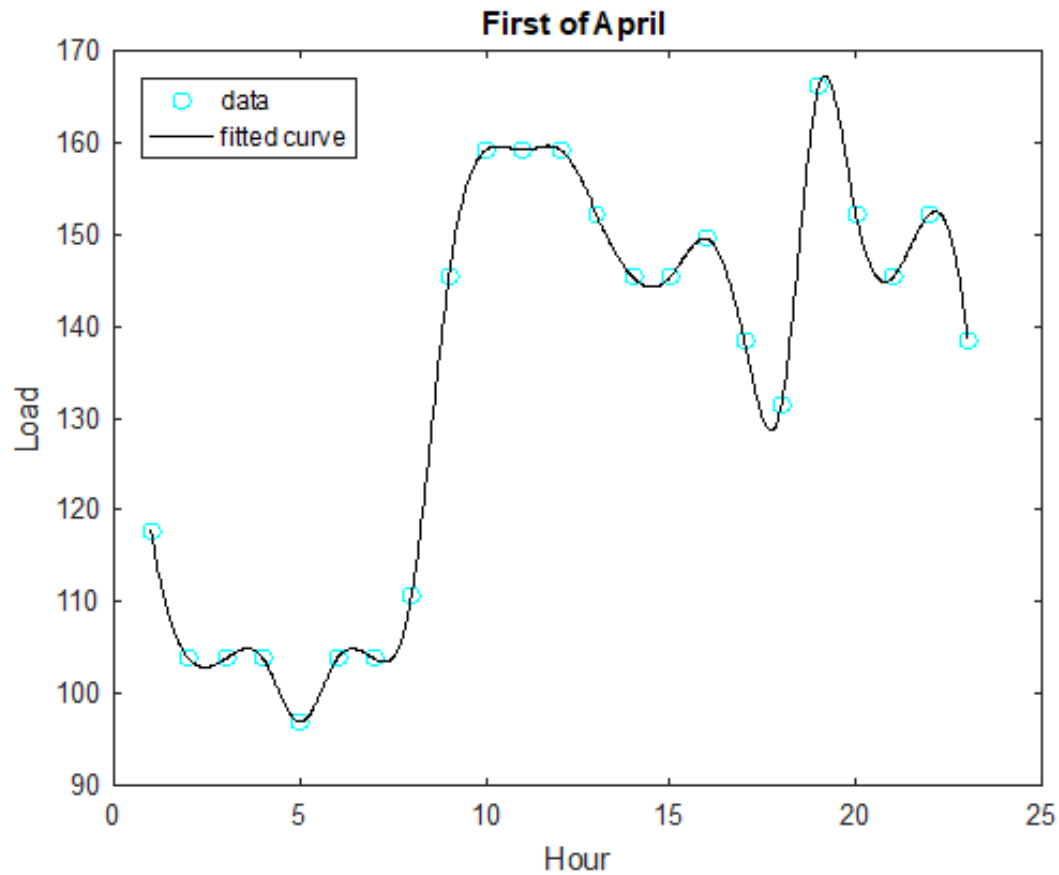
Figure 4.5: Load Curve of the 1ˢᵗ of April 2010

(Source: Matlab file "SamplingOneDayOfEachSeason.m")

- 1ˢᵗ of July:

In figure 4.6 is presented the load demand for the first of July of 2010. The cyan circles represent the data gathered from Corvo, while the black line shows the fitted curve created in the Matlab file.
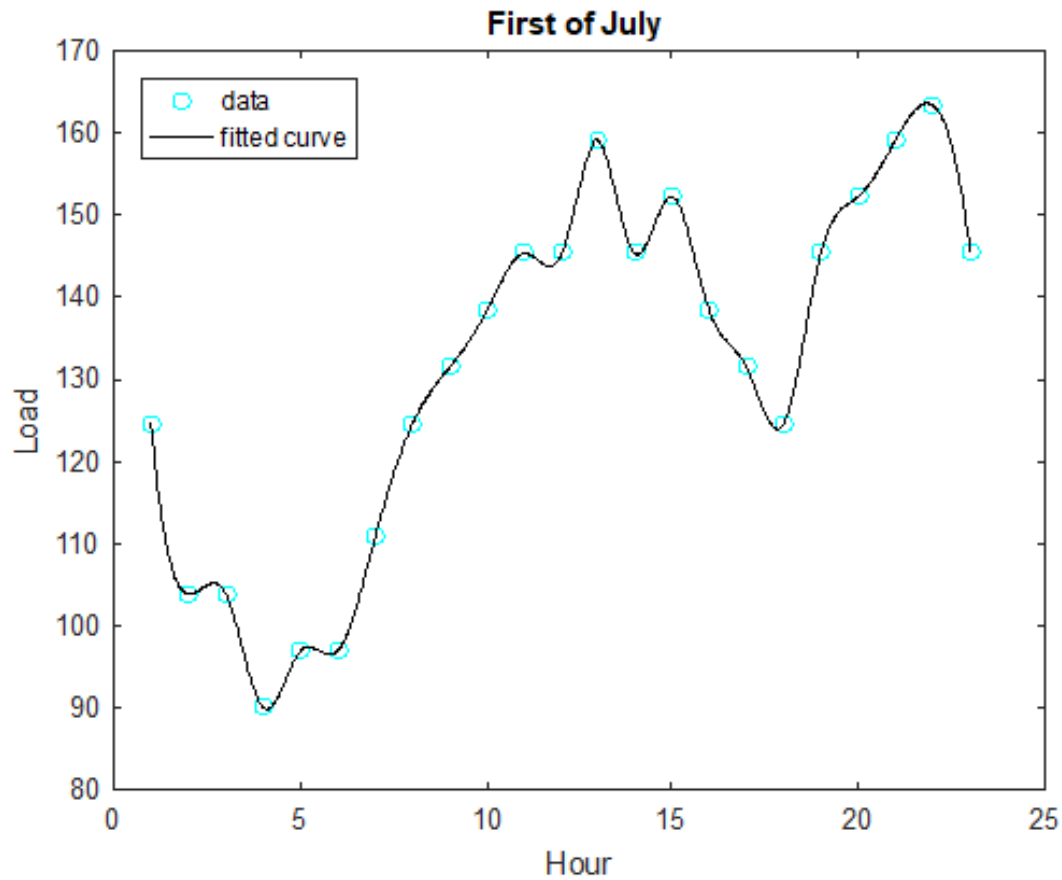
Figure 4.6: Load Curve of the 1st of July 2010

(Source: Matlab file "SamplingOneDayOfEachSeason.m")

- 1st of October:

In figure 4.7 is presented the load demand for the first of October of 2010. The cyan circles represent the data gathered from Corvo, while the black line shows the fitted curve created in the Matlab file.
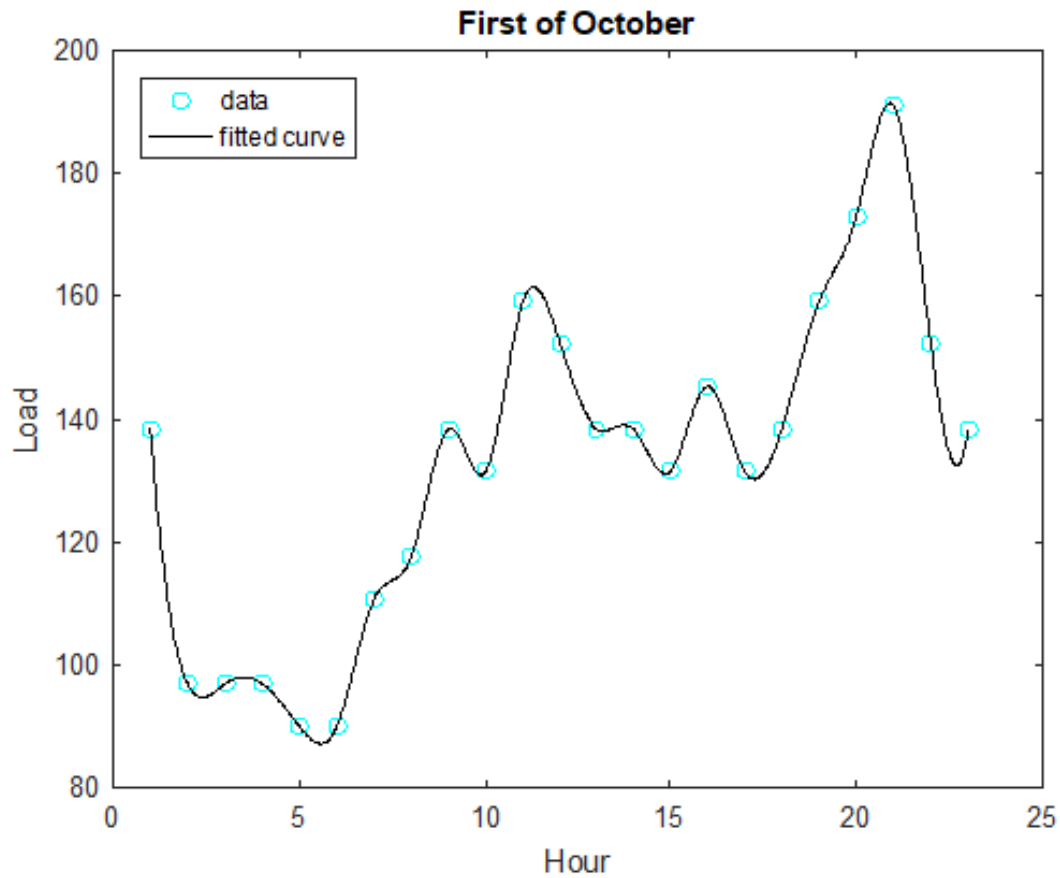
Figure 4.7: Load Curve of the 1st of October 2010

(Source: Matlab file "SamplingOneDayOfEachSeason.m")

4.3 Water Data – Stream Flow

For this project, a sampling of the hourly stream flow in Corvo Island throughout the year is presented in table 4.3 in order to calculate the minimum and maximum flow per second. The table shows the flow in m^3 of one random hour of a random day of each month.

As it can be seen from the table, the minimum hourly flow is $13.939m^3$ and the maximum is $41.382m^3$. Thus, the minimum flow per second is $0.232m^3/s$ and the maximum is $0.690m^3/s$.

Table 4.3 - Sampling of the flow

DAYHOUR	DAY	MONTH	FLOW (m^3)
1	1	1	41.382
3	3	2	35.719
6	6	3	30.492
8	9	4	21.998
10	12	5	18.513
12	15	6	13.939
14	17	7	15.682
16	20	8	18.731
18	23	9	27.661
20	26	10	31.581
22	28	11	33.977
24	30	12	33.977

4.4   Temperature and Solar Data

Corvo Island is the smallest and the northernmost island of the Azores archipelago.

In figure 4.8 the maximum, minimum and average temperatures in Corvo are presented for each month of the year. Table 4.4 shows numerically the same temperatures.
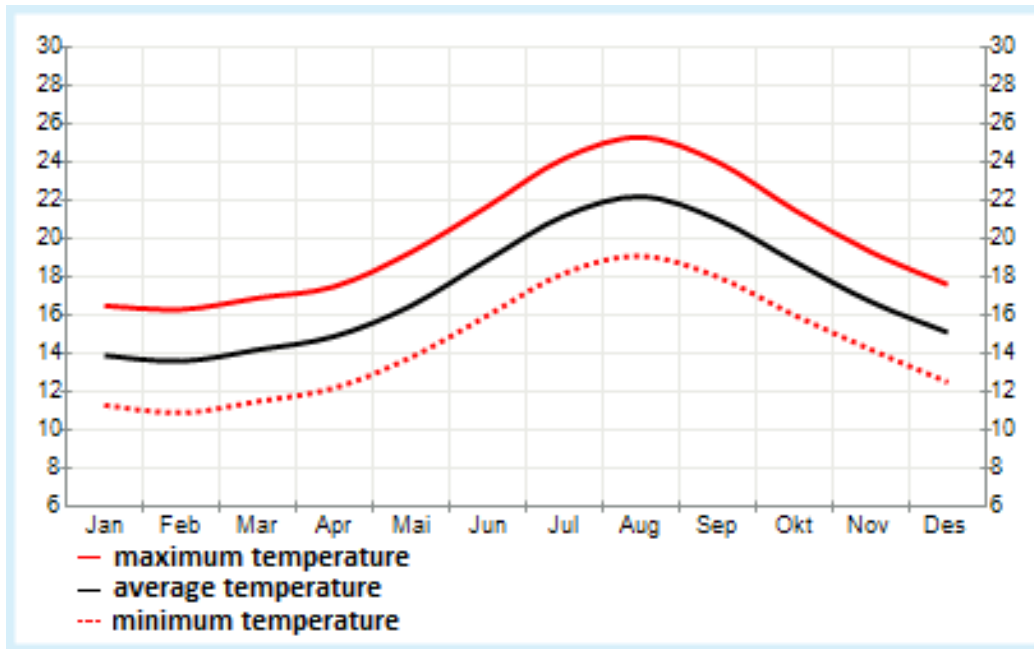
Figure 4.8: Temperature (°C) in Corvo, measured in the period 1961-1990

(Source: WMO)

Table 4.4 - Temperature (°C) in Corvo, measured in the period 1961-1990

MONTH	NORMAL TEMP	WARMEST TEMP	COLDEST TEMP
January	13.9°C	16.5°C	11.3°C
February	13.6°C	16.3°C	10.9°C
March	14.2°C	16.9°C	11.5°C
April	14.9°C	17.5°C	12.2°C
May	16.5°C	19.3°C	13.8°C
June	18.9°C	21.7°C	16.0°C
July	21.2°C	24.2°C	18.2°C
August	22.2°C	25.3°C	19.1°C
September	21.0°C	24.0°C	18.0°C
October	18.8°C	21.5°C	16.0°C
November	16.7°C	19.3°C	14.2°C
December	15.1°C	17.6°C	12.5°C

For the solar data the climate database of NASA has been used [38].

In table 4.5 the average daylight hours are presented for each month. This table includes very important information due to the inability of the photovoltaic applications to produce energy during the rest of the day.

Table 4.5 - Monthly Average Daylight Hours

MONTH	AVERAGE
January	9.71h
February	10.70h
March	11.90h
April	13.20h
May	14.30h
June	14.90h
July	14.60h
August	13.70h
September	12.40h
October	11.20h
November	10.00h
December	9.41h
Average	12.17h

Below, table 4.6 shows the solar radiation for each month for the purpose of sizing and pointing of solar panels, as well as for solar thermal applications. As one can observe, the columns are divided according to the degrees that a tilted PV system is able to have. The last column provides the optimal radiation, which is the radiation that a concentrating PV system may absorb. It's important to draw to one's attention that this table presents the average values through a twenty two-year period.

Table 4.6 - Monthly Average Radiation Incident On An Equator-Pointed Tilted Surface (kWh/m^2/day)

MONTH	DIRECT	TILT 0	TILT 24	TILT 39	TILT 54	TILT 90	OPT
January	2.82	1.83	2.57	2.87	3.01	2.69	3.02
February	3.50	2.59	3.31	3.55	3.60	2.96	3.60
March	4.28	3.76	4.37	4.48	4.35	3.21	4.48
April	5.37	5.13	5.44	5.29	4.87	3.08	5.45
May	5.88	5.96	5.92	5.52	4.85	2.71	6.04
June	6.17	6.32	6.10	5.58	4.80	2.52	6.34
July	7.16	6.71	6.56	6.03	5.21	2.72	6.75
August	7.36	6.30	6.54	6.24	5.62	3.26	6.56
September	5.84	4.73	5.41	5.46	5.23	3.63	5.48
October	4.36	3.23	4.10	4.37	4.40	3.55	4.41
November	3.34	2.13	2.97	3.30	3.44	3.03	3.45
December	2.68	1.63	2.39	2.70	2.87	2.62	2.89

Table 4.7 - Minimum and Maximum Difference From Monthly Average Direct Normal Radiation

MONTH	MINIMUM	MAXIMUM
January	-20%	23%
February	-19%	38%
March	-20%	22%
April	-14%	14%
May	-7%	16%
June	-14%	8%
July	-7%	9%
August	-6%	6%
September	-5%	11%
October	-7%	18%
November	-13%	28%
December	-22%	29%

Table 4.7, above, shows the minimum and maximum difference from the monthly average presented in table 4.6.

CHAPTER 5.   OPTIMAL SIZING

In this chapter, optimal sizing of an isolated microgrid, consisting of a Hydro-PV-BESS hybrid system, is presented with the HOMER software. (Without loss of generality, the sum of the hydro turbine power generators, the photovoltaic power generators or the energy storage system is equivalently regarded as one hydro system, one PV system or one storage system respectively, which are examined as three subsystems on the microgrid that is considered the main system.)

The PV and Hydro energy are intermittent sources due to their dependence with the weather conditions. Therefore, it is difficult to match production and demand. This makes the sizing process complex in many aspects. The optimization problem not only concerns the sizing of each component, but it is also affected by the dependence between the components.

5.1   Introduction to HOMER

The HOMER (Hybrid Optimization of Multiple Energy Resources) software application is used to design and evaluate technically and financially the options for off-grid and on-grid power systems for remote, stand-alone and distributed generation applications. It allows one to consider a large number of technology options to account for energy resource availability that can include a combination of renewable power sources, storage, and a fossil-based generation. [40][50]

Originally, HOMER was designed at the National Renewable Energy Laboratory for the village power program (U.S.) [40].

5.2   Homer System

HOMER can model both technical and economic factors involved in the project. If a larger scale of sensitivity is provided, HOMER can provide an important overview that compares

the cost and feasibility of different configurations, so that designers can use more specialized software to model technical performance [40].

Nevertheless, in this project, our goal is to take advantage of the hydro power as more as possible. This means that the sources left to optimize is the BESS and PV system which are two interconnected systems that could be considered as one.

In this chapter the main simulation will be presented, which covers the island's load needs of the measurements of 2010. The schematic is presented in figure 5.1.
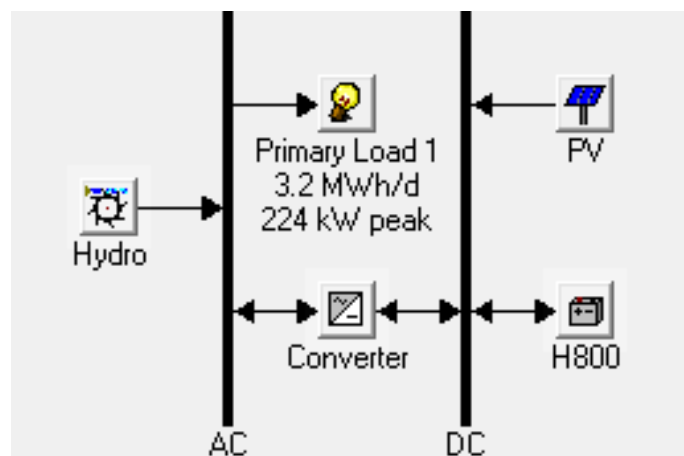
Figure 5.1: HOMER Simulated Microgrid Schematic

(Source: HOMER)

Subsequently, the simulated equipment will be presented in detail, as well as all the necessary resources.

5.2.1   Electric Load

A load is a portion of the system that consumes energy. Primary load is the electrical load that the system must meet immediately in order to avoid unmet load. In each time step, HOMER dispatches the power-producing components of the system to serve the total primary load.

In HOMER, after the selection of load type (AC or DC), one can specify an electric load by choosing one of three options:

1. Creating a synthetic load from a profile (after entering 24 values which correspond to the average electric demand for every single hour of the day in the load table and a scaled annual average, HOMER replicates this profile throughout the year unless you define different load profiles for different months or day types),
2. Importing a load from a time series file (demand data file *.dmd or text files *.txt),
3. Download OpenEl Load Profiles (this option is available only in HOMER Pro) [42].

In this case, option two was chosen. Figure 5.2 shows the imported file with the load data for a year.
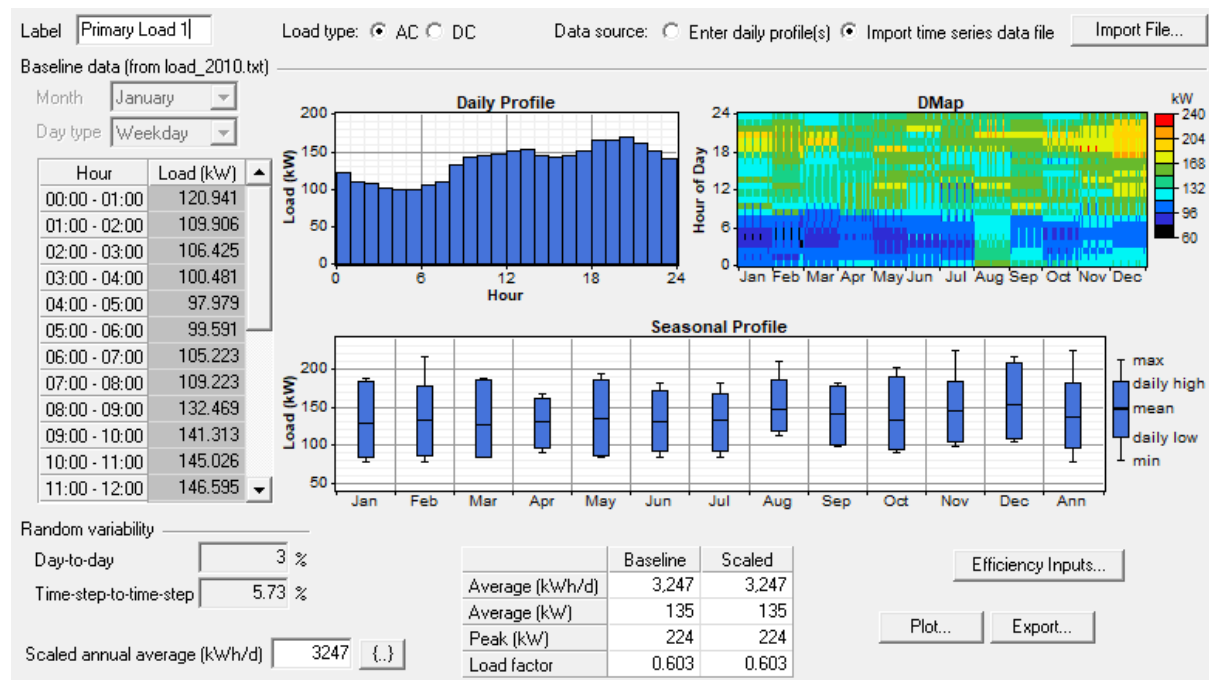
Figure 5.2: Electric Load of measurement of 2010 in Corvo Island, HOMER software

(Source: HOMER Pro)

In the left side of the Figure 5.2 an hourly sequence for a weekday during January is presented, adjacent to a daily profile per hour and in the right side one can observe a seasonal map of the load. Below these profiles there is a yearly profile per hour and one can clearly specify the difference between the months.

In figure 5.3 there are twelve different profiles, one for each month showing the load per hour during an average day.
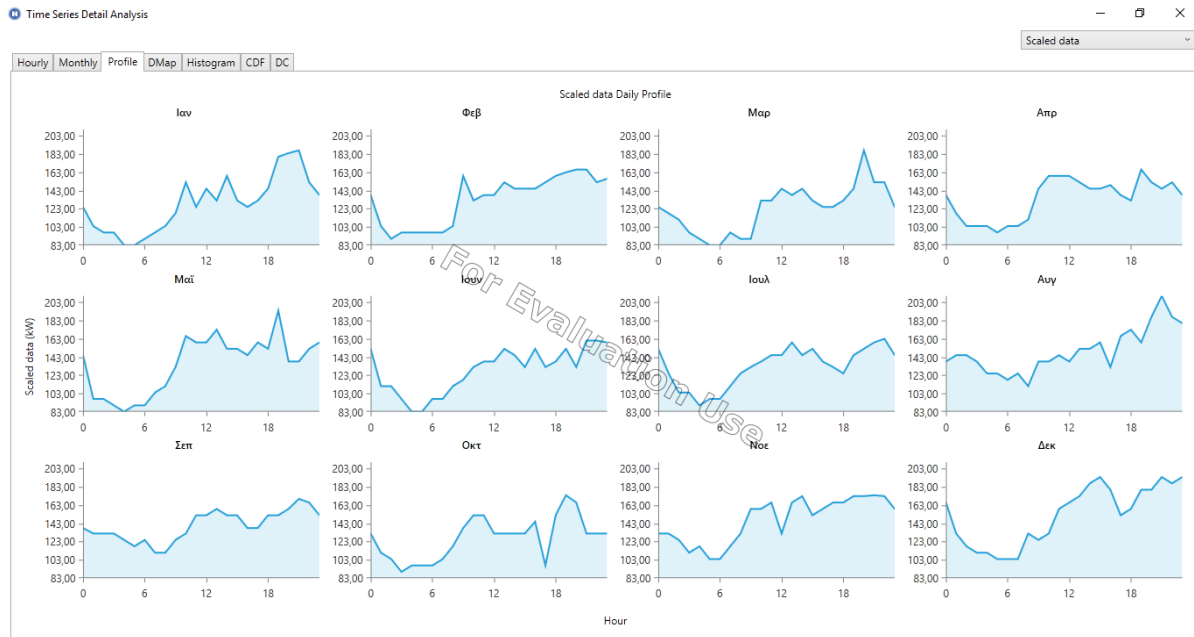
Figure 5.3: Electric Load profiles for an average day of each month of measurements of 2010 in Corvo Island, HOMER software

(Source: HOMER Pro)

5.2.2 Converter

In figure 5.4 the converter is presented. The converter is an essential part of the system because it keeps the balance between different amplitudes of current and between the AC and DC subsystems. A converter can be an inverter (DC to AC), rectifier (AC to DC) or both.
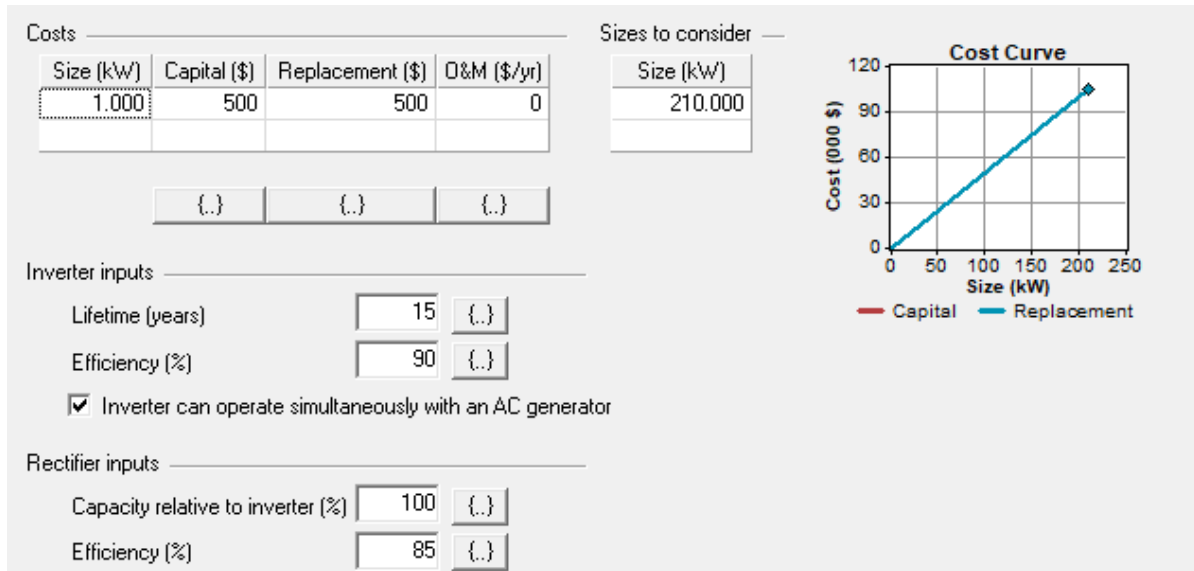
Figure 5.4: HOMER Simulated System Converter

(Source: HOMER)

5.2.3 Hydro Module

The Hydro module adds the hydro resource and the hydro component. You can specify the stream flow in the Hydro resource, either as twelve monthly values, or as an imported time series [41].

In this project the hydro resource was calculated as follows, inserted in "hydro_resource.hyd" specified as twelve monthly values and imported in HOMER software (Figure 5.5).

The data from table 4.3 showing a sampling of the flow in m^3 per hour will be used in order to calculate the monthly values in Liters per second which are necessary to import in HOMER software. Table 5.1 shows this conversion.

 – Cubic meters to Liters: 1 m^3 = 1000 L

- Liters per hour to Liters per second: $1L/h = 1/60$ L/s

Table 5.1 - Calculation of flow in Liters per second, Corvo Island 2010

MONTH	FLOW(m^3/h)	FLOW(L/h)	FLOW (L/s)
1	41,382	41382	690
2	35,719	35719	595
3	30,492	30492	508
4	21,998	21998	367
5	18,513	18513	309
6	13,939	13939	232
7	15,682	15682	261
8	18,731	18731	312
9	27,661	27661	461
10	31,581	31581	526
11	33,977	33977	566
12	33,977	33977	566

In the left side of the figure 5.5, 12 average monthly values are shown, adjacent to a visual representation on the right side. As calculated by HOMER, the scaled annual average is 449 L/s.
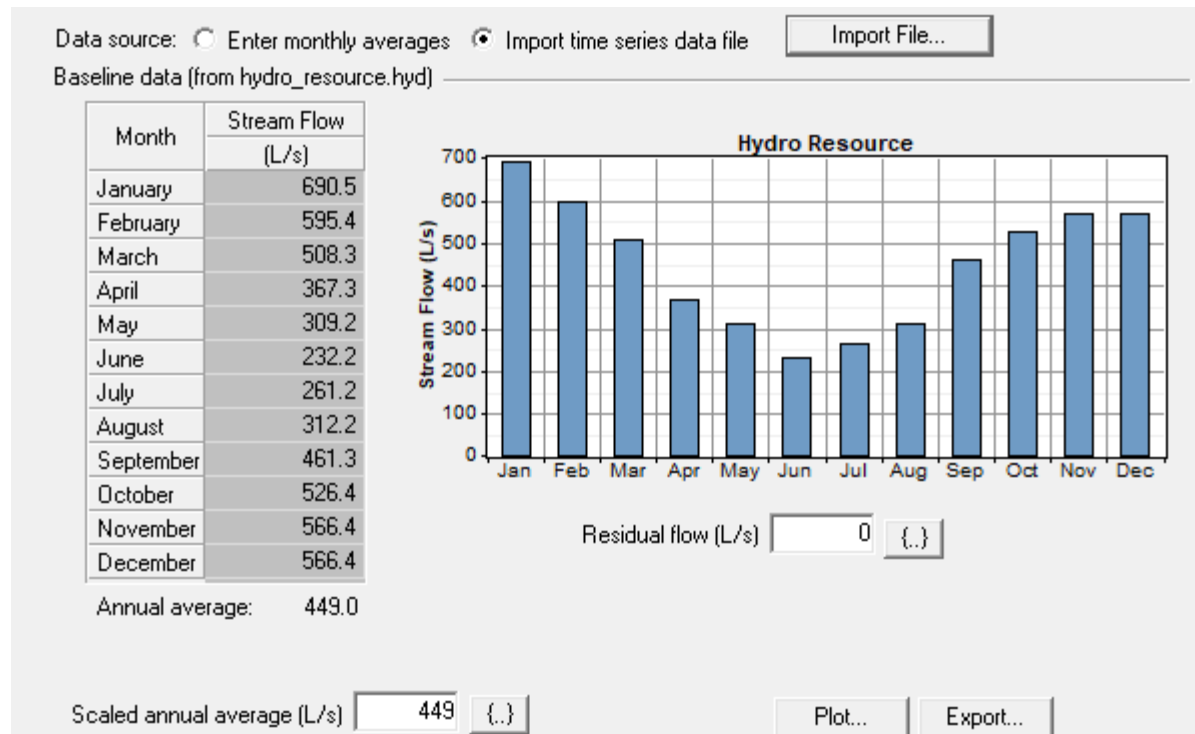
Figure 5.5: Hydro Resource (L/s) in Corvo Island 2010, HOMER software

(Source: HOMER)

Figure 5.6 shows the hydro component of the system. In the middle section of the Figure the specification of the turbine is presented:

− Available head is 100 m,

− Design flow rate is considered at 464 L/s (0,464 m³/s),

− Minimum flow ration is 50% (0,232 m³/s which is a lot more than 0,1 m³/s which is calculated in "Appendix: III. Calculation of minimum Hydro Contribution" as the minimum flow rate entering the penstock and this is why the efficiency (%) below is so low, in order to have a realistic production from the Hydro System),

− Maximum flow ration is 150% (0,696 m³/s > 0,690 m³/s Maximum stream flow during January).

– Efficiency is only 45% due to the type of hydro that is used in the project (there are no tank or dam to ensure minimum loss of the flow).

Figure 5.6: Hydro Component, HOMER software

(Source: HOMER)

5.2.4 Storage Module

In HOMER and HOMER Pro the Storage page allows one to choose a storage component from the library, look at the technical details, and specify storage costs. One can define new storage models in the Storage Library or select from existing options.

There are several types of storage components:

- Idealized Battery: The idealized battery model allows users to size energy and power independently.

- Kinetic Battery: The Kinetic Battery model is a two-tank system that separates available energy for electricity generation from bound energy that cannot be used.

- Modified Kinetic Battery: The Modified Kinetic Battery Model accounts for rate dependent losses, temperature dependence on capacity, and temperature effects on calendar life.

- Supercapacitor: The Supercapacitor is based on the Idealized Storage Model, which replicates a simple storage model with a flat discharge curve because the supply voltage stays mostly constant during the discharge cycle.

- Flywheel: A flywheel provides operating reserve on the AC bus, helping to absorb sudden increases or make up for sudden decreases in renewable power output.

- Pumped Hydro: A Pumped Hydro System builds potential energy by storing water in a reservoir at a certain height when there is excess energy, and converts the potential energy to electricity by releasing the potential energy to turn the turbine generator when there is a demand. [43]

In this BESS, the "Hoppecke 8 OPzS 800" model is chosen (Figure 5.7). This is a vented lead-acid, tubular-plate, deep-cycle battery and some of her specifications are listed below.

The nominal capacity of the model used below (Figure 5.7) is:

$$C_H = 800Ah$$

The nominal voltage of each battery is 2V. As a result in order to create a 48V bus the quantity needed per string is (Figure 5.8):

$$N_{BS} = \frac{48V}{2V} = 24 \ batteries \ per \ string$$

The Minimum State of Charge (or Maximum Depth of Discharge) of the battery model is:

$$SOC_{min} = DOD_{max} = 30\%$$

Battery Details

The properties of this battery appear below. Once a battery is created you cannot edit its properties. To change a battery's properties, create a copy (click New in the Battery Inputs window) and modify the properties of the copy.
Hold the pointer over an element name or click Help for more information.

General

Description:	Hoppecke 8 OPzS 800
Abbreviation:	H800
Manufacturer:	Hoppecke
Website:	www.hoppecke.com
Notes:	Vented lead-acid, tubular-plate, deep-cycle battery.

Nominal capacity:	800 Ah
Nominal voltage:	2 V
Round trip efficiency:	86 %
Min. state of charge:	30 %
Float life:	20 yrs
Max. charge rate:	1 A/Ah
Max. charge current:	162 A
Lifetime throughput:	2,742 kWh
Suggested value:	2,743 kWh

Calculated parameters

Maximum capacity:	958 Ah
Capacity ratio, c:	0.332
Rate constant, k:	1.10 1/hr

Capacity curve

Current (A)	Capacity (Ah)
81.00	810.00
139.60	698.00
201.00	603.00
432.00	432.00

Lifetime curve

Depth of Discharge [%]	Cycles to Failure
20	7,820
30	4,960
40	3,600
50	2,780
60	2,270
70	1,930
80	1,640

Figure 5.7: Battery chosen for the BESS in HOMER software

(Source: HOMER)

In figure 5.8 there is a middle section for inserting values for sizes to consider. HOMER provides a tool for optimization, simulating all the theoretical scenarios depending on the values inserted in this section called the "Consider table" and choosing the value that minimizes the cost of the system. This is why the right completion of the costs in each sub-system is so important. It is indicated that the same pattern can be used in other sub-systems of a larger system, in this case in the PV system (Figure 5.10).
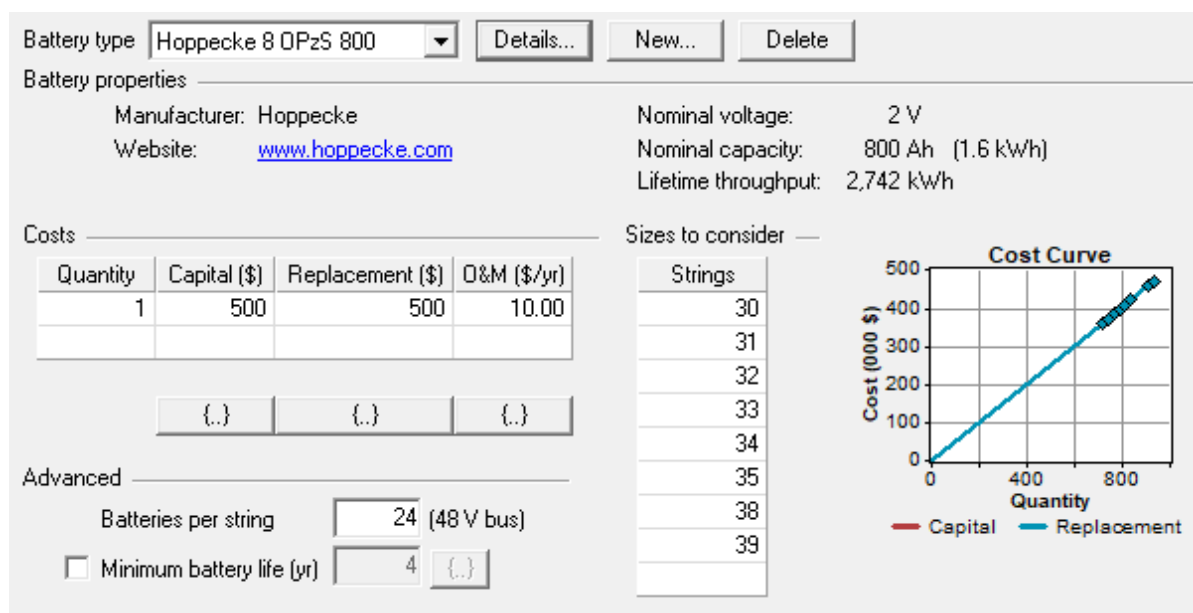
Figure 5.8: Simulated BESS with Consider table Optimization, HOMER software

(Source: HOMER)

5.2.5 Photovoltaics

The PV page in HOMER software allows one to enter the cost, performance characteristics, and orientation of an array of photovoltaic (PV) panels and if desired one is able to allow the software itself to calculate the optimal sizing after fill in all the possible values, as mentioned earlier (page 86). Note that by default, HOMER sets the slope value equal to the latitude from the Solar Resource (Figure 5.9) Inputs window.

In order to insert a PV system in the project, solar resource and temperature are needed to calculate the array's output for each hour of the year.

For solar resource, after entering the latitude and an average daily radiation value for each month, HOMER uses the latitude value to calculate the average daily radiation captured by

the panels. In HOMER the data is available to download from the Internet. In Figure 5.9 the Solar Resource is presented.
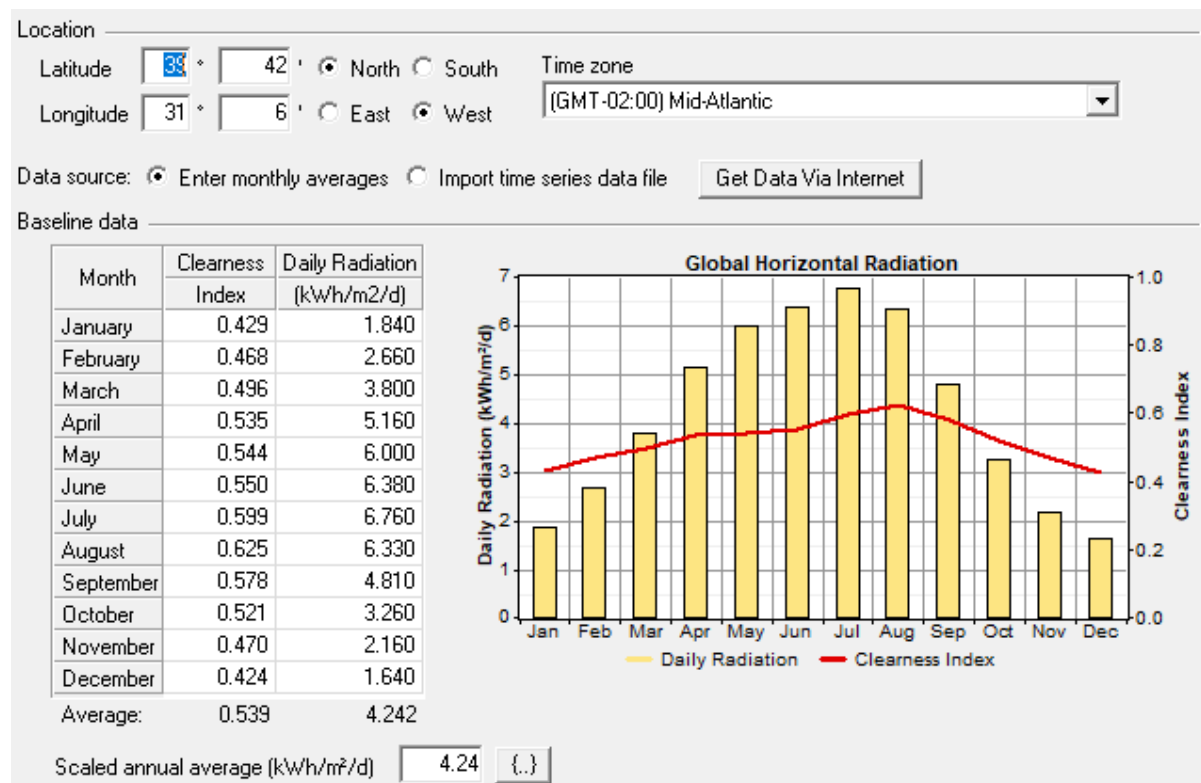
Figure 5.9: Solar Resource showing the Average Daily radiation in Corvo Island, HOMER software

(Source: HOMER, Nasa Data)

For temperature, after entering monthly average values, HOMER uses the ambient temperature data to calculate the power produced by the PV array in each time step. In Figure 5.10 the Temperature Resource is presented.
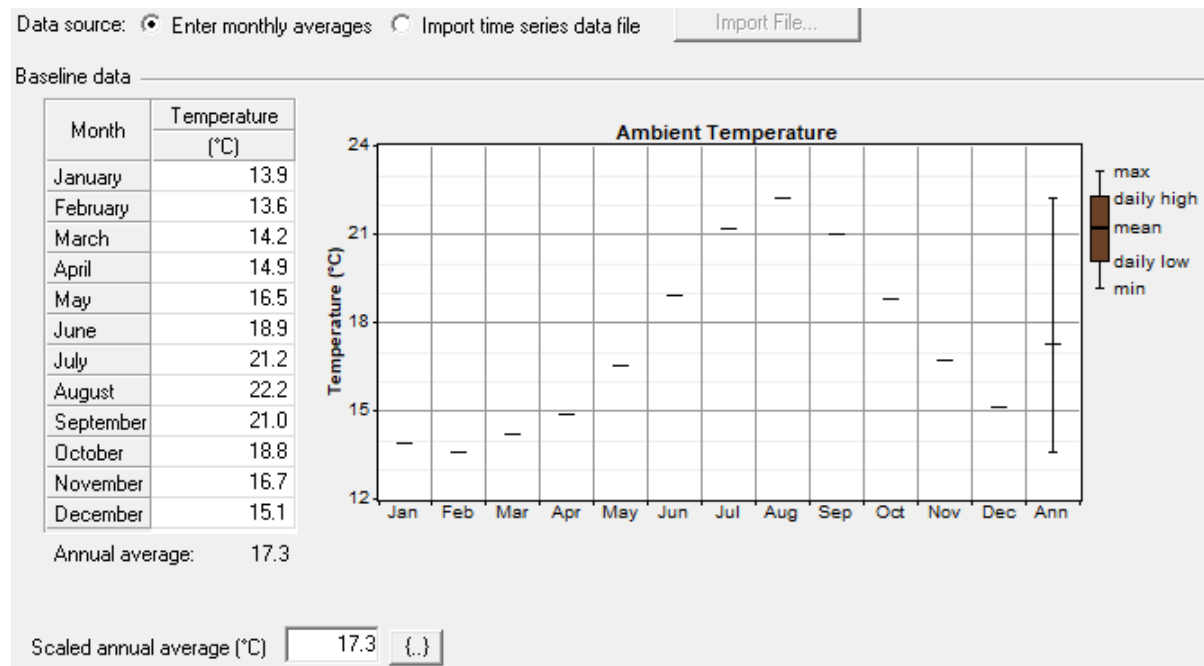
Figure 5.10: Temperature Resource showing the Average Monthly temperature in Corvo Island, HOMER software

(Source: HOMER)

The PV component includes all costs associated with the PV system (cost of modules, mounting hardware and installation). As the optimization tool searches for the optimal system size, HOMER considers each PV array capacity in the Consider table (Figure 5.11).
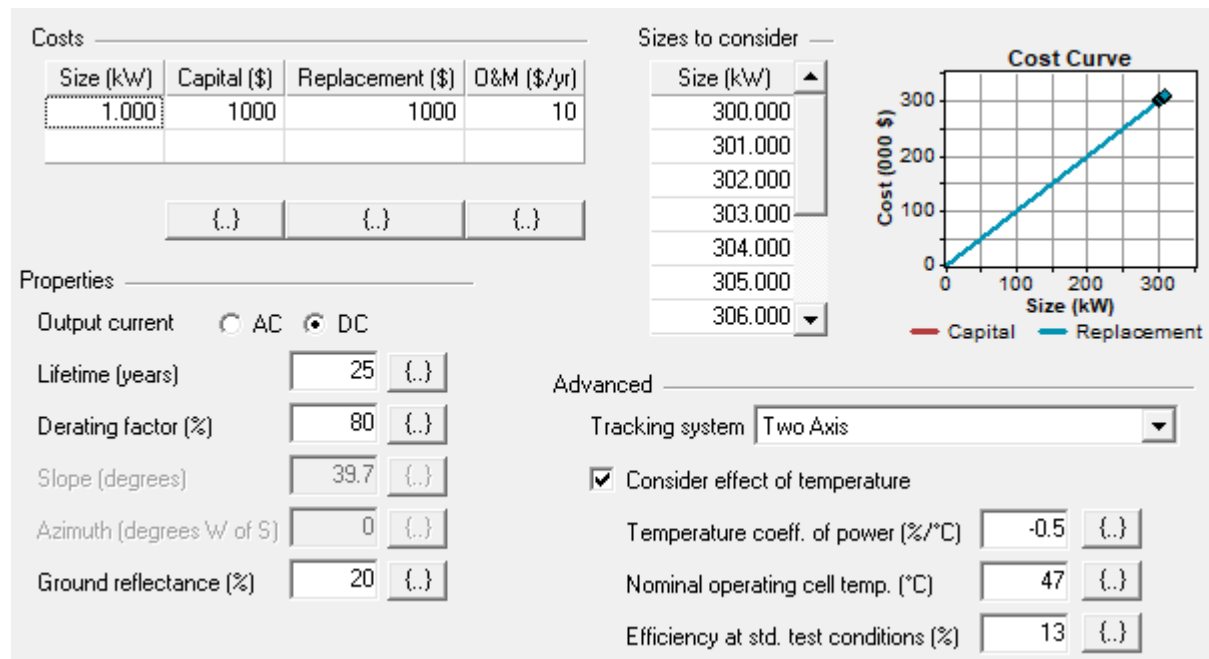
Figure 5.11: Simulated PV System with Consider table Optimization, HOMER software

(Source: HOMER)

5.2.6 Simulated System Results

Lastly, the system is ready for the final run. The simulation analysis lastedfor only two seconds and the results are shown in Figure 5.12.

Sensitivity Results | Optimization Results

Double click on a system below for simulation results.   ○ Categorized ● Overall   Export...   Details...

PV (kW)	Hydro (kW)	H800	Conv. (kW)	Disp. Strgy	Initial Capital	Operating Cost ($/yr)	Total NPC	COE ($/kWh)	Ren. Frac.
304	205	840	210	CC	$ 909,000	21,132	$ 1,179,143	0.078	1.00
304	205	840	210	LF	$ 909,000	21,132	$ 1,179,143	0.078	1.00
305	205	840	210	CC	$ 910,000	21,142	$ 1,180,271	0.078	1.00
305	205	840	210	LF	$ 910,000	21,142	$ 1,180,271	0.078	1.00
306	205	840	210	CC	$ 911,000	21,152	$ 1,181,399	0.078	1.00
306	205	840	210	LF	$ 911,000	21,152	$ 1,181,399	0.078	1.00
307	205	840	210	CC	$ 912,000	21,162	$ 1,182,526	0.078	1.00
307	205	840	210	LF	$ 912,000	21,162	$ 1,182,526	0.078	1.00
308	205	840	210	CC	$ 913,000	21,172	$ 1,183,654	0.078	1.00
308	205	840	210	LF	$ 913,000	21,172	$ 1,183,654	0.078	1.00
309	205	840	210	CC	$ 914,000	21,182	$ 1,184,782	0.078	1.00
309	205	840	210	LF	$ 914,000	21,182	$ 1,184,782	0.078	1.00
310	205	840	210	CC	$ 915,000	21,192	$ 1,185,910	0.078	1.00
310	205	840	210	LF	$ 915,000	21,192	$ 1,185,910	0.078	1.00
300	205	912	210	CC	$ 941,000	22,198	$ 1,224,770	0.081	1.00
300	205	912	210	LF	$ 941,000	22,198	$ 1,224,770	0.081	1.00
301	205	912	210	CC	$ 942,000	22,208	$ 1,225,898	0.081	1.00
301	205	912	210	LF	$ 942,000	22,208	$ 1,225,898	0.081	1.00
302	205	912	210	CC	$ 943,000	22,218	$ 1,227,025	0.081	1.00
302	205	912	210	LF	$ 943,000	22,218	$ 1,227,025	0.081	1.00
303	205	912	210	CC	$ 944,000	22,228	$ 1,228,153	0.081	1.00
303	205	912	210	LF	$ 944,000	22,228	$ 1,228,153	0.081	1.00
304	205	912	210	CC	$ 945,000	22,238	$ 1,229,281	0.081	1.00
304	205	912	210	LF	$ 945,000	22,238	$ 1,229,281	0.081	1.00
305	205	912	210	CC	$ 946,000	22,248	$ 1,230,409	0.081	1.00
305	205	912	210	LF	$ 946,000	22,248	$ 1,230,409	0.081	1.00
306	205	912	210	CC	$ 947,000	22,258	$ 1,231,537	0.081	1.00
306	205	912	210	LF	$ 947,000	22,258	$ 1,231,537	0.081	1.00
307	205	912	210	CC	$ 948,000	22,268	$ 1,232,665	0.081	1.00
307	205	912	210	LF	$ 948,000	22,268	$ 1,232,665	0.081	1.00
308	205	912	210	CC	$ 949,000	22,278	$ 1,233,792	0.081	1.00
308	205	912	210	LF	$ 949,000	22,278	$ 1,233,792	0.081	1.00
309	205	912	210	CC	$ 950,000	22,288	$ 1,234,920	0.082	1.00
309	205	912	210	LF	$ 950,000	22,288	$ 1,234,920	0.082	1.00
310	205	912	210	CC	$ 951,000	22,298	$ 1,236,048	0.082	1.00
310	205	912	210	LF	$ 951,000	22,298	$ 1,236,048	0.082	1.00
300	205	936	210	CC	$ 953,000	22,567	$ 1,241,482	0.082	1.00
300	205	936	210	LF	$ 953,000	22,567	$ 1,241,482	0.082	1.00
301	205	936	210	CC	$ 954,000	22,577	$ 1,242,610	0.082	1.00
301	205	936	210	LF	$ 954,000	22,577	$ 1,242,610	0.082	1.00
302	205	936	210	CC	$ 955,000	22,587	$ 1,243,738	0.082	1.00
302	205	936	210	LF	$ 955,000	22,587	$ 1,243,738	0.082	1.00
303	205	936	210	CC	$ 956,000	22,597	$ 1,244,866	0.082	1.00
303	205	936	210	LF	$ 956,000	22,597	$ 1,244,866	0.082	1.00
304	205	936	210	CC	$ 957,000	22,607	$ 1,245,994	0.082	1.00
304	205	936	210	LF	$ 957,000	22,607	$ 1,245,994	0.082	1.00
305	205	936	210	CC	$ 958,000	22,617	$ 1,247,122	0.082	1.00
305	205	936	210	LF	$ 958,000	22,617	$ 1,247,122	0.082	1.00
306	205	936	210	CC	$ 959,000	22,627	$ 1,248,249	0.082	1.00
306	205	936	210	LF	$ 959,000	22,627	$ 1,248,249	0.082	1.00
307	205	936	210	CC	$ 960,000	22,637	$ 1,249,377	0.083	1.00
307	205	936	210	LF	$ 960,000	22,637	$ 1,249,377	0.083	1.00
308	205	936	210	CC	$ 961,000	22,647	$ 1,250,505	0.083	1.00
308	205	936	210	LF	$ 961,000	22,647	$ 1,250,505	0.083	1.00
309	205	936	210	CC	$ 962,000	22,657	$ 1,251,633	0.083	1.00
309	205	936	210	LF	$ 962,000	22,657	$ 1,251,633	0.083	1.00
310	205	936	210	CC	$ 963,000	22,667	$ 1,252,761	0.083	1.00
310	205	936	210	LF	$ 963,000	22,667	$ 1,252,761	0.083	1.00

ⓘ Completed in 2 seconds.

Figure 5.12: Results of the simulated system, HOMER software

(Source: HOMER)

In Figure 5.12 there is a column for operating strategies of the system. There are two choises:

- the LF strategy (load following strategy), whereby whenever a generator operates, it produces only enough power to meet the primary load. Lower-priority objectives such as charging the storage bank or serving the deferrable load are left to the renewable power sources. The generator can still ramp up and sell power to the grid if it is economically advantageous. [48]
- the CC strategy (cycle charging strategy), whereby whenever a generator needs to serve the primary load, it operates at full output power. Surplus electrical production goes toward the lower-priority objectives such as, in order of decreasing priority: serving the deferrable load or charging the storage bank. [49]

In this case where the system's load is covered exclusively by RES there isn't any difference between the two strategies. In chapter 6, discovering various scenarios related to this microgrid these strategies may cause changes in the sizing that lead to changes in cost.

The optimum economic layout (highlited alternative in Figure 5.12) includes 205kW Hydro, 304kW PV, 840 batteries and a 210kW converter.

Table 5.2– Cost analysis of optimized simulated system, HOMER software

COMPONENT	CAPITAL ($)	REPLACEMENT ($)	O&M ($)	FUEL ($)	SALVAGE ($)	TOTAL ($)
PV	304,000	0	38,861	0	0	342,861
HYDRO	80,000	0	30,680	0	0	110,680
BESS	420,000	130,958	107,380	0	-73,395	584,944
CONVERTER	105,000	43,813	0	0	-8,155	140,658
SYSTEM	909,000	174,771	176,922	0	-81,550	1,179,143

A visual representation of the cost is available in Figure 5.13 and 5.14 below.
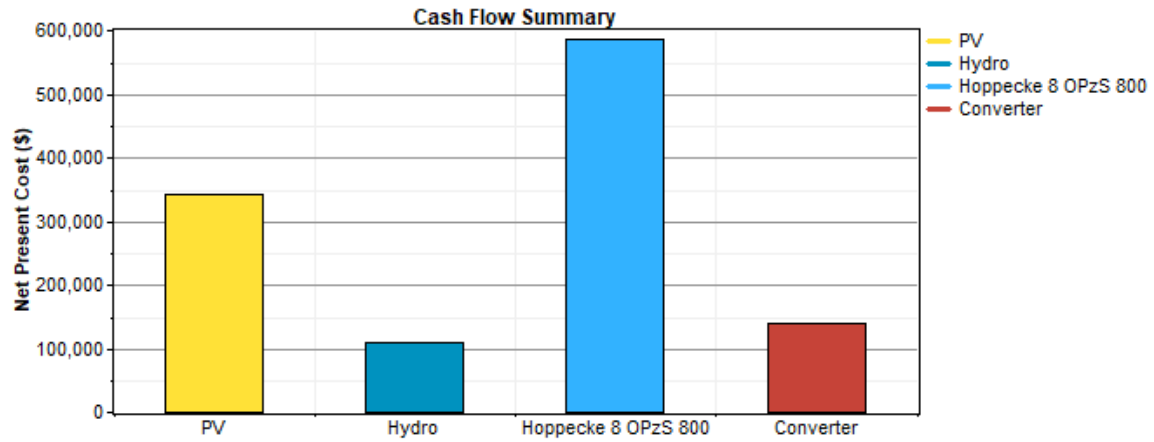
Figure 5.13: Cash Flow Summary of the simulated system by component, HOMER software

(Source: HOMER)

The net present cost (Total NPC) is 1,179,143$, and the cost of electricity (COE) is 0.078$/kWh. The operating cost of the microgrid is 21,132$/year.
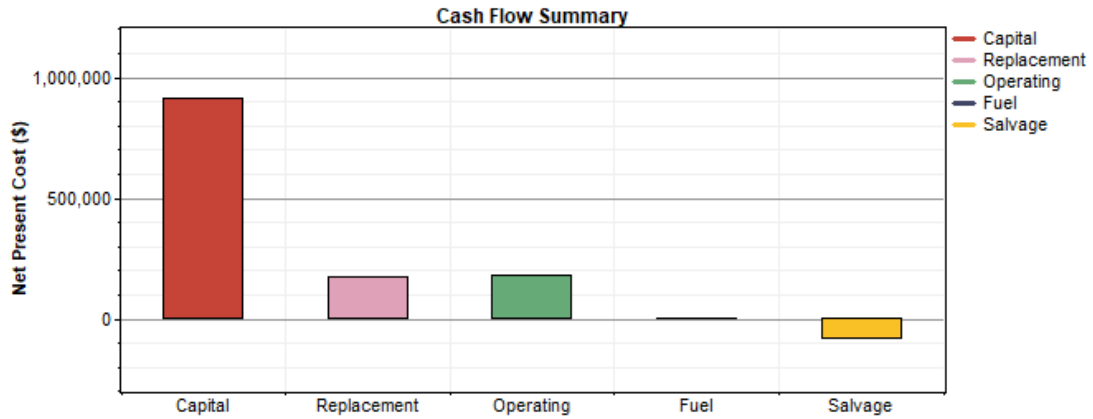
Figure 5.14: Cash Flow Summary of the simulated system by cost type, HOMER software

(Source: HOMER)

The Figure 5.15 describes the monthly average electric production by RES. During the winter months more than 80% of the electric production comes from the Hydro system, while during the summer months the rate tends to reach 50%.
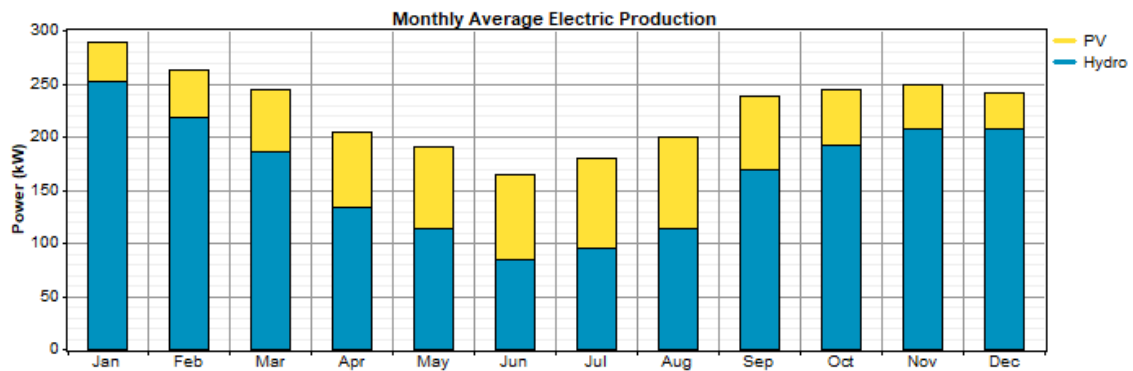
Figure 5.15: Monthly Average Electric Production of the simulated system by RES, HOMER software

(Source: HOMER)

The Figure 5.16 shows the monthly statistics of BESS. During June batteries reach the minimum SOC limit which is 30%.
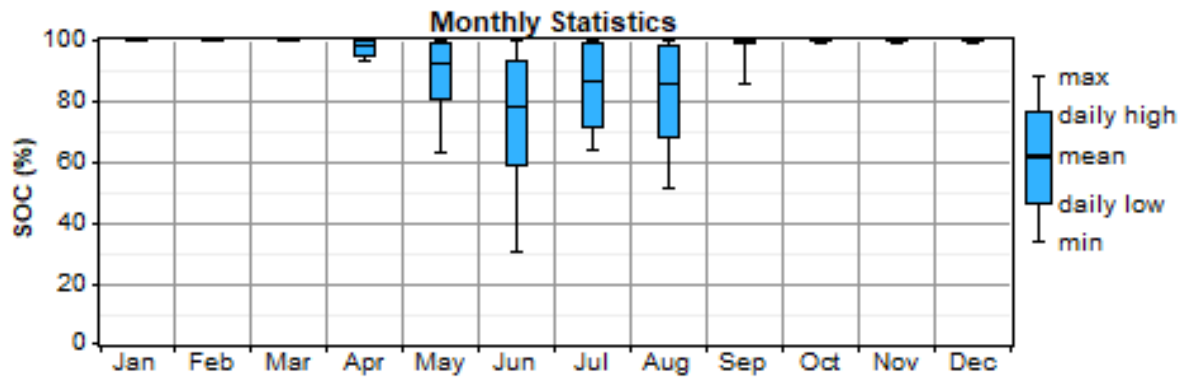
Figure 5.16: Monthly Statistics of the BESS of the simulated system, HOMER software

(Source: HOMER)

CHAPTER 6.   EXTENDED SIMULATION RESULTS

In this chapter four additional simulated scenarios are provided. Through these scenarios the course of load as it increases over time is highlighted, as is the anew examination of optimal sizing of the components in order to meet the new load.

6.1   Load

In subchapter "4.2 Load" the load demand of Corvo Island is presented through the load demand dataset. The Figure 4.1 presents the load demand in 1999 and in 2010. Every year the load increases an average 3%. The "ScenariosLoadDemand" dataset presents the load demand during 2015 (scenario 1), 2020 (scenarios 2 and 3) and 2035 (scenario 4).

The calculations are presented below:

- After 5 years:

$$load_{2015} = load_{2010}1.03^5 = load_{2010}1.16$$

- After 10years:

$$load_{2020} = load_{2010}1.03^{10} = load_{2010}1.34$$

- After 25 years:

$$load_{2035} = load_{2010}1.03^{25} = load_{2010}2.09$$

6.2   Scenarios

6.2.1   Scenario 1: Prediction for the next five years

This scenario presents the load demand after 5 years and highlights how quickly the microgrid needs to evolve in order to avoid unmet load, while still remains dependent exclusively by RESs to produce electricity.

The significant difference from our microgrid in chapter 5 is the load. After the selection of load type (AC or DC), follows the insertion of the load from a time series file ("LoadOf2015.txt"). Figure 6.1 shows the load component produced from the imported file with data for a year.
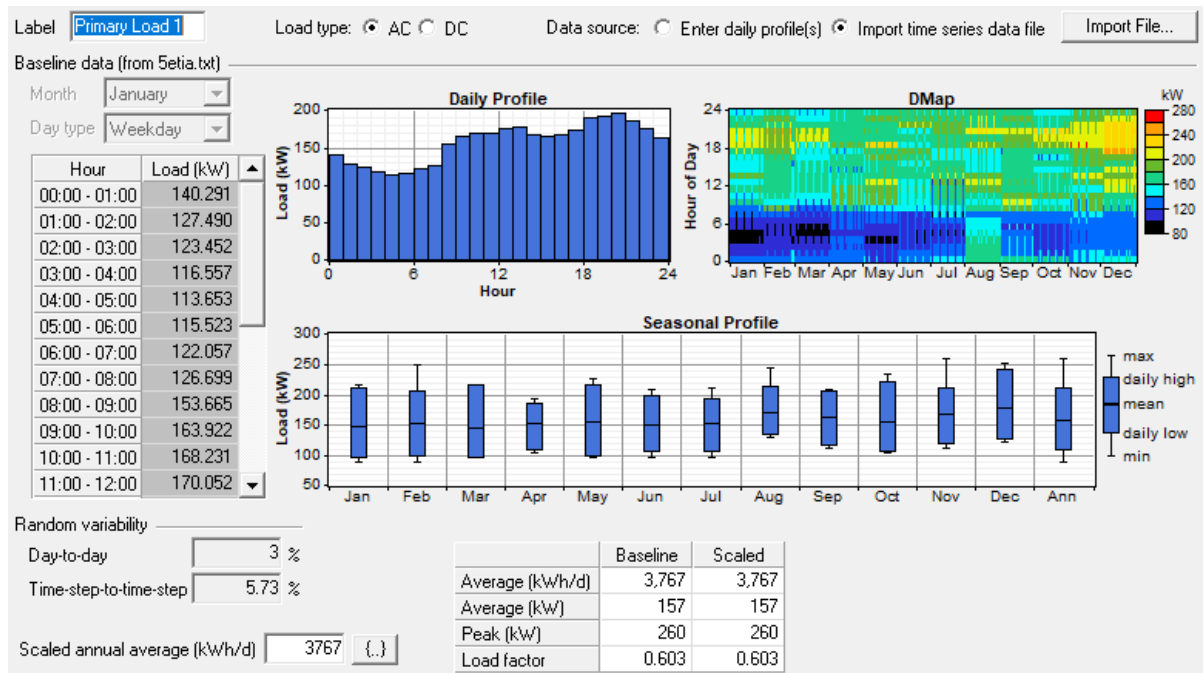
Figure 6.1: Electric Load of measurement of 2015 in Corvo Island, scenario 1, HOMER software

(Source: HOMER)

The system is ready for the final run. The simulation analysis lasted for only two seconds and the results are shown in Figure 6.2.

Sensitivity Results | Optimization Results

Double click on a system below for simulation results.   ○ Categorized ◉ Overall   [Export...]   [Details...]

	PV (kW)	Hydro (kW)	H800	Conv. (kW)	Disp. Strgy	Initial Capital	Operating Cost ($/yr)	Total NPC	COE ($/kWh)	Ren. Frac.
	600	205	936	210	CC	$ 1,253,000	25,567	$ 1,579,832	0.090	1.00
	600	205	936	210	LF	$ 1,253,000	25,567	$ 1,579,832	0.090	1.00
	590	205	960	210	CC	$ 1,255,000	25,836	$ 1,585,267	0.090	1.00
	590	205	960	210	LF	$ 1,255,000	25,836	$ 1,585,267	0.090	1.00
	580	205	984	210	CC	$ 1,257,000	26,104	$ 1,590,701	0.091	1.00
	580	205	984	210	LF	$ 1,257,000	26,104	$ 1,590,701	0.091	1.00
	585	205	984	210	CC	$ 1,262,000	26,154	$ 1,596,340	0.091	1.00
	585	205	984	210	LF	$ 1,262,000	26,154	$ 1,596,340	0.091	1.00
	600	205	960	210	CC	$ 1,265,000	25,936	$ 1,596,545	0.091	1.00
	600	205	960	210	LF	$ 1,265,000	25,936	$ 1,596,545	0.091	1.00
	590	205	984	210	CC	$ 1,267,000	26,204	$ 1,601,979	0.091	1.00
	590	205	984	210	LF	$ 1,267,000	26,204	$ 1,601,979	0.091	1.00
	580	205	1008	210	CC	$ 1,269,000	26,473	$ 1,607,414	0.092	1.00
	580	205	1008	210	LF	$ 1,269,000	26,473	$ 1,607,414	0.092	1.00
	585	205	1008	210	CC	$ 1,274,000	26,523	$ 1,613,053	0.092	1.00
	585	205	1008	210	LF	$ 1,274,000	26,523	$ 1,613,053	0.092	1.00
	600	205	984	210	CC	$ 1,277,000	26,304	$ 1,613,258	0.092	1.00
	600	205	984	210	LF	$ 1,277,000	26,304	$ 1,613,258	0.092	1.00
	590	205	1008	210	CC	$ 1,279,000	26,573	$ 1,618,692	0.092	1.00
	590	205	1008	210	LF	$ 1,279,000	26,573	$ 1,618,692	0.092	1.00
	580	205	1032	210	CC	$ 1,281,000	26,842	$ 1,624,127	0.092	1.00
	580	205	1032	210	LF	$ 1,281,000	26,842	$ 1,624,127	0.092	1.00
	585	205	1032	210	CC	$ 1,286,000	26,892	$ 1,629,766	0.093	1.00
	585	205	1032	210	LF	$ 1,286,000	26,892	$ 1,629,766	0.093	1.00
	600	205	1008	210	CC	$ 1,289,000	26,673	$ 1,629,971	0.093	1.00
	600	205	1008	210	LF	$ 1,289,000	26,673	$ 1,629,971	0.093	1.00
	590	205	1032	210	CC	$ 1,291,000	26,942	$ 1,635,405	0.093	1.00
	590	205	1032	210	LF	$ 1,291,000	26,942	$ 1,635,405	0.093	1.00
	580	205	1056	210	CC	$ 1,293,000	27,210	$ 1,640,839	0.093	1.00
	580	205	1056	210	LF	$ 1,293,000	27,210	$ 1,640,839	0.093	1.00
	585	205	1056	210	CC	$ 1,298,000	27,260	$ 1,646,478	0.094	1.00
	585	205	1056	210	LF	$ 1,298,000	27,260	$ 1,646,478	0.094	1.00
	600	205	1032	210	CC	$ 1,301,000	27,042	$ 1,646,683	0.094	1.00
	600	205	1032	210	LF	$ 1,301,000	27,042	$ 1,646,683	0.094	1.00
	590	205	1056	210	CC	$ 1,303,000	27,310	$ 1,652,117	0.094	1.00
	590	205	1056	210	LF	$ 1,303,000	27,310	$ 1,652,117	0.094	1.00
	600	205	1056	210	CC	$ 1,313,000	27,410	$ 1,663,396	0.095	1.00
	600	205	1056	210	LF	$ 1,313,000	27,410	$ 1,663,396	0.095	1.00

⚠ PV search space may be insufficient.

ⓘ Completed in 1 seconds.

Figure 6.2: Results of scenario 1, system in 5 year time, HOMER software

(Source: HOMER)

It is reminded that LF and CC are two potential operating strategies (page 91). In this case where the system's load is covered exclusively by RES there isn't any difference between the two strategies.

The optimum economic layout (highlited alternative in Figure 6.2) includes 205kW Hydro, 600kW PV, 936 batteries and a 210kW converter.

Table 6.1– Cost analysis of optimized simulated system, HOMER software

COMPONENT	CAPITAL ($)	REPLACEMENT ($)	O&M ($)	FUEL ($)	SALVAGE ($)	TOTAL ($)
PV	600,000	0	76,700	0	0	676,700
HYDRO	80,000	0	30,680	0	0	110,680
BESS	468,000	145,925	119,652	0	-81,783	651,795
CONVERTER	105,000	43,813	0	0	-8,155	140,658
SYSTEM	1,253,000	189,738	227,033	0	-89,938	1,579,833

A visual representation of the cost is available in Figure 6.3 and 6.4 below.
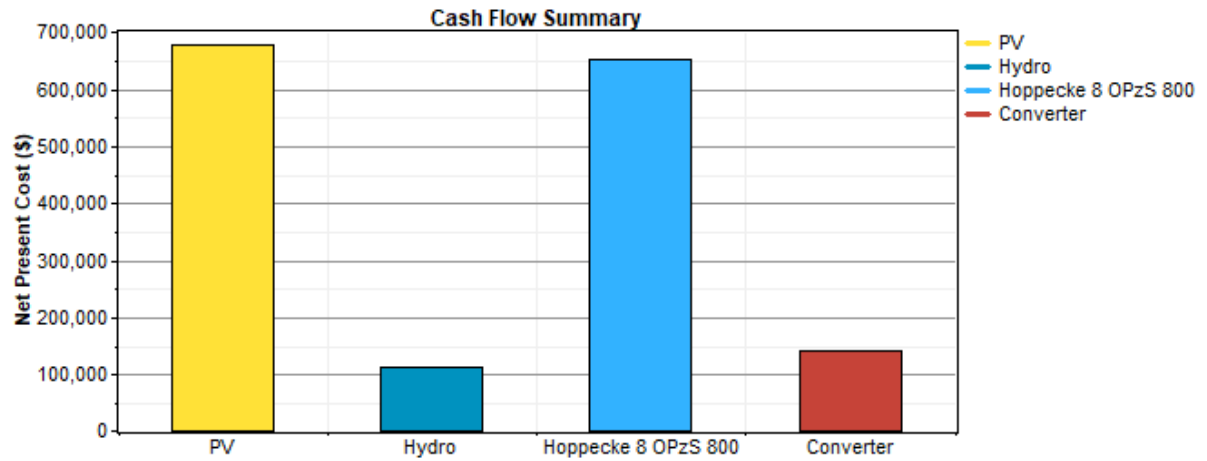
Figure 6.3: Cash Flow Summary of the simulated system by component, scenario 1, HOMER software

(Source: HOMER)

The net present cost (Total NPC) is 1,579,832$, and the cost of electricity (COE) is 0.090$/kWh. The operating cost of the microgrid is 25,567$/year.
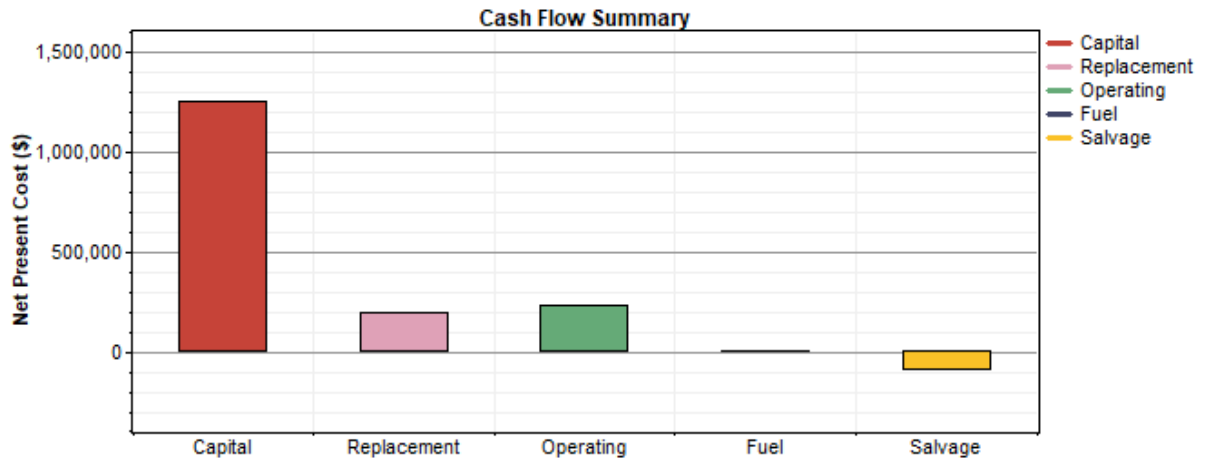
Figure 6.4: Cash Flow Summary of the simulated system by cost type, scenario 1, HOMER software

(Source: HOMER)

The Figure 6.5 describes the monthly average electric production by RES. During the winter months more than 80% of the electric production comes from the Hydro system, while during the summer months the rate tends to reach 50%.
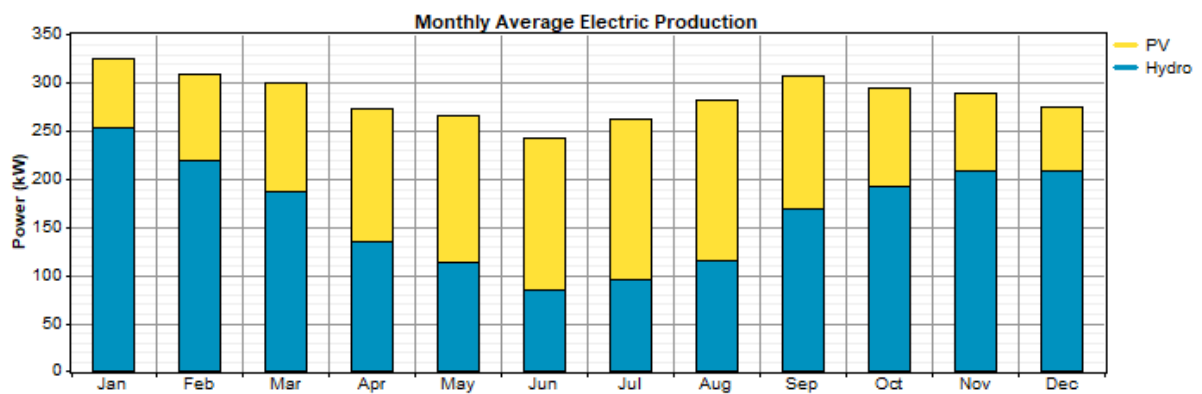
Figure 6.5: Monthly Average Electric Production of the simulated system by RES, scenario 1, HOMER software

(Source: HOMER)

The Figure 6.6 shows the monthly statistics of BESS. During June batteries reach the minimum SOC limit which is 30%.
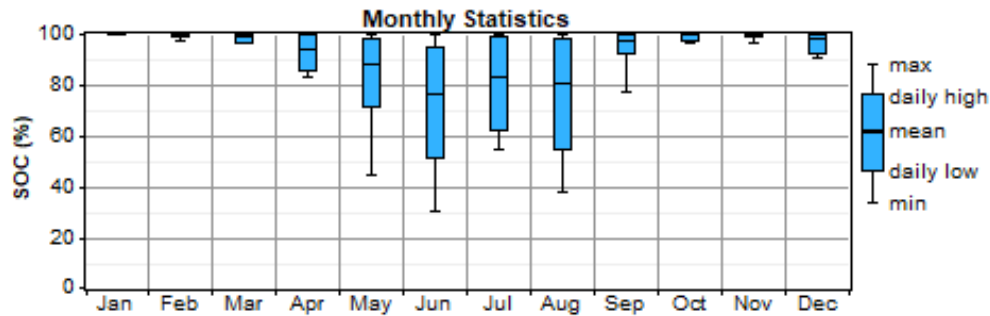
Figure 6.6: Monthly Statistics of the BESS of the simulated system, scenario 1, HOMER software

(Source: HOMER)

6.2.2   *Scenario 2: Prediction for the next ten years*

This scenario presents the load demand after 10 years and highlights how quickly the microgrid needs to keep evolving in order to avoid unmet load, while still remains dependent exclusively by RESs to produce electricity. As load increases it is very difficult to keep the electric production completely friendly towards the environment especially in an island like Corvo which is very limited in space. (Larger battery storage and more PV panels mean more terrain.)

The significant difference from our microgrid in chapter 5 is the load. After the selection of load type (AC or DC), follows the insertion of the load from a time series file ("LoadOf2020.txt"). Figure 6.7 shows the load component produced from the imported file with data for a year.
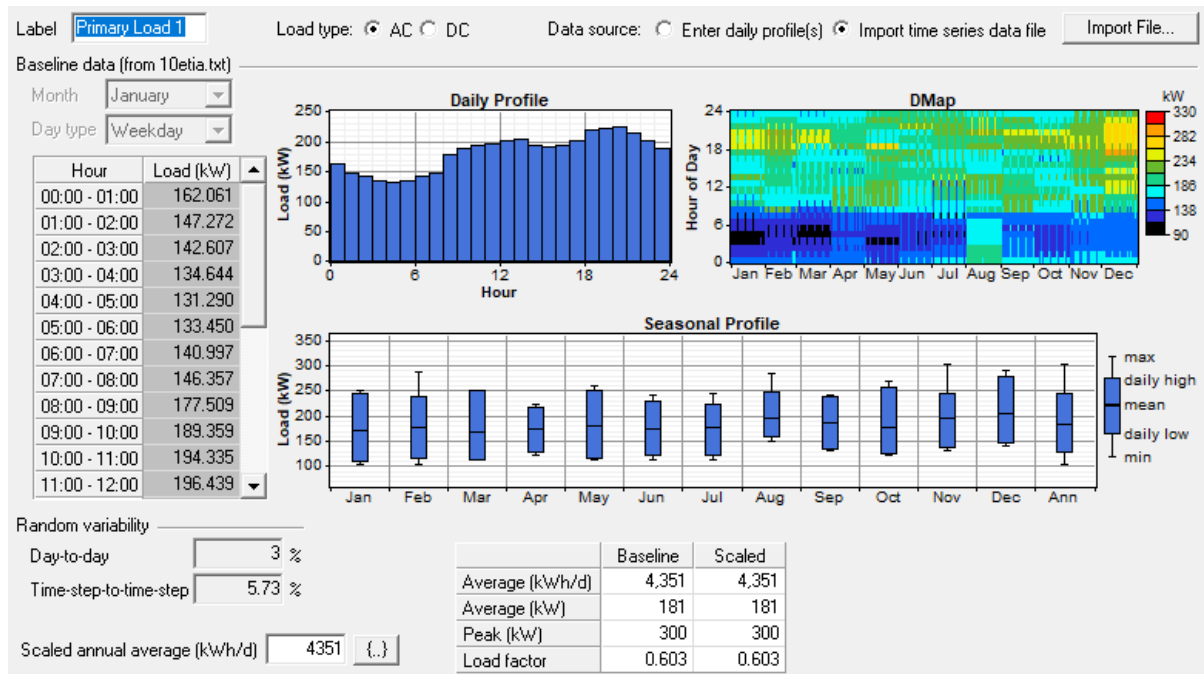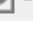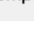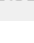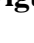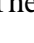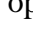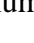
Figure 6.7: Electric Load of measurement of 2020 in Corvo Island, scenario 2, HOMER software

(Source: HOMER)

The system is ready for the final run. The simulation analysis lastedfor only three seconds and the results are shown in Figure 6.8.

	PV (kW)	Hydro (kW)	H800	Conv. (kW)	Disp. Strgy	Initial Capital	Operating Cost ($/yr)	Total NPC	COE ($/kWh)	Ren. Frac.
	875	205	1248	210	CC	$ 1,684,000	33,110	$ 2,107,251	0.104	1.00
	875	205	1248	210	LF	$ 1,684,000	33,110	$ 2,107,251	0.104	1.00
	890	205	1224	210	CC	$ 1,687,000	32,951	$ 2,108,221	0.104	1.00
	890	205	1224	210	LF	$ 1,687,000	32,951	$ 2,108,221	0.104	1.00
	900	205	1200	210	CC	$ 1,685,000	33,270	$ 2,110,303	0.104	1.00
	900	205	1200	210	LF	$ 1,685,000	33,270	$ 2,110,303	0.104	1.00
	880	205	1248	210	CC	$ 1,689,000	33,160	$ 2,112,891	0.104	1.00
	880	205	1248	210	LF	$ 1,689,000	33,160	$ 2,112,891	0.104	1.00
	855	205	1296	210	CC	$ 1,688,000	33,647	$ 2,118,120	0.104	1.00
	855	205	1296	210	LF	$ 1,688,000	33,647	$ 2,118,120	0.104	1.00
	870	205	1272	210	CC	$ 1,691,000	33,428	$ 2,118,325	0.104	1.00
	870	205	1272	210	LF	$ 1,691,000	33,428	$ 2,118,325	0.104	1.00
	900	205	1224	210	CC	$ 1,697,000	33,045	$ 2,119,431	0.104	1.00
	900	205	1224	210	LF	$ 1,697,000	33,045	$ 2,119,431	0.104	1.00
	860	205	1296	210	CC	$ 1,693,000	33,697	$ 2,123,759	0.105	1.00
	860	205	1296	210	LF	$ 1,693,000	33,697	$ 2,123,759	0.105	1.00
	875	205	1272	210	CC	$ 1,696,000	33,478	$ 2,123,964	0.105	1.00
	875	205	1272	210	LF	$ 1,696,000	33,478	$ 2,123,964	0.105	1.00
	890	205	1248	210	CC	$ 1,699,000	33,260	$ 2,124,169	0.105	1.00
	890	205	1248	210	LF	$ 1,699,000	33,260	$ 2,124,169	0.105	1.00
	850	205	1320	210	CC	$ 1,695,000	33,966	$ 2,129,194	0.105	1.00
	850	205	1320	210	LF	$ 1,695,000	33,966	$ 2,129,194	0.105	1.00
	880	205	1272	210	CC	$ 1,701,000	33,528	$ 2,129,603	0.105	1.00
	880	205	1272	210	LF	$ 1,701,000	33,528	$ 2,129,603	0.105	1.00
	840	205	1344	210	CC	$ 1,697,000	34,234	$ 2,134,628	0.105	1.00
	840	205	1344	210	LF	$ 1,697,000	34,234	$ 2,134,628	0.105	1.00
	855	205	1320	210	CC	$ 1,700,000	34,016	$ 2,134,833	0.105	1.00
	855	205	1320	210	LF	$ 1,700,000	34,016	$ 2,134,833	0.105	1.00
	870	205	1296	210	CC	$ 1,703,000	33,797	$ 2,135,038	0.105	1.00

Completed in 3 seconds.

Figure 6.8: Results of the simulated system, scenario 2, HOMER software

(Source: HOMER)

The optimum economic layout (highlited alternative in Figure 6.8) includes 205kW Hydro, 875kW PV, 1248 batteries and a 210kW converter.

Table 6.2– Cost analysis of optimized simulated system, HOMER software

COMPONENT	CAPITAL ($)	REPLACEMENT ($)	O&M ($)	FUEL ($)	SALVAGE ($)	TOTAL ($)
PV	875,000	0	111,854	0	0	986,855
HYDRO	80,000	0	30,680	0	0	110,680
BESS	624,000	194,566	159,536	0	-109,044	869,059
CONVERTER	105,000	43,813	0	0	-8,155	140,658
SYSTEM	1,684,000	238,379	302,071	0	-117,198	2,107,252

A visual representation of the cost is available in Figure 6.9 and 6.10 below.
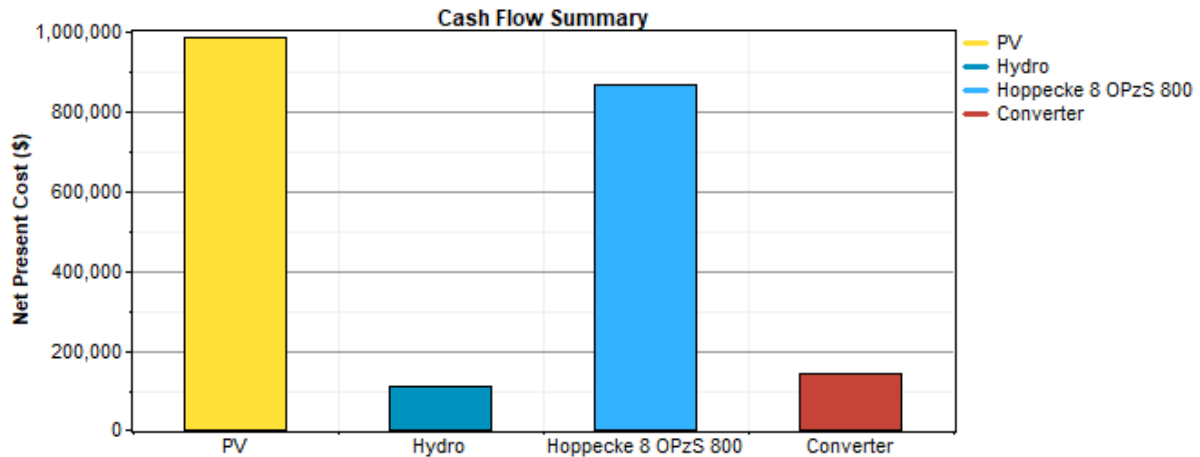
Figure 6.9: Cash Flow Summary of the simulated system by component, scenario 2, HOMER software

(Source: HOMER)

The net present cost (Total NPC) is 2,107,251$, and the cost of electricity (COE) is 0.104$/kWh. The operating cost of the microgrid is 33,110$/year.
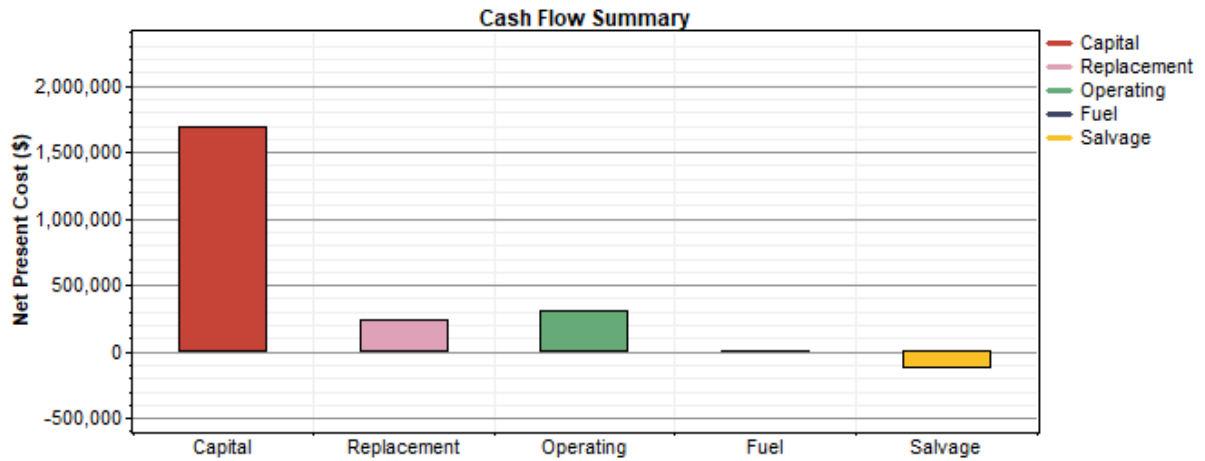
Figure 6.10: Cash Flow Summary of the simulated system by cost type, scenario 2, HOMER software

(Source: HOMER)

The Figure 6.11 describes the monthly average electric production by RES. During the winter months more than 60% of the electric production comes from the Hydro system, while during the summer months the rate drops lower than 30%.
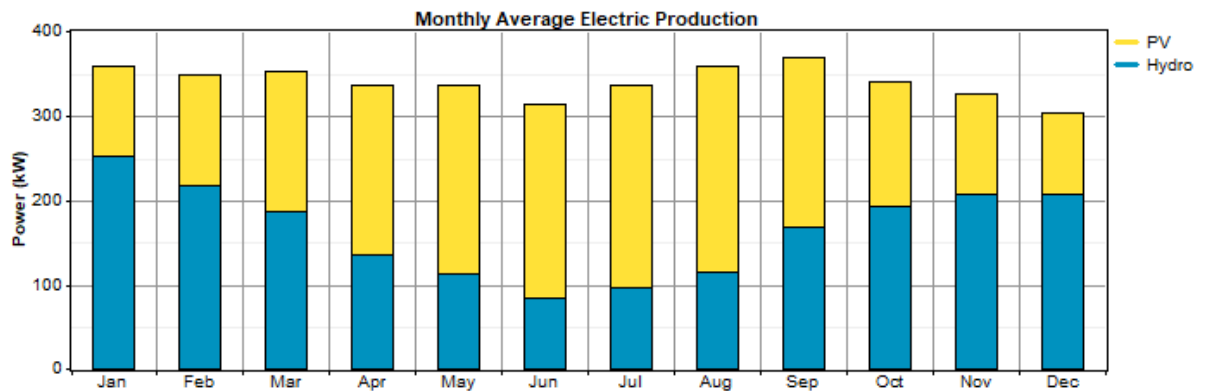
Figure 6.11: Monthly Average Electric Production of the simulated system by RES, scenario 2, HOMER software

(Source: HOMER)

The Figure 6.12 shows the monthly statistics of BESS. During May, June and August batteries reach the minimum SOC limit which is 30%.
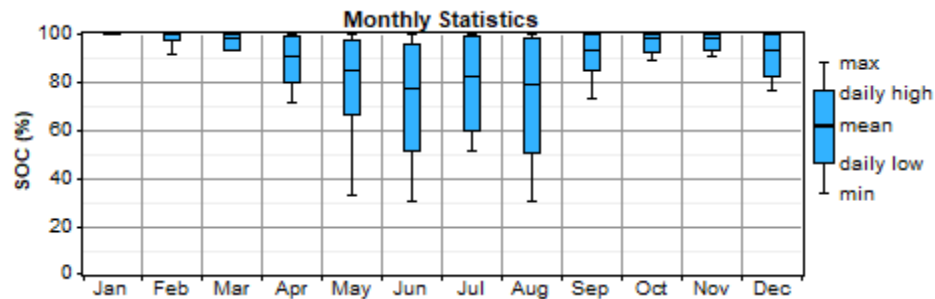
Figure 6.12: Monthly Statistics of the BESS of the simulated system, scenario 2, HOMER software

(Source: HOMER)

6.2.3 Scenario 3: Prediction for the next ten years, RES and generator combined

As seen from the previous scenario above, a 100% renewable system would require extremely large battery storage which leads in need of more space for the increased number of both batteries and PV panels. This is very difficult for a small island such as Corvo with limited soil. This is why in this scenario oil generators are introduced, while the load remains the same (load prediction for 2020).

The significant difference from our microgrid in chapter 5 is the load (the same as of scenario 2, page 101, imported time series file "LoadOf2020.txt") and the insertion of one generator. In this scenario the rest of the components remain the same as of scenario 1. This means that our microgrid consists of 205kW Hydro, 600kW PV, 936 batteries, a 210kW converter and an oil generator yet to be optimum sized.
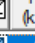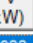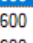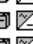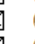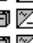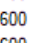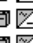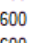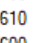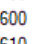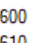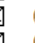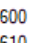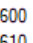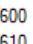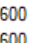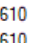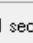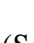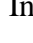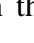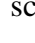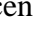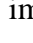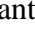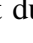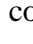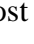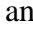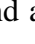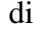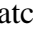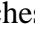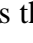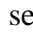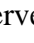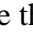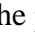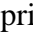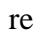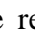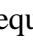
The generator component in HOMER (Figure 6.13) allows the user to choose a fuel (b), enter sizes for optimization through the Consider table (a), enter capital cost and operation&maintenance (O&M) value (a).

124
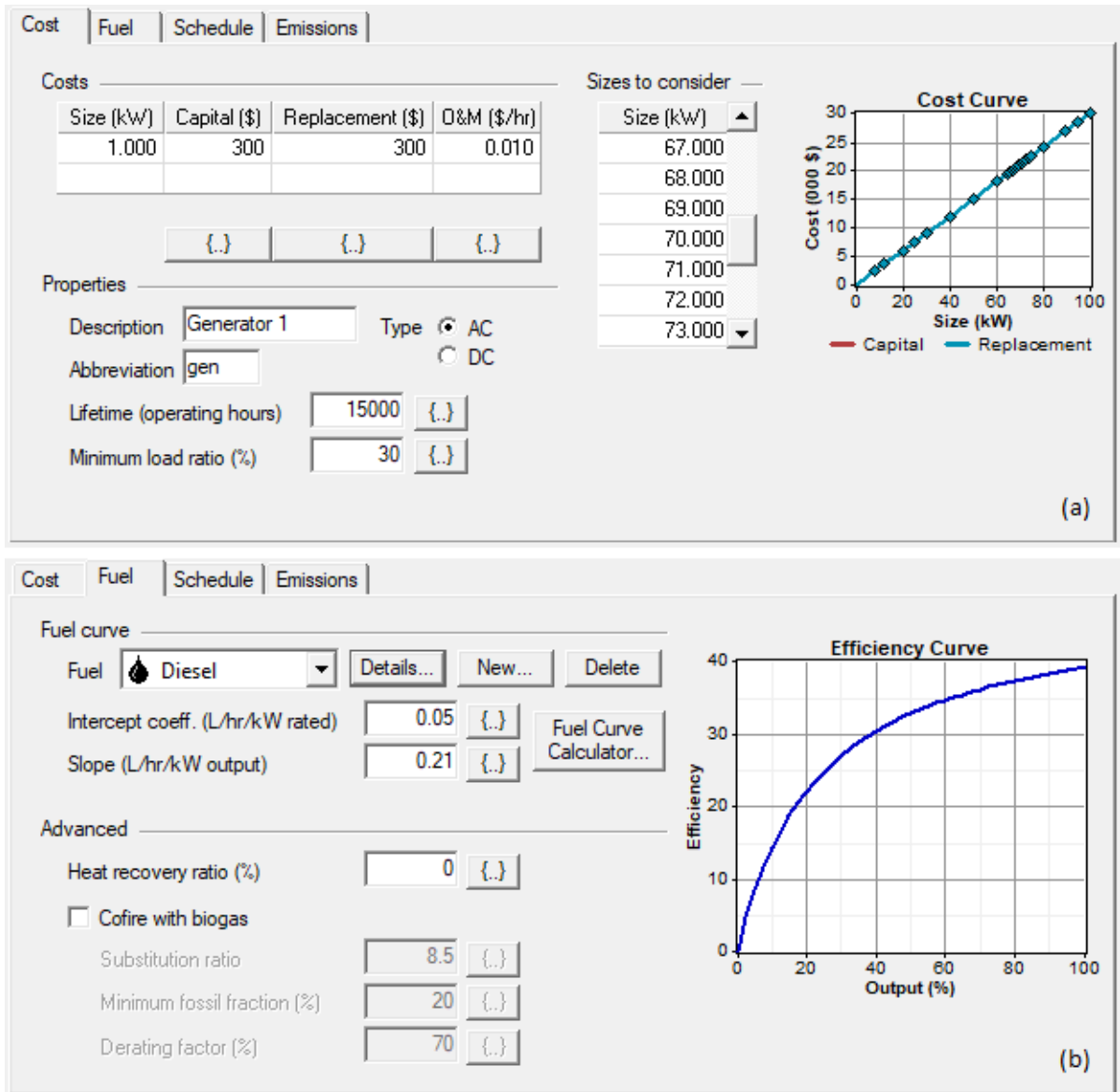
Figure 6.13: Simulated Diesel Generator, (a) Cost Tab with Consider table Optimization, (b) Fuel Tab, scenario 3, HOMER software

(Source: HOMER)

The system is ready for the final run. The simulation analysis lastedfor only forty two seconds and the results are shown in Figure 6.14.

Figure 6.14: Results of the simulated system, scenario 3, HOMER software

(Source: HOMER)

In this scenario (as well as in scenario 4) the operating strategy of the system is very important due to the generator. If the strategy is misselected may cause increase in fuel cost and added impact in the environmen. Under the Load Following strategy, HOMER dispatches the system's controllable power sources (generators and storage bank) so as to serve the primary load at the least total cost each time step, while satisfying the operating reserve requirement. (The operating reserve requirement is the minimum amount of operating reserve that the system must be capable of providing.) The total cost includes the cost of fuel, operation and maintenance, and replacement [48].

The optimum economic layout (highlited alternative in Figure 6.14) includes 205kW Hydro, 600kW PV, 936 batteries, 210kW converter and a 70kW generator.

Table 6.3– Cost analysis of optimized simulated system, scenario 3, HOMER software

COMPONENT	CAPITAL ($)	REPLACEMENT ($)	O&M ($)	FUEL ($)	SALVAGE ($)	TOTAL ($)
PV	600,000	0	76,700	0	0	676,700
HYDRO	80,000	0	30,680	0	0	110,680
GENERATOR 1	21,000	0	1,253	20,824	-3,751	39,326
BESS	468,000	189,091	119,652	0	-42,807	733,936
CONVERTER	105,000	43,813	0	0	-8,155	140,658
SYSTEM	1,274,000	232,904	228,285	20,824	-54,713	1,701,300

A visual representation of the cost is available in Figure 6.15 and 6.16 below.
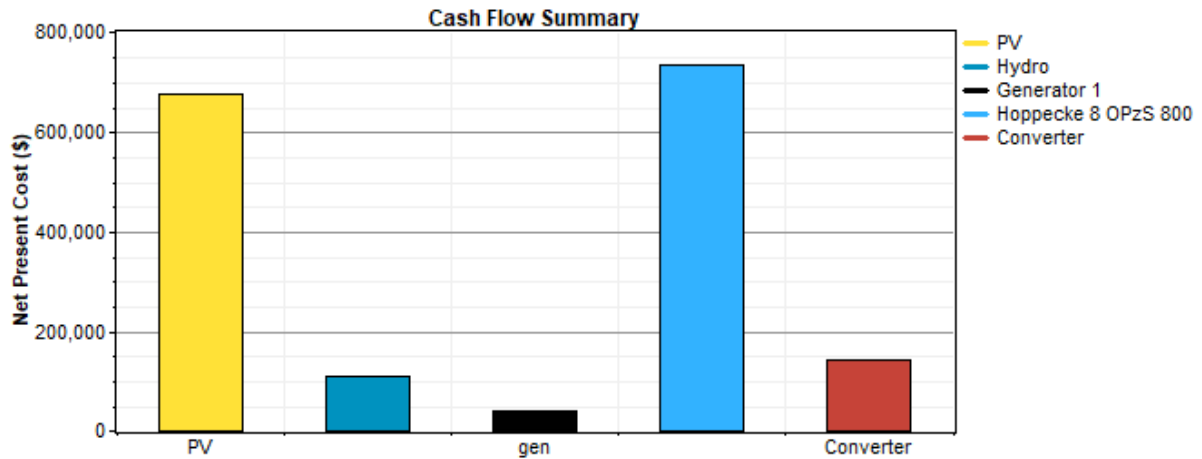
Figure 6.15: Cash Flow Summary of the simulated system by component, scenario 3, HOMER software

(Source: HOMER)

The net present cost (Total NPC) is 1,701,300$, and the cost of electricity (COE) is 0.084$/kWh. The operating cost of the microgrid is 33,426$/year.
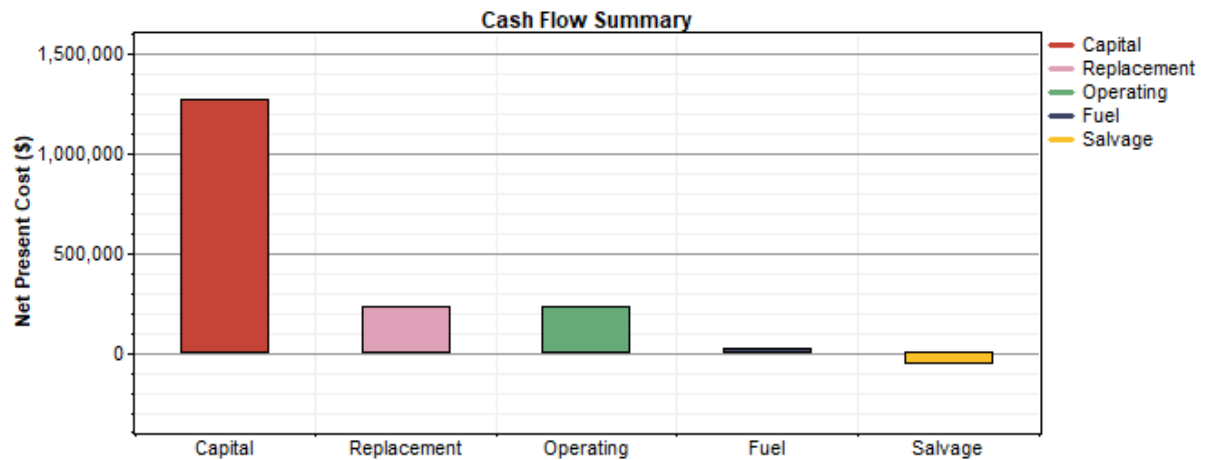
Figure 6.16: Cash Flow Summary of the simulated system by cost type, scenario 3, HOMER software

(Source: HOMER**)**

The Figure 6.17 describes the monthly average electric production by RES. During the winter months more than 80% of the electric production comes from the Hydro system, while during the summer months the rate drops lower than 40%.
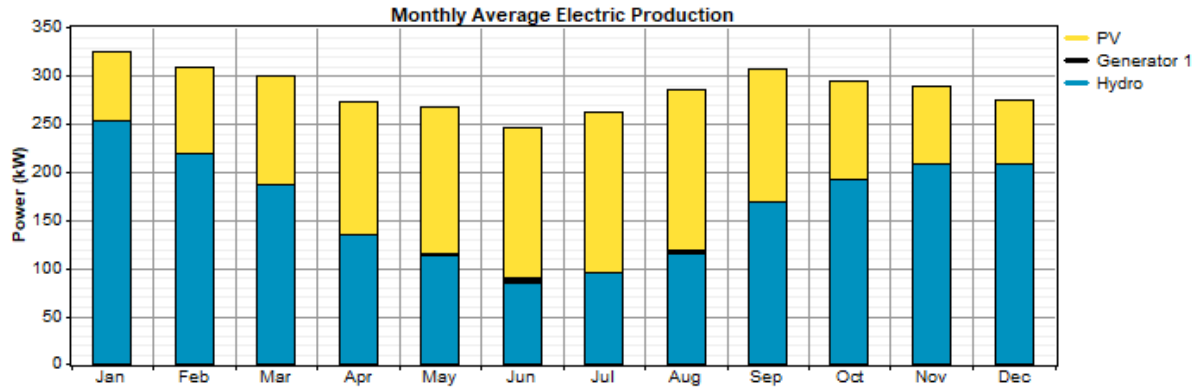
Figure 6.17: Monthly Average Electric Production of the simulated system by source, scenario 3, HOMER software

(Source: HOMER)

The Figure 6.18 shows the monthly statistics of BESS. During May, June, July and August batteries reach the minimum SOC limit which is 30%.
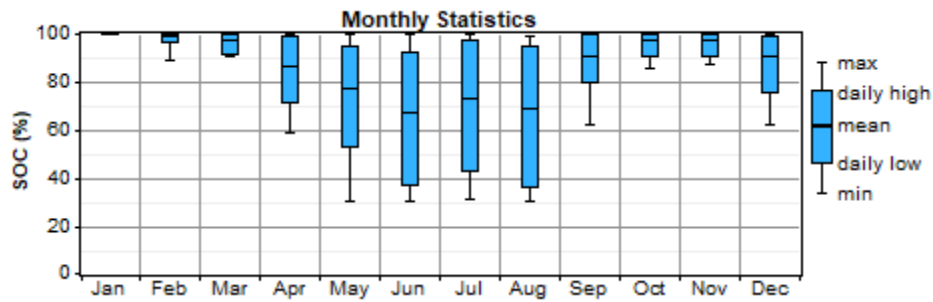
Figure 6.18: Monthly Statistics of the BESS of the simulated system, scenario 3. HOMER software

(Source: HOMER)

6.2.4 Scenario 4: Prediction for the next twenty five years, RES and generators combined

In scenario 4 the load has been increased over 2 times (page 95) since the demand in 2010. As mentioned before, a 100% renewable system would require extremely large battery storage and PV production which leads in need of more space for the increased number of both batteries and PV panels. This is very difficult for a small island such as Corvo with limited soil.

In this scenario electricity produced dy diesel generators is escalated. The significant difference from our microgrid in chapter 5 is the load and the generators. In this scenario the rest of the components remain the same as of the scenario 3. This means that our microgrid consists of 205kW Hydro, 600kW PV, 936 batteries, a 210kW converter and a 70kW diesel generator already.

- Load: After the selection of load type (AC or DC), follows the insertion of the load from a time series file ("LoadOf2035.txt"). Figure 6.19 shows the load component produced from the imported file with data for a year.
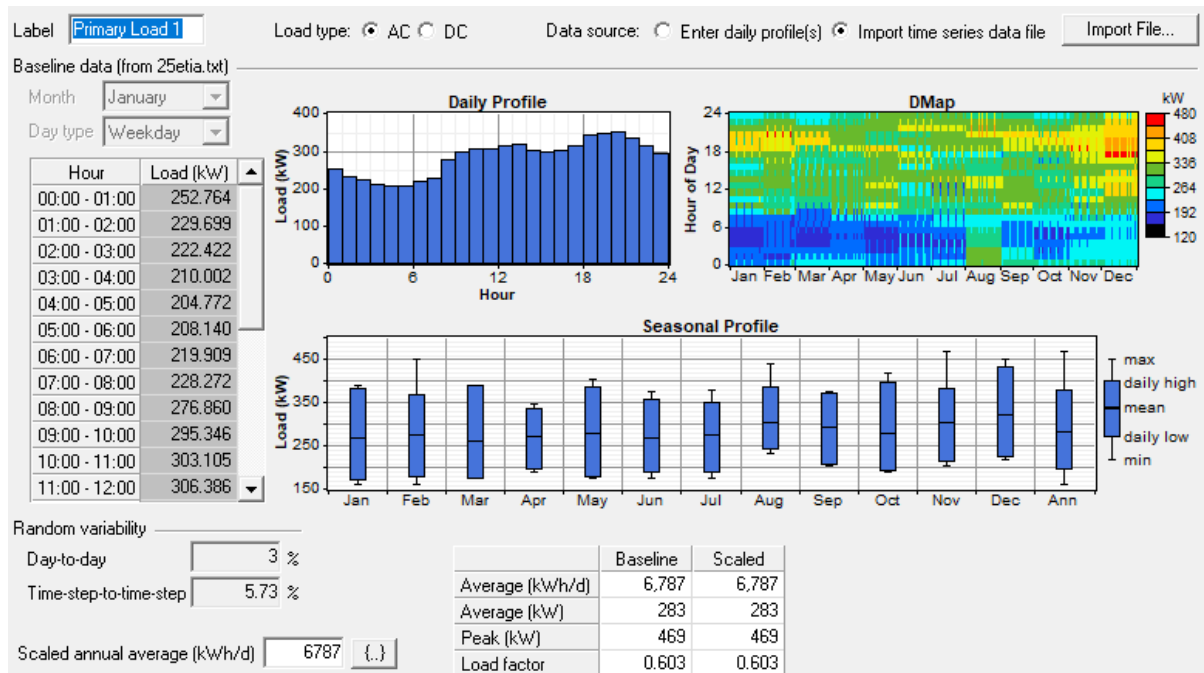
Figure 6.19: Electric Load of measurement of 2035 in Corvo Island, scenario 4, HOMER software
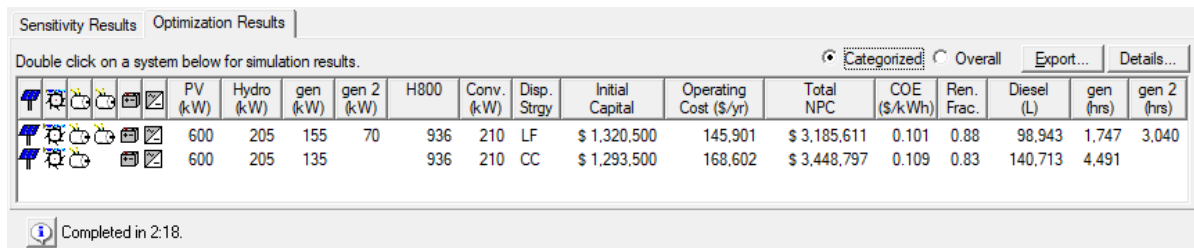
(Source: HOMER)

130

-   Second Generator:

The generator component in HOMER (Figure 6.13) allows the user to choose a fuel (b), enter sizes for optimization through the Consider table (a), enter capital cost and operation&maintenance (O&M) value (a) (page 106).

(a)

(b)
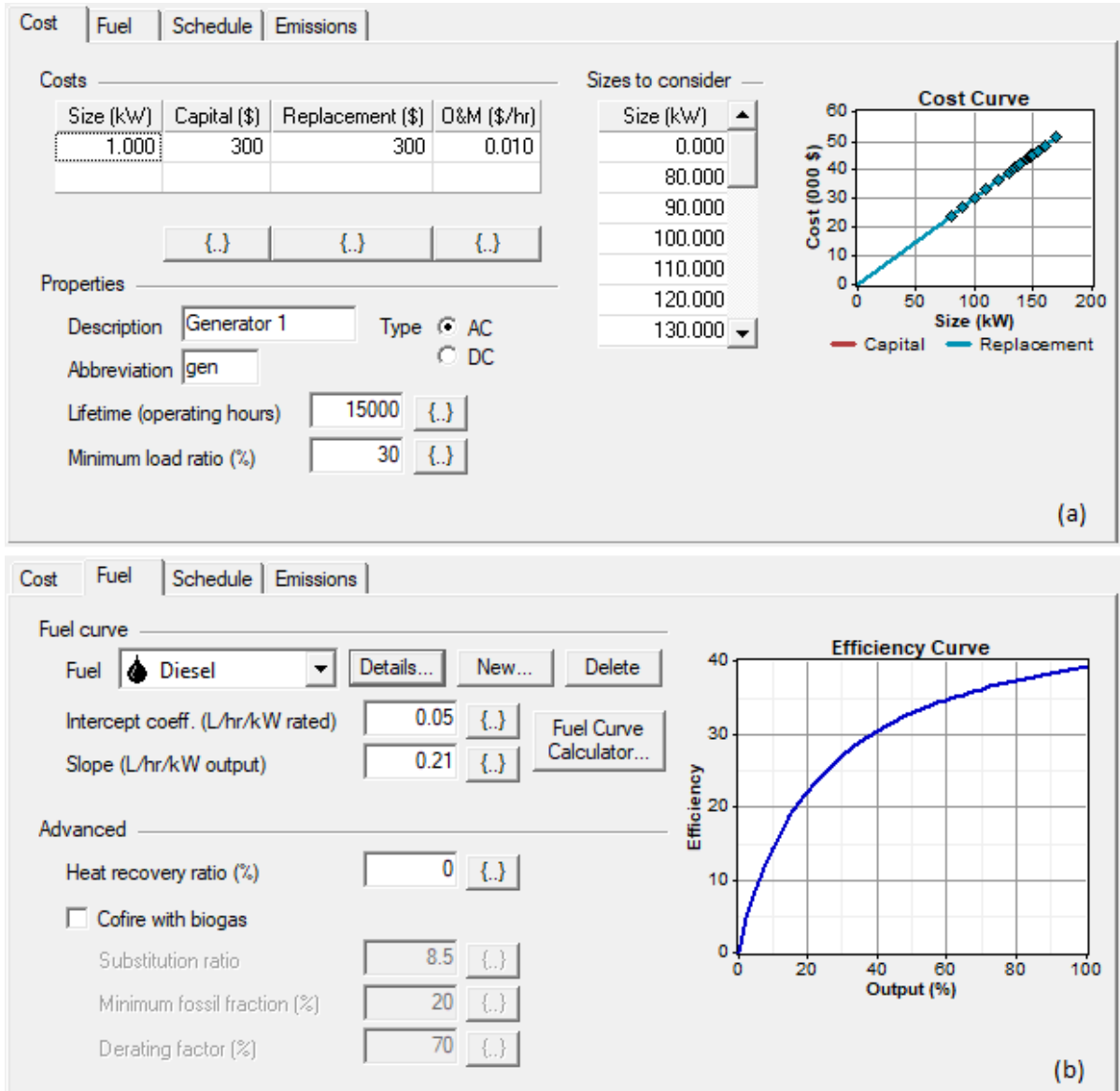
Figure 6.20: Second Simulated Diesel Generator, (a) Cost Tab with Consider table Optimization, (b) Fuel Tab, scenario 4, HOMER software

(Source: HOMER)

Lastly, the system is ready for the final run. The simulation analysis lastedfor two minutes and eighteen seconds and the optimum results for each operational strategy are shown in Figure 6.21.

	PV (kW)	Hydro (kW)	gen (kW)	gen 2 (kW)	H800	Conv. (kW)	Disp. Strgy	Initial Capital	Operating Cost ($/yr)	Total NPC	COE ($/kWh)	Ren. Frac.	Diesel (L)	gen (hrs)	gen 2 (hrs)
	600	205	155	70	936	210	LF	$ 1,320,500	145,901	$ 3,185,611	0.101	0.88	98,943	1,747	3,040
	600	205	135		936	210	CC	$ 1,293,500	168,602	$ 3,448,797	0.109	0.83	140,713	4,491	

Figure 6.21: Results of the simulated system, optimum alternative for LF and CC strategy, scenario 4, HOMER software

(Source: HOMER)

The optimum economic layout includes 205kW Hydro, 304kW PV, 840 batteries, 210kW converter and two generators, one of 70kW and one of 155kW.

Table 6.4– Cost analysis of optimized simulated system, scenario 4, HOMER software

COMPONENT	CAPITAL ($)	REPLACEMENT ($)	O&M ($)	FUEL ($)	SALVAGE ($)	TOTAL ($)
PV	600,000	0	76,700	0	0	676,700
HYDRO	80,000	0	30,680	0	0	110,680
GENERATOR	46,500	45,291	34,615	605,478	-957	730,927
GENERATOR 2	21,000	48,070	27,203	406,377	-4,567	498,083
BESS	468,000	453,195	119,652	0	-12,284	1,028,568
CONVERTER	105,000	43,813	0	0	-8,155	140,658
SYSTEM	1,320,500	590,369	288,851	1,011,855	-25,963	3,185,612

A visual representation of the cost is available in Figure 6.22 and 6.23 below.
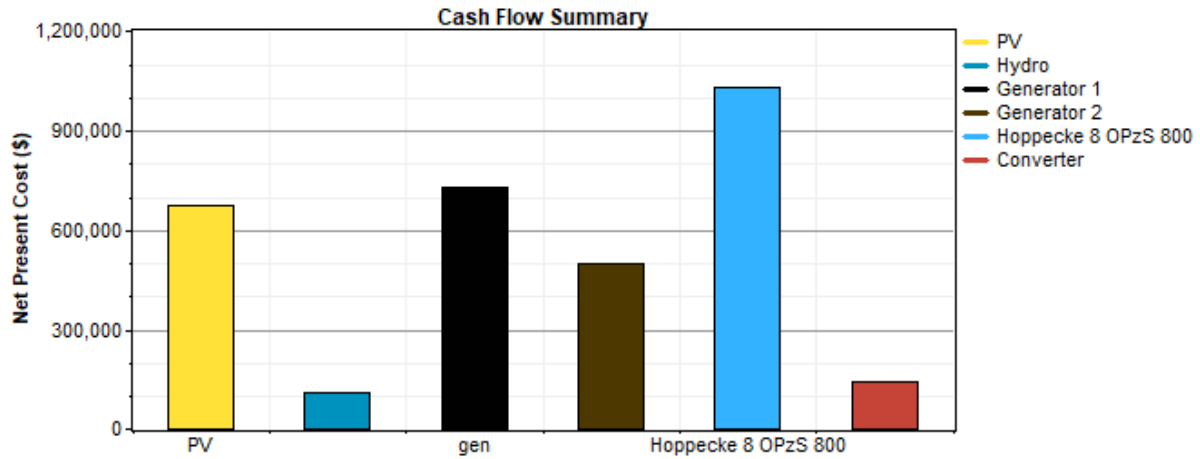
Figure 6.22: Cash Flow Summary of the simulated system by component, scenario 4, HOMER software

(Source: HOMER)

The net present cost (Total NPC) is 3,185,611$, and the cost of electricity (COE) is 0.101$/kWh. The operating cost of the microgrid is 145,901$/year.
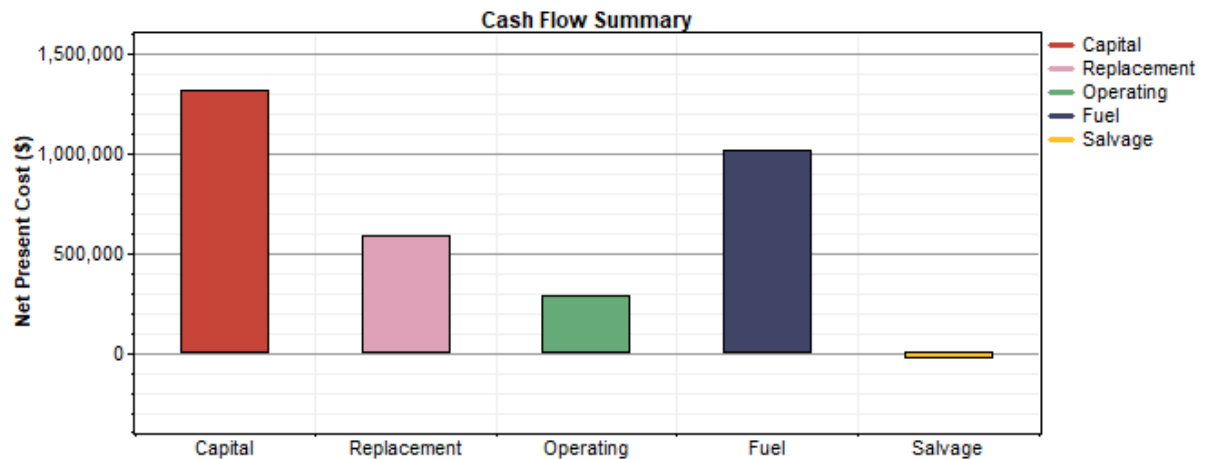
Figure 6.23: Cash Flow Summary of the simulated system by cost type, scenario 4, HOMER software

(Source: HOMER)

The Figure 6.24 describes the monthly average electric production by RES. During the winter months more than 80% of the electric production comes from the Hydro system, while during the summer months the rate tends to reach 30%.
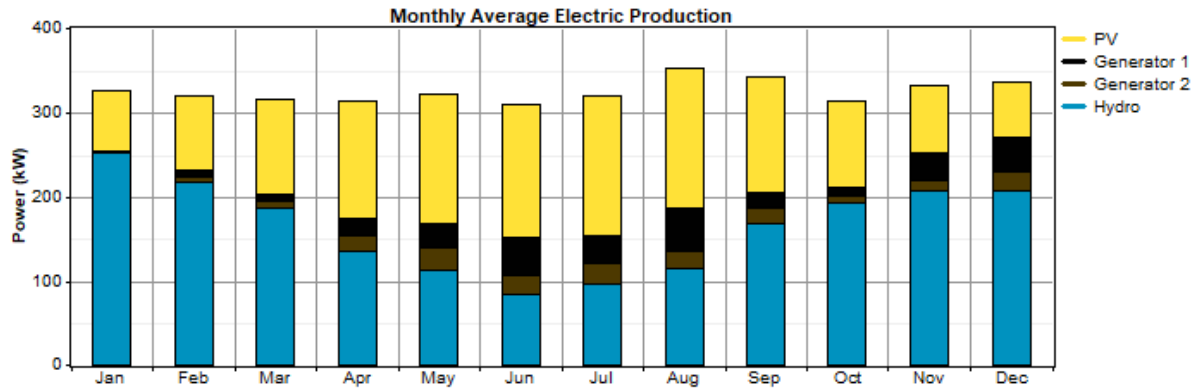
Figure 6.24: Monthly Average Electric Production of the simulated system by RES, scenario 4, HOMER software

(Source: HOMER)

The Figure 6.25 shows the monthly statistics of BESS. During June batteries reach the minimum SOC limit which is 30%.
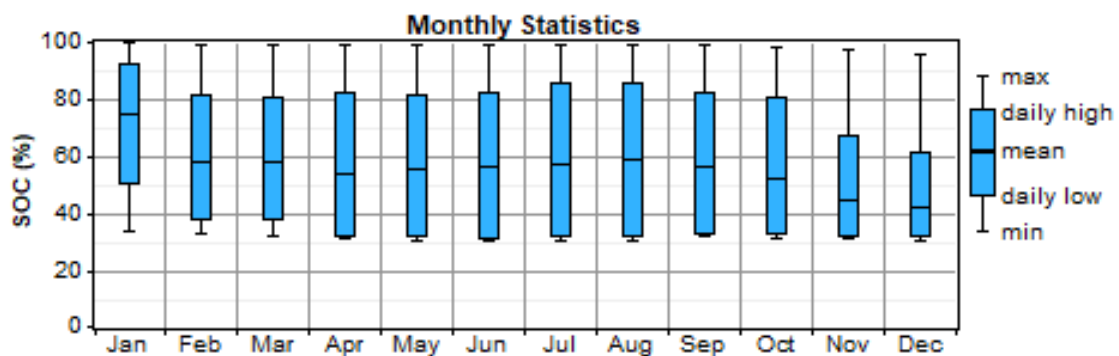
Figure 6.25: Monthly Statistics of the BESS of the simulated system, scenario 4, HOMER software

(Source: HOMER)

6.3   Results of the simulated scenarios

The architecture of each scenario is displayed in table 6.5, including the initial microgrid of 2010, while the same values in percentage are presented in comparison with the initial microgrid in table 6.6.

Table 6.5– Presentation of the architecture of each simulated system per scenario, HOMER software

SYSTEM of	LOAD (kW)	HYDRO (kW)	PV (kW)	BATTERIES	GEN. 1 (kW)	GEN. 2 (kW)
2010	135	205	304	840	-	-
2015	157	205	600	936	-	-
2020 RES	181	205	875	1248	-	-
2020	181	205	600	936	70	-
2035	283	205	600	936	70	155

Table 6.6– Comparison of the architecture of each simulated system per scenario, HOMER software

SYSTEM of	LOAD	HYDRO	PV (kW)	BATTERIES
2015	+16.3%	0%	+97.4%	+11.4%
2020 RES	+34.1%	0%	+187.8	+48.6%
2020	+34.1%	0%	+97.4%	+11.4%
2035	+109.6%	0%	+97.4%	+11.4%

A description of the most important economic values associated with each scenario is presented in table 6.7, as well as the Carbon dioxide emissions. Table 6.8 compares the economic results from the initial microgrid with the microgrids in all four scenarios in percentage.

Table 6.7– Cost analysis and Carbon dioxide Emissions of each simulated system, HOMER software

SYSTEM of	TOTAL NPC ($)	LCOE ($/kWh)	OPERATING COST ($/yr)	EMISSIONS (kg/yr)
2010	1,179,143	0.078	21,132	-
2015	1,579,832	0.090	25,567	-
2020 RES	2,107,251	0.104	33,110	-
2020	1,701,300	0.084	33,426	5,362
2035	3,185,611	0.101	145,901	250,548

Table 6.8– Comparison of cost analysis of each simulated system, HOMER software

SYSTEM of	TOTAL NPC	LCOE	OPERATING COST
2015	+34%	+15.4%	+21%
2020 RES	+78.7%	+33.3%	+56.7%
2020	+44.3%	+7.7%	+58.2%
2035	+170.2%	+29.5%	+590.4%

For the first 5 years the avoidance of fossil fuels penetrating the microgrid is feasible. Observing the next scenarios of 2020, it's clear that each of the two combinations of grid is capable of meeting the load. (HOMER have set that it only performs economic calculations when the system is technically feasible.) Despite the amount of emissions, the system with the generator prevails due to the reduced cost.

The same philosophy expands in scenario 4, which the percentage of the load has reached 209.6%. Without the use of generators the system couldn't possibly produce enough energy to cover the demand considering the prohibitive costs and the huge quantities of batteries and PV panels. This leads to the conclusion that under these circumstances (with limited soil and money and using current technology of reduced efficiency of the components), trying to

create a microgrid depending exclusively in RESs would not only be a luxury, but a futile attempt.

CHAPTER 7.   CONCLUSION AND FUTURE WORK

7.1   Conclusion

The aim of this thesis is to determine the possibility of a stand-alone renewable energy system which is able to satisfy the load demand and to present the optimal sizing of its components by using HOMER software. Stand-alone power system can eliminate the need to build expensive grid to rural area. Solar and hydro offer tremendous advantages as the main supply for this system.

However, stand-alone system depending exclusively in RESs has its own weaknesses where it is very high in cost due to low efficiency of some of its components, such as the PV subsystem. The proper design of the system is vital to ensure its feasibility, while the cost remains affordable, as it takes full advantage of the electrical potential.

Wide range of factors need to be considered prior to start developing a system which include suitable selection of site, hydro flow rates, solar irradiances and balance of a system components such as inverters, batteries and controllers. Due to the high rates of feed in tariff and capital cost, it is necessary to identify the system life cycle cost or Total Net Present Cost (TNPC) to achieve optimal hybrid energy system. It is important to observe the realistic effect on power system and its economic parameters, also to assess the effect of uncertainty or changes in sensitivity variable which affect the simulated result.

The increased cost in operation and maintenance may result in high rates of Levelized Cost of Energy (LCOE). Expanding the lifetime of a system should decrease the rate of cost of energy. However, due to the escalation of the load demand with time, the energy sources must expand, increasing the cost. From an economic point of view, a high annual increasing rate of the load may raise the COE substantially, which will inevitably lead in a hybrid system depending on renewable energy and fossil fuels.

From an experimental point of view, our contribution lies in the comparison of the multiple scenarios, in both pure RESs depending and fossils depending microgrids, with HOMER's optimization and sensitivity. These simulations were performed for different load demand, different types of operating strategies, and applied to microgrids' optimum size problem.

7.2   Future Work

Many different adaptations, tests, and experiments have been left for the future due to lack of time. Future work concerns deeper analysis of particular methodologies, new proposals to try different scenarios, or simply curiosity.

A mathematical model could be implemented to determine the optimal sizing of the Hydro, BESS and PV system, in order to validate the results from the simulation. A combination of various methodologies mentioned in literature could be used.

There are some ideas worth trying, born during the description and the development of simulated scenarios in Chapter 6. This thesis has been mainly focused on the use of BESS as a system inextricably linked with PVs, incurious of the nature of the batteries and their ability to be charged by any source of power. A scenario of a system exclusively depending on a RoR hydro subsystem and a BESS replacing the non-existent dam would be intriguing, as would be expensive.

An additional research for creating a microgrid with another type of hydro system would be interesting. A hydro with a dam would probably be enough as the only source of power to cover the island's load. Taking advantage of as much flow rate as possible, in a manner of usage and storage, hydro system could have achieved its finest electrical potential.

REFERENCES

Ngoc An Luu. Control and management strategies for a Microgrid. Electric power. Université de Grenoble, 2014.

Learning about renewable energy. https://www.nrel.gov.

Renewable Energy Sources, http://www.ypeka.gr/Default.aspx?tabid=285&language=el-GR

Energy Statics, http://www.mof.gov.cy/mof/cystat/statistics.nsf/energy_environment_81main_gr/energy_environment_81main_gr?OpenForm&sub=1&sel=4.

PV Statics, Hellenic Association of Photovoltaic Companies, http://helapco.gr/wp-content/uploads/pv-stats_greece_2015_10Feb2016.pdf

Photovoltaic (Solar Electric), http://www.seia.org/policy/solar-technology/photovoltaic-solar-electric

Energy Storage in EU, https://ec.europa.eu/energy/en/topics/technology-and-innovation/energy-storage

Country profiles: Greece, EU energy in figures, https://ec.europa.eu/energy/sites/ener/files/documents/pocketbook_energy-2016_web-final_final.pdf

A. Zahedi. Maximizing solar PV energy penetration using energy storage technology, James Cook University, 2010.

Jim Eyer, Garth Corey. Energy Storage for the Electricity Grid: Benefits and Market
Potential Assessment Guide, Sandia National Laboratories, 2010.

A. Varela Souto. Management of a Microgrid Based on Frequency Communications, Delft
University of Technology, 2016.

Preety Mathema. Optimization of Integrated Renewable Energy System – Microgrid,
Tribhuvan University, 2011

Orhan Ekren and Banu Yetkin Ekren (2011). Size Optimization of a Solar-wind Hybrid
Energy System Using Two Simulation Based Optimization Techniques, Fundamental
and Advanced Topics in Wind Power, Dr. Rupp Carriveau (Ed.), InTech, DOI:
10.5772/18007.

F. Tooryan, S.M. Moghaddas Tafreshi, S.M. Bathaee and H. Hamidhassanzadeh-Fard.
Distributed Energy Resources Optimal Sizing and Placement in a Microgrid, (IEEJ)
Vol. 4 (2013) No. 2, pp. 1059-1070, ISSN 2078-2365.

History of hydropower, USA Office of Energy Efficiency and Renewable Energy,
https://energy.gov/eere/water/history-hydropower.

Types of Hydropower Turbines, USA Office of Energy Efficiency and Renewable Energy,
https://energy.gov/eere/water/types-hydropower-turbines.

Hydroelectric Plants in Greece – other regions, power plants around the world,
http://www.industcards.com/hydro-greece.htm.

How much does a hydropower system cost to build?,
https://www.renewablesfirst.co.uk/hydropower/hydropower-learning-centre/how-
much-do-hydropower-systems-cost-to-build/

Control of Microgrid for Different Modes of Operation, Megha Prakash, M.Tech Student , Dept. of EEE, Adi Shankara Institute of Engineering & Technology, Kalady, Kerala,India.

Microgrid Controller and Advanced Distribution Management System Survey Report, Guodong Liu, Michael R. Starke, Drew Herron, OAK Ridge National Laboratory, July 2016.

Demand and Response in Smart Grids for Modern Power System, Muhammad Qamar Raza, Muhammad Usman Haider, S. Muhammad Ali, Muhammad Zeeshan Rashid, Farooq Sharif, University of Faisalabad, 2013.

Microsource Interface for a Microgrid, Prabath Janaka Binduhewa, University of Manchester, 2010.

Feed-in tariffs for promotion of energy storage technologies, Goran Krajacic, Neven Duic, Antonis Tsikalakis, Manos Zoulias, George Caralis, Eirini Panteri, Maria da Graca Carvalho, 2010.

The Overview of Research on Microgrid Protection Development, Wei Jiang, Zheng-you He, Zhi-qian Bo, Intelligent System Design and Engineering Application (ISDEA), 2010 International Conference on Intelligent System Design and Engineering Application.

Progress and problems in microgrid protection schemes, Sohrab Mirsaeidi, Dalila Mat Said, Mohd, Wazir Mustafa, Mohd, Hafiz Habibuddin, Elsevier, 2014.

Solar Electric Photovoltaic Modules, http://www.solardirect.com/pv/pvlist/pvlist.htm.

Types of Hydropower Turbines, https://energy.gov/eere/water/types-hydropower-turbines.

Note on Water Turbine, https://www.kullabs.com/classes/subjects/units/lessons/notes/note-detail/4209.

Hydro Resource Evaluation Tool, Lancaster University, http://www.engineering.lancs.ac.uk/lureg/nwhrm/engineering/turbine_costs.php.

Run-of-the-river hydroelectricity, https://en.wikipedia.org/wiki/Run-of-the-river_hydroelectricity

Electrochemical Supercapacitors: Scientific Fundamentals and Technological Applications, B. E. Conway

Cost Optimization of Hydro Solar, Micro-Hydro and Hydrogen Fuel Cell Using HOMER Software, Nader Barsoum, Pearl Dianne Petrus, Department of Electrical and Electronics Engineering, UniversitY Malaysia Sabah, August 2015

NUMBERED REFERENCES

[1] C. Wang and M. H. Nehrit, "Power management of a stand-alone wind/photovoltaic/fuel cell energy system" IEEE Trans. Energy Convers., vol. 23, no. 3, pp. 957-967, Sep. 2008.

[2] A. W. Yang, "Design of energy management strategy in hybrid vehicles by evolutionary fuzzy system part I: Fuzzy logic controlled development" in Proc. 6th World Congress on Intelligent Control and Automation, Dalian, China, Jun. 21-23, 2006.

[3] Faisal A. Mohamed, "Microgrid modeling and online management". Helsinki University of Technology Control Engineering, Finland. PhD Thesis, Jun. 2008.

[4] Zheng Zhao, "Optimal Energy Management for Microgrids". Clemson University, United States, PhD Thesis, Oct. 2009.

[5] N. Hatziargyriou, "Microgrids: Architectures and Control" Wiley-IEEE Press, 2014.

[6] Y. A. R. I. Mohamed and A. A. Radwan, "Hierarchical control system for robust microgrid operation and seamless mode transfer in active distribution systems", IEEE Trans, Smart Grid, vol. 2, pp. 352-362, Jun. 2011.

[7] A. P. Martins, A. S. Carvalho and A. S. Araujo, "Design and implementation of a current controller for the parallel operation of standard UPSs", in Proc. IEEE IECON, 1995, pp. 584-589.

[8] Jiefeng HU. "Advanced Control in Smart Microgrids". University of Technology, Sydney, Australia. PhD Thesis, Jun. 2013

[9] S. M. Moghaddas-Tafreshi, H. A. Zamani, and S. M. Hakimi, J. Renewable Sustainable Energy, 3, (2011).

[10] Bernal-Agustın, Jose L., and Rodolfo Dufo-Lopez. "Simulation and optimization of stand-alone hybrid renewable energy systems." Renewable and Sustainable Energy Reviews 13 (2009): 2111-2118.

[11] Phrakonkham, S., Le Chenadec, J. Y., Diallo, D., Remy, G., & Marchand, C. (2010). Reviews on Micro-Grid Configuration and Dedicated Hybrid System Optimization Software Tools: Application to Laos. Engineering Journal, 14(3), 15-34. SIZING.

[12] HOGA (Hybrid Optimization by Genetic Algorithms). [Online]. Available http://www.unizar.es/rdufo.hoga - eng.htm.

[13] T. Khatib, A. Mohamed, K. Sopian "A review of photovoltaic system size optimization techniques," Renewable and Sustainable Energy Reviews, 22 (2013), pp. 454–46.

[14] Koutroulis Eftichios, Kolokotsa Dionissia, Portirakis Antonis, Kalaitzakis Kostas. J. Solar energy, 80, 1072 (200).

[15] J.L. Bernal-Agustín, R. Dufo-López, D.M. Rivas-Ascaso, "Design of isolated hybrid systems minimizing costs and pollutant emissions," Renew Energy, 31 (14) (2006), pp. 2227–2244.

[16] J.L. Bernal-Agustín, R. Dufo-López, D.M. Rivas-Ascaso, "Design of isolated hybrid systems minimizing costs and pollutant emissions," Renew Energy, 31 (14) (2006), pp. 2227–2244.

[17] S. Diaf, M. Belhamelb, M. Haddadic, A. Louchea, "Technical and economic assessment of hybrid photovoltaic/wind system with battery storage in Corsica Island," Energy Policy, 36 (2) (2008), pp. 743–754.

[18] R. Dufo-López et al, "Multi-objective optimization minimizing cost and life cycle emissions of stand-alone PV–wind–diesel systems with batteries storage," Applied Energy,88 (2011), pp. 4033–4041. [2-] Faisal A. Mohamed and Heikki N. Kio, Proceeding of the International conference on renewable energies and power quality (ICREPQ'07), Sevilla, Spain, 2007.

[19] Yu Ru; Kleissl, J.; Martinez, S., "Storage Size Determination for Grid-Connected Photovoltaic Systems," Sustainable Energy, IEEE Transactions on , vol.4, no.1, pp.68-81, Jan. 2013.

[20] Kornelakis, A., and E. Koutroulis. "Methodology for the design optimisation and the economic analysis of grid-connected photovoltaic systems." IET Renewable Power Generation, vol. 3, no 4, p. 476-492, 2009.

[21] Hernández, J. C., A. Medina, and F. Jurado. "Optimal allocation and sizing for profitability and voltage enhancement of PV systems on feeders." Renewable Energy 32.10 (2007): 1768-1789.

[22] Kornelakis, Aris, and Yannis Marinakis. "Contribution for optimal sizing of gridconnected PV-systems using PSO", vol. 35, no 6, p. 1333-1341, 2010.

[23] Microgrids: "Large Scale Integration of Micro-Generation to Low Voltage Grids", ENK5-CT-2002-00610. 2003–2005.

[24] More microgrids: "Advanced Architectures and Control Concepts for More microgrids", FP6 STREP, Proposal/Contract no.: PL019864. 2006–2009.

[25] How Microgrid Work, Office of Electricity Delivery & Energy Reliability (US Department of Energy).

[26] The Microgrid Solution, Mohommed Shahidehpour, bodine Distinguished Chair Professor and Director at Illinois Institute of Technology.

[27] Microgrids, https://sustainability.ucsd.edu/highlights/microgrids.html , US San Diego, University of California.

[28] The microgrid concept, Berkeley lab, https://building-microgrid.lbl.gov/microgrid-concept , 2017.

[29] Importance of a Distribution Management System (DMS) in Grid Modernization, Kevin Normandeau, https://microgridknowledge.com/importance-of-distribution-management-system-dms-grid-modernization/, 2015.

[30] R. H. Lasseter and P. Piagi,"Control and design of microgrids components", PSERC Publication 06-03, University of Wisconsin-Madison, January 2006.

[31] Ngoc An Luu. Control and management strategies for a Microgrid. Electric power. Université de Grenoble, 2014.

[32] Ziyad M. Salameh, Margaret A. Casacca, William A. Lynch, "A Mathematical Model for Lead-Acid Batteries", Department of Electrical Engineering, University of Lowell, 1992.

[33] Riffonneau Y., Bacha S., Barruel F., Ploix S., "Optimal Power Flow Management for Grid Connected PV Systems With Batteries", Sustainable Energy, IEEE Transactions on, vol.2, no.3, pp.309, 320, July 2011.

[34] Yann Riffoneau, "Gestion Des flux energitiques dans un systeme photovoltaique avec stockage connecte au reseau", University Joseph Fourier, France, October 2009.

[35] Modeling for control of run-of-river power plant Gronvollfoss, Liubomyr Vytvytskyi, Roshan Sharma, Ingunn Granstrom, Bernt Lie, Telemark University College, Norway.

[36] A staggered conservative scheme for every Froude number in rapidly varied shallow water flows, Sterling, G. S., Duinmeijer, S. P. A., International Journal for Numerical Methods In Fluids, 2003.

[37] Momentum and energy conserving discretizations on general grids for the compressible Euler and shallow water equations, Van't Hof B., Veldman, Journal of Computational Physics, 2012.

[38] Nasa, "atmospheric Science Data Center" [Online]. Available: https://eosweb.larc.nasa.gov/sse/

[39] Vasiliki Nikolopoulou, "Study of autonomous photovoltaic system" ("Μελέτη Αυτόνομου Φωτοβολταϊκού Συστήματος"), University of Patras, 2012.

[40] The HOMER Microgrid Software, www.homerenergy.com/products/software.html.

[41] Hydro Module, www.homerenergy.com/products/pro/modules/hydro.html.

[42] Electric Load, www.homerenergy.com/products/grid/docs/1.1/electric_load.html.

[43] Storage, www.homerenergy.com/products/pro/docs/3.11/storage.html.

[44] Photovoltaic (PV) Library, HOMER ENERGY, www.homerenergy.com/products/pro/docs/3.10/photovoltaic_pv_library.html.

[45] Solar GHI Resource, HOMER ENERGY, www.homerenergy.com/products/pro/docs/3.10/solar_ghi_resource.html.

[46] Solar DNI Resource, HOMER ENERGY, www.homerenergy.com/products/pro/docs/3.10/solar_dni_resource.html.

[47] Feed-in tariffs for promotion of energy storage technologies, Goran Krajacic, Neven Duic, Antonis Tsikalakis, Manos Zoulias, George Caralis, Eirini Panteri, Maria da graca Carvalho, 2010.

[48] Load Following Strategy, HOMER software, https://www.homerenergy.com/products/pro/docs/3.11/load_following_strategy.html

[49] Cycle Charging Strategy, HOMER software, https://www.homerenergy.com/products/pro/docs/3.11/cycle_charging_strategy.html

[50] HOMER Software Training Guide for Renewable Energy Base Station Design, https://www.gsma.com/mobilefordevelopment/wp-content/uploads/2012/06/HOMER-Software-Training-Guide-June-2011.pdf

APPENDIX

I.   Turbine selection:

There are two main types of Hydro turbines: impulse and reaction. The type of hydropower turbine selected for a project is based on the height of standing water -referred to as "head"- and the flow, or volume of water, at the site. Figure 5.1 shows an application chart in which one can decide what type of turbine needs to be selected for a specific project.
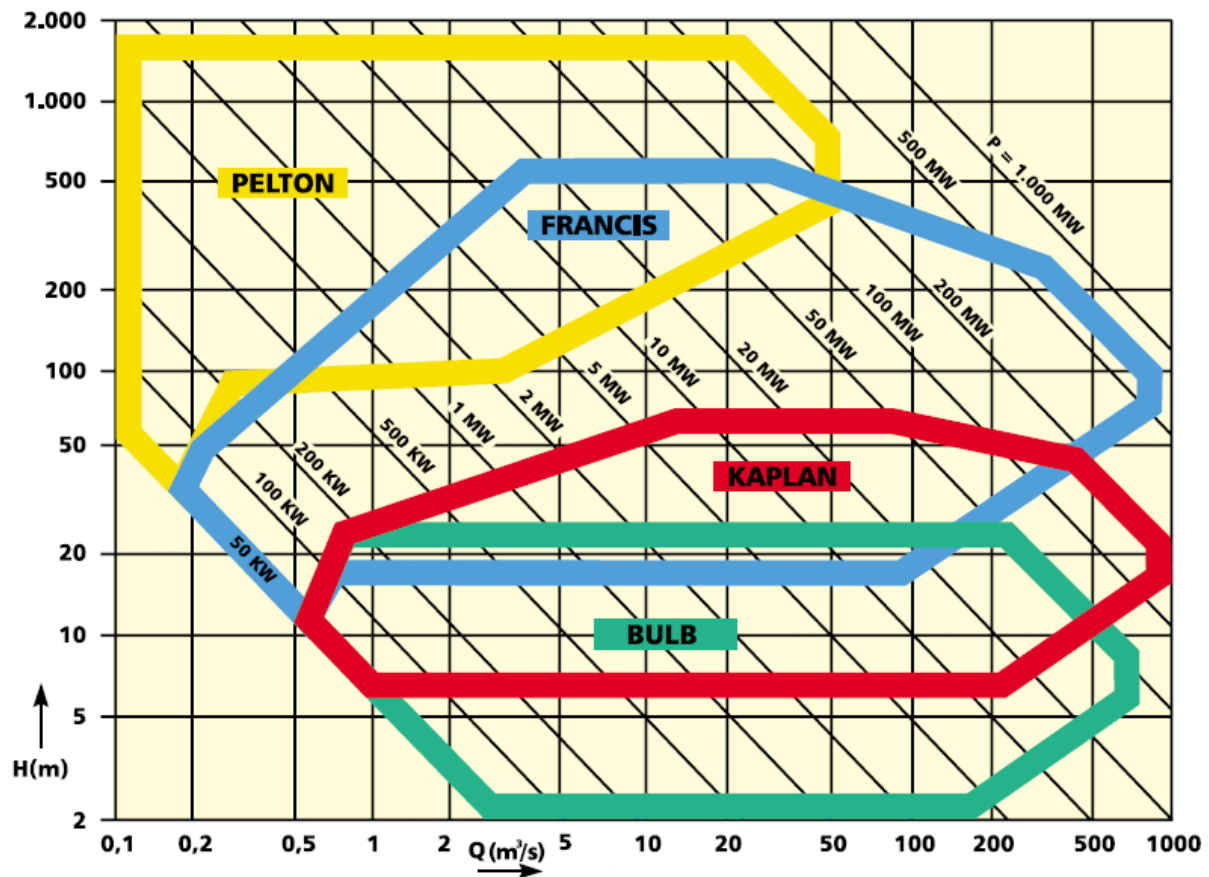
Figure A I: Turbine application charts

(Source: https://www.researchgate.net/figure/312577028_fig2_Figure-4-Turbine-
    application-range-charts)

The impulse turbine generally uses the velocity of the water to move the runner and discharges to atmospheric pressure. The water stream hits each bucket on the runner. There is no suction on the down side of the turbine, and the water flows out the bottom of the turbine housing after hitting the runner. An impulse turbine is generally suitable for high head, low flow applications. Examples of impulse turbines are the Pelton turbine and the Cross-flow turbine.

A reaction turbine develops power from the combined action of pressure and moving water. The runner is placed directly in the water stream flowing over the blades rather than striking each individually. Reaction turbines are generally used for sites with lower head and higher flows than compared with the impulse turbines. Examples of reaction turbines are the Propeller turbine (Bulb, Straflo, tube, Kaplan), Francis turbine and Kinetic energy turbine.

II.   Pelton Turbine:

Pelton turbines are usually used for the high head, low flow power plants. It was invented by Lester Ella Pelton in about 1870s. Nozzles are direct powerful, high-speed streams of water against a rotary series of spoon-shaped buckets, also known as impulse blades, which are mounted on the circumferential frame of a drive wheel also called a runner. As the water jet strikes the bucket-blades, the direction of water velocity is changed to follow the contours of the bucket. Water impulse energy puts forth the torque on the bucket and wheel system, spinning the wheel; the water stream itself does a "u- turn" and exits at the outer sides of the bucket. Figure 3.4 describes an example of the operation of a Pelton turbine attached to a dam.
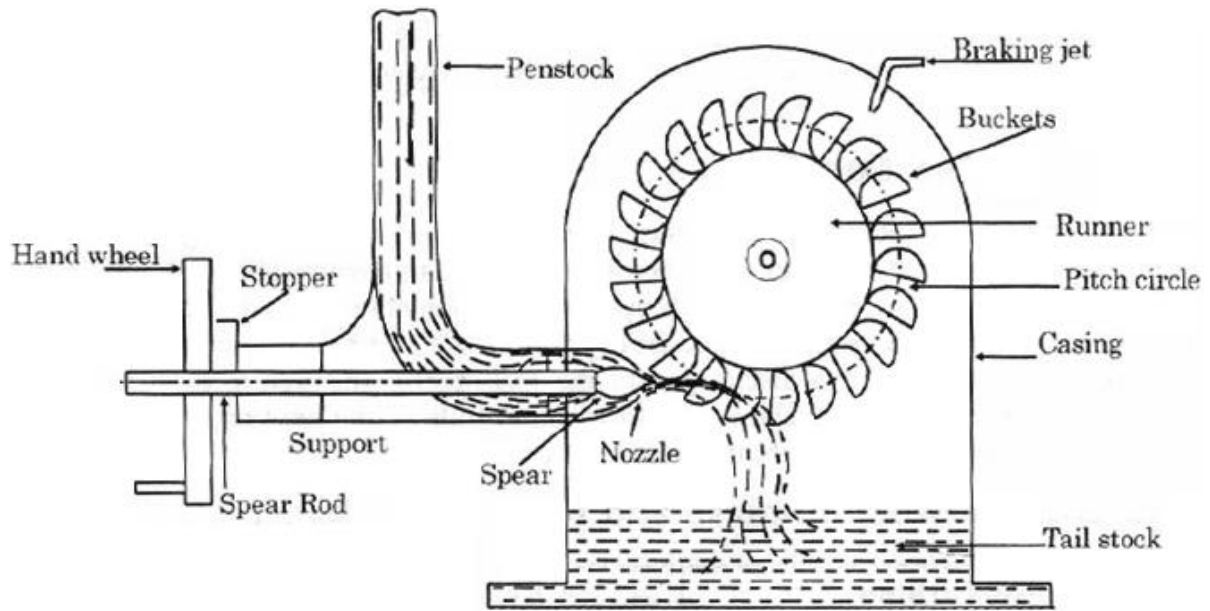
Figure A II: Pelton Turbine operation

(Source: https://www.kullabs.com/classes/subjects/units/lessons/notes/note-detail/4209)

Pelton wheels are made in all sizes. For maximum power and efficiency, the wheel and turbine system are designed such that the water jet velocity is two times the velocity of the rotating buckets.

The penstock, presented in the above Figure, conveys pressurized water from the river to the turbine. In addition to the pressure caused by static head, the penstock must be able to withstand the pressure rise caused by the so-called water hammer, i.e., the pressure rise that occurs due to rapid turbine shutdown in emergencies. Pipe thickness is based on the internal pressure the pipe material must withstand; higher internal pressure requires greater pipe thickness. The penstock can be implemented on the ground or as a buried pipe. The penstock is always laid on a stable site, towards the hill slope and is held by anchor blocks, or supported by piers when necessary. Anchor blocks must be located everywhere the penstock changes incline or direction to ensure safe handling of the arising forces.

III. Calculation of minimum Hydro contribution

It is known from the literature that the island's highest point is Circa, 720 m. To preserve the eco system of the area, the river flow must be restored as soon as possible, the height has to be reduced to the minimum possible. Due to the type of hydro that will be used to this project (ROR without a dam) it's impossible to ensure that all the water is going to enter the penstock. In the application chart presented above it is observed that at the correct height (about 100 m) and for about half (and maybe less) of the minimum flow (0,1 m^3/s) calculated in subchapter 4.3 (page 74), the appropriate turbine that should be used is Pelton. Figure 5.2 shows a Pelton turbine.

Figure A III: Pelton Turbine

(Source: http://www.mechanicalbooster.com/2016/10/pelton-turbine-working-main-parts-application-with-diagram.html)

IV.   Hydroelectric System Cost Estimation

The relationship between the cost of Pelton turbine C_{Pelton} and a flow rate Q in m^3/s can be expressed by the following formula (in Euro):

$$C_{Pelton}=8300 \cdot (Q \cdot H)^{0.54} \cdot Ex$$

Where

Q: flow rate (m^3/s),

H: head (m),

Ex: currency exchange rates from British Pound to Euro, currently 1.0779 (€/£).

The cost of the penstock $C_{penstock}$ of the turbine, as indicated in [47], is calculated as follows:

$$C_{penstock} = 1.25 \cdot \sum_{I} \left\{ \left[\left(W_M \cdot \pi \cdot D_I \cdot e_I \cdot L \right) C_M + \left(\pi \cdot \pi_I \cdot L \right) C_I + \left(1.5 \cdot \frac{\pi \cdot D_I^2}{4} \cdot L \right) C_E \right] \right\}$$

The cost of the generator $C_{generator}$ of the turbine depends on the model.

The cost of the control System C_{cs} of the turbine, as indicated in [a1], is calculated as follows:

$$C_{cs}=(C_{Pelton} + C_{penstock} + C_{generator}) \cdot 1.6\%$$

The cost of transportation of equipment C_T, as indicated in [a1], is presented as follows:

$$C_T=(C_{Pelton} + C_{penstock} + C_{generator}) \cdot 2.4\%$$

The cost of personel C_{pe} needed for the hydro system, as indicated in [a1], is shown below:

$$C_{pe} = (C_{Pelton} + C_{penstock} + C_{generator}) \cdot 30\%$$

The cost of operation and maintenance OMC, as indicated in [a1], is shown below:

$$OMC = (C_{Pelton} + C_{penstock} + C_{generator}) \cdot 2\%$$

Some other expenses C_o, as indicated in [a1], are calculated as follows:

$$C_o = (C_{Pelton} + C_{penstock} + C_{generator}) \cdot 2\%$$

Finally, to calculate the total cost of the Hydro system C_{HS} one must sum up all the above:

$$C_{HS} = C_{Pelton} + C_{penstock} + C_{generator} + C_{cs} + C_T + C_{pe} + OMC + C_o$$

V. Photovoltaic System Sizing

A PV system consists of many PV panels wired in parallel to increase current and in series to produce a higher voltage. The required number of PV panels in series is estimated by the number of panels needed to match the bus operation voltage. Thus, the PV panel number in series is calculated as follows:

$$n_{pv,series} = \frac{U_{bus}}{U_{panel}}$$

Where

$n_{pv,series}$: the number of PV panels in series,

U_{bus}: the bus operation voltage,

U_{panel}: the PV panel voltage.

Each PV string includes $n_{pv,series}$ panels connected in series. In order to match the current requirement of the system, this PV string is needed to be installed in parallel with other strings. <u>The parallel string number is the sizing variable that is able to be optimized.</u>

The parallel PV string number $x_{pv,parallel}$ relates with the amount of the available output current from the overall PV array. Thus, when one changes the value of $x_{pv,parallel}$, the value of the output current is also changed. Therefore, in the optimal sizing system, the parallel PV string number is handled as a variable value to be found through the optimization algorithm. The current output of PV array at time t is calculated as follows:

$$I_{pv,array}(t) = I_{pv,panel}(t, x_{size,type,pv}) \cdot x_{pv,parallel} \cdot f_{mm}$$

Where

$x_{pv,parallel}$: the parallel PV string number,

$x_{size,type,pv}$: PV panel size of a certain PV panel type,

$I_{pv,array}(t)$: the current output of PV array at time t,

$I_{pv,panel}(t, x_{size,type,pv})$: the PV panel output current at time t depending on panel type,

f_{mm}: mismatch factor.

The PV panels number can range from 0 to the highest amount of PV panels needed when a PV stand-alone system must cover the load demand. Thus, $x_{pv,parallel}$ is bounded as follows:

$$0 \leq x_{pv,parallel} \leq \frac{E_{L\_day}}{n \cdot W \cdot n_{pv,series} \cdot Hours_{sunshine/day}}$$

Where

n: efficiency loss of conversion,

W: the expected PV panel output power (Watt),

Hours$_{sunshine/day}$: the average number of estimated sunshine hours per day (h).

The output power of the PV array is calculated as follows:

$$P(t) = I_{pv,panel}(t, x_{size,type,pv}) \cdot U_{panel} \cdot n_{pv,series} \cdot x_{pv,parallel} \cdot f_{mm}$$

Where

P(t): The output power of the PV array at time t (Watt).

The PV sizing variables are given as the **PV panel number** and the **amount of string in a PV array**.

VI.   Alternative mathematical way of Sizing of BESS and PV system:

Following the methodology indicated by literature [39] the parameters A and C will be calculated below.

- Calculation of load in Ah/day:

The load that must be covered from the PV system is 45 kW, with 48 V voltage. The formula used for the calculation of the average load for one day of each month is presented below:

$$\bar{L}'_d = \frac{\bar{L}}{V}\frac{24h}{day} = \frac{45kW}{48V}\frac{24h}{day} = \frac{22,5kAh}{day}$$

$$\bar{L}_d = \bar{L}\frac{24h}{day} = 45kW\frac{24h}{day} = \frac{1,08MWh}{day}$$

Repeating the process for an average daily load of each month leads to the following calculations, presenting in table 5.1. It's important to point out that the results are showing in both kW (power) and kAh (energy).

Table A I- Daily Average Load Calculation For Each Month

MONTH	TOTAL LOAD (kW)	LOAD COVERED FROM PV SYSTEM (kW)	LOAD COVERED FROM PV SYSTEM (kAh)
July	132	42	21
August	145	55	27,5
September	139	49	24,5
October	133	43	21,5
November	145	55	27,5
December	153	63	31,5
January	128	38	19
February	132	42	21
March	125	35	17,5
April	130	40	20
May	133	43	21,5
June	129	39	19,5

- Calculation of STBS:

The STBS corresponds in 2 consecutive cloudy days are presented below.

$$STBS = \frac{2 days\, 22,5 kAh}{day} = 45 kAh$$

- Calculation of C:

The battery capacity C is calculated as follows. DOD_{max} for electrochemical storage is approximately 60%.

$$C = \frac{STBS}{1 - DOD_{max}} = \frac{45 kAh}{1 - 0,6} = 112,5 kAh$$

(For example, if the capacity of every battery is 500 Ah, then 225 batteries will be used.)

- Calculation of $\bar{n}_i$:

Initially, from the mean ambient temperature values, the average efficiency of the array for each month will be calculated based on the following formula:

$$\bar{n}_i = n_R\left[1 - 0{,}004\left(\bar{T}_{C_i} - T_R\right)\right]$$

Where,

$\bar{n}_i$: the average efficiency of the array for each month.

n_R: the nominal efficiency of the array (14%).

T_R: the reference temperature (25 °C).

$\bar{T}_{C_i}$: the mean temperature of the cells' operation of the array for each month and is calculated from the formula presented below:

$$\bar{T}_{C_i} = \bar{T}_{a_i} + 20$$

Where

$\bar{T}_{a_i}$: the mean ambient temperature of one day of each month (table 4.4, page 76).

The results of the calculations above are presented in table 5.2 below.

Table A II- The average efficiency of the array for each month

MONTH	$\bar{n}_i$
January	0,135
February	0,135
March	0,135
April	0,134
May	0,134
June	0,132
July	0,131
August	0,130
September	0,131
October	0,132
November	0,133
December	0,134

- Calculation of A_{min}:

$$A_{min} = \frac{\frac{1}{12}\sum_{i=1}^{12}(\bar{L}_d)_i\, V_{PV}}{\frac{1}{12}\sum_{i=1}^{12}(\bar{H}_T)_i\bar{n}_i n_D} = 1981,81 m^2$$

Where,

$\bar{H}_T$: the average daily radiation of one month on a tilted surface (table 4.6 at page 77, tilt=54).

$(\bar{L}_d)_i$: the average load for one day of each month.

V_{PV}: the PV system's voltage.

n_D: the efficiency rate of the array due to dust (95%).

- Calculation of A_{max}:

$$A_{max} = max\left\{\frac{(\bar{L}_d)_i V_{PV}}{(\bar{H}_T)_i \bar{n}_i n_D}\right\} = \frac{V_{PV}}{n_D} max\left\{\frac{(\bar{L}_d)_i}{(\bar{H}_T)_i \bar{n}_i}\right\} = 4138,49m^2$$

Where,

$max\left\{\frac{(\bar{L}_d)_i}{(\bar{H}_T)_i \bar{n}_i}\right\}$: During December

- Calculation of A_{opt}:

The optimal surface A_{opt} of the PV array can be found between A_{min} and A_{max}. It also has to gratify the following Treaty: the charge level of the batteries must not drop below the value found from the following equation.

$$1 - DOD_{max} = 1 - 0,4 = 0,6 = 60\%$$

To calculate the average energy that is produced daily every month in kAh the following function is used.

$$E = \frac{A(\bar{H}_T)_i \bar{n}_i n_D}{48V}$$

The process is repeated for every day during the period of one year in Matlab file "Aopt.m". From a combination of "Aopt.m" and trial and error the optimal size of the PV array is:

$$A_{opt} = 3941,4m^2$$

A sample of the results is presented in table 5.3. In columns where the results differ from day to day in period of a month, the last day of the month is presented (such as in column "Initial Capacity" and "Final Capacity").

Table A III- Daily Average Load Calculation For Each Month

| MONTH (days) | $\bar{H}_T$ [kWh/m2/day] | $\bar{n}_i$ | MONTHLY VALUES | | | LEVEL OF CHARGE | | | |
			Energy (kAh) Produced	Load (kAh)	Subtraction (kAh)	Initial (kAh) Capacity	Initial SOC	Final (kAh) Capacity	Final SOC
July(31)	5,21	0,131	30,4	21	9,4	112,5	100%	112,5	100%
August(31)	5,62	0,130	32,5	27,5	5	112,5	100%	112,5	100%
September(30)	5,23	0,131	30,5	24,5	6	112,5	100%	112,5	100%
October(31)	4,40	0,132	25,8	21,5	4,3	112,5	100%	112,5	100%
November(30)	3,44	0,133	20,3	27,5	-7,2	112,5	100%	112,5	100%
December(31)	2,87	0,134	17,1	31,5	-14,4	69	61,3%	67,5	60%
January(31)	3,01	0,135	18,1	19	-0,9	112,5	100%	112,5	100%
February(28)	3,60	0,135	21,6	21	0,6	112,5	100%	112,5	100%
March(31)	4,35	0,135	26,1	17,5	8,6	112,5	100%	112,5	100%
April(30)	4,87	0,134	29	20	9	112,5	100%	112,5	100%
May(31)	4,85	0,134	28,9	21,5	7,4	112,5	100%	112,5	100%
June(30)	4,80	0,132	28,2	19,5	8,7	112,5	100%	112,5	100%

VII.   Matlab flie: SamplingOneDayOfEachSeason.m

%get the values from the Excel file using xlsread.

```
[num2,txt2,raw2]  =  xlsread('FourDaysLoadCorvo2010.xlsx', 'C1:C24');
[num3,txt3,raw3]  =  xlsread('FourDaysLoadCorvo2010.xlsx', 'D1:D24');
[num4,txt4,raw4]  =  xlsread('FourDaysLoadCorvo2010.xlsx', 'E1:E24');
[num0,txt0,raw0]  =  xlsread('FourDaysLoadCorvo2010.xlsx', 'A1:A24');
[num1,txt1,raw1]  =  xlsread('FourDaysLoadCorvo2010.xlsx', 'B1:B24');

f1 = fit(num0,num1,'cubicinterp')
f2 = fit(num0,num2,'cubicinterp')
f3 = fit(num0,num3,'cubicinterp')
f4 = fit(num0,num4,'cubicinterp')
```

```matlab
figure(1)
plot(f1,'k',num0,num1,'co')
title('First of January')
xlabel('Hour')
ylabel('Load')


figure(2)
plot(f2,'k',num0,num2,'co')
title('First of April')
xlabel('Hour')
ylabel('Load')


figure(3)
plot(f3,'k',num0,num3,'co')
title('First of July')
xlabel('Hour')
ylabel('Load')


figure(4)
plot(f4,'k',num0,num4,'co')
title('First of October')
xlabel('Hour')
ylabel('Load')
```

VIII.   Matlab file: Aopt.m

```matlab
n = [0.131 0.130 0.131 0.132 0.133 0.134 0.135 0.135 0.135 0.134 0.134 0.132];
L = [21 27.5 24.5 21.5 27.5 31.5 19 21 17.5 20 21.5 19.5];
H = [5.21 5.62 5.23 4.4 3.44 2.87 3.01 3.6 4.35 4.87 4.85 4.8];
```

```matlab
Aop = 3941.4;
nd = 0.95;
Ctot = 112.5;
Cin = zeros(12, 30);
Cf = zeros(12, 30);
SOC = zeros(12, 30);
E = zeros(size(n));
Sub = zeros(size(n));


for i = 1:12
    if i==1
        Cin(i) = Ctot;
    end
    for j = 1:30

        %for Aop = 1950.85: 0.01: 2955.79
        E(i) = (Aop*H(i)*n(i)*nd)/48;
        Sub(i) = E(i)-L(i);
        if L(i) > E(i)
            Cf(i,j) = Cin(i,j)+Sub(i);
            SOC(i,j) = Cf(i,j)/Ctot;
            if i < 12
                if j < 30
                    Cin(i,j+1) = Cf(i,j);
                else
                    Cin(i+1,1) = Cf(i,j);
                end
            else
                if j < 30
                    Cin(i,j+1) = Cf(i,j);
                end
```

```
            end
        else
            if i == 12
                if (Cin(i,j)+Sub(i)) < Ctot
                    Cf(i,j) = Cin(i,j)+Sub(i);
                    if j < 30
                        Cin(i,j+1) = Cf(i,j);
                    end
                else
                    Cf(i,j) = Ctot;
                    if j < 30
                        Cin(i,j+1) = Cf(i,j);
                    end
                end
            else
                if (Cin(i,j)+Sub(i)) < Ctot
                    Cf(i,j) = Cin(i,j)+Sub(i);
                    if j < 30
                        Cin(i,j+1) = Cf(i,j);
                    else
                        Cin(i+1,1) = Cf(i,j);
                    end
                else
                    Cf(i,j) = Ctot;
                    if j < 30
                        Cin(i,j+1) = Cf(i,j);
                    else
                        Cin(i+1,1) = Cf(i,j);
                    end
                end
            end
```

```
        SOC(i,j) = Cf(i,j)/Ctot;
    end
  end
end
```